HANOI METROPOLITAN UNIVERSITY

# SCIENTIFIC
# JOURNAL

ISSN 2354-1504

---

## N°35 – TECHNOLOGICAL AND NATURAL SCIENCE

---

NOVEMBER – 2019

## SCIENTIFIC JOURNAL OF HANOI METROPOLITAN UNIVERSITY

(Frequency of issue: Monthly)

*The MIC issued License No. 571/GP-BTTTT dated on Oct. 26th, 2015*
*Publishing 300 volumes at Hanoi Metropolitan University.*
*Finishing and legal copyrighting on November 2019.*

# CONTENTS

# CONVEX FUNCTIONS AND APPLICATIONS THAT PROVE INEQUALITY

**Hoang Ngoc Tuyen**
*Hanoi Metropolitaln University*

***Abstract:*** *In this paper, we refer to the concept of function and convex (Convex function) with an application of convex function in solving the problem of proof of Inequality and the Extreme problem about inequality.*

***Keywords:*** *Convex function, inequalities, extreme*

Email: hntuyen@hnmu.edu.vn

Received 18 October 2019
Accepted for publication 20 November 2019

## 1. BACKGROUND

Convex analytic plays an important role in the theoretical study of extreme problems. Applied math majors are using convex analytical knowledge and linear space as an effective tool when solving related problems. There are many problems, if solved in the usual way is very difficult. However, if viewed from a functional perspective, the problem solved will be much simpler.

In this article, please mention such a function class - that is, a convex function, with the concepts and results involved to apply them to prove some inequalities.

## 2. SOME PREPARE KNOWLEDGE

### 2.1. Definitions and results

**Definitions 1:**

a) The f**unction** $f(x)$ is called convex on paragraph [a,b], if all $x_1, x_2 \in [a, b]$ and all $\lambda \in [0,1]$, we all have $f(\lambda . x_1 + (1 - \lambda). x_2) \geq \lambda f(x_1) + (1 - \lambda) f(x_2)$

Equality occurs when $x_1 = x_2$

b) $f(x)$ is the concave function on $[a,b]$, if $-f(x)$ is the convex function on $[a,b]$.

**Definitions 2:**

The f**unction** $f(x)$ identified on$[a,b]$ is called convex if all $x_1,x_2 \in [a,b]$ we have:

$$f(\frac{x_1+x_2}{2}) \geq \frac{f(x_1)+f(x_2)}{2}$$

Equality occurs when $x_1 = x_2$

**Comment:**

If $f(x)$ is a continuous function on [*a, b*] then definition (1) and definition (2) are equivalent.

**Theorem 1:**

Suppose the function $f(x)$ has a second derivative $f''(x)$ on $[a,b]$

Then:

1, If $f''(x) \geq 0$ with all $x \in [a,b]$ then $f(x)$ concave on paragraph [a,b]

2, If $f''(x) \leq 0$ with all $x \in [a,b]$ than $f(x)$ convex on paragraph [a,b]

## 2.2. Basic properties

**Properties 1:**

Give $f(x)$ is a convex function, continuous on $[a,b]$ then every $q_1$, $q_2$, $q_3$ positive such that $q_1 + q_2 + q_3 = 1$ we have:

$$f(q_1x_1+q_2x_2+q_3x_3) \geq q_1f(x_1)+q_2f(x_2)+q_3f(x_3)$$

*Prove:*

We have:

$$f(q_1x_1+q_2x_2+q_3x_3) = f\left[q_1x_1+(q_2+q_3)\frac{q_2x_2+q_3x_3}{q_2+q_3}\right]$$

Apply the definition (1) we obtain:

$$f(q_1x_1+q_2x_2+q_3x_3) \geq \ q_1f(x_1)+(q_2+q_3)f(\frac{q_2x_2+q_3x_3}{q_2+q_3})$$
$$\geq \ q_1f(x_1)+q_2f(x_2)+q_3f(x_3)$$

**Properties 2:**

If $f(x)$ is a convex function, continuous on $[a,b]$ then every $x_1,x_2,\dots x_n \in [a,b]$ and with all $\lambda_1,\lambda_2,\dots\lambda_n \in [0,1]$ so that $\lambda_1+\lambda_2+\cdots+\lambda_n=1$ we all have:

$$f\left(\sum_{i=1}^{n}\lambda_i\, x_i\right) \geq \sum_{i=1}^{n}\lambda_i\, f(x_i)$$

Equality only occurs when $x_1=x_2=\cdots=x_n$. Especially if selected $\lambda_1=\lambda_2=\cdots=\lambda_n=\frac{1}{n}$, I obtained:

$$f\left(\frac{x_1+x_2+\cdots+x_n}{n}\right) \geq \left(\frac{f(x_1)+f(x_2)+\cdots f(x_n)}{n}\right)$$

*Prove:* Based on definition (1) and inductive

**Properties 3:**

To put $f(x)$ is convex function on $[a,b]$. Then for all $x_1,x_2,\dots x_n \in [a,b]$, with all $\lambda_i > 0, i=\overline{1,n}$ we all have:

$$f\left(\frac{\lambda_1\, x_1+\lambda_2\, x_2+\cdots+\lambda_n\, x_n}{\lambda_1+\lambda_2+\cdots+\lambda_n}\right)$$
$$\geq \left(\frac{1}{\lambda_1+\lambda_2+\cdots+\lambda_n}\right)(\lambda_1\, f(x_1)+\lambda_2\, f(x_2)+\cdots+\lambda_n\, f(x_n))$$

Equality only occurs when $x_1=x_2=\cdots=x_n$.

**Comment:**

This property is a consequence of property 2. If $f(x)$ is concave function on [a,b] we have similar inequalities in the opposite direction.

## 3. USING CONVEX FUNCTIONS AND PROPERTIES OF CONVEX FUNCTIONS TO PROVE INEQUALITY (SOME ILLUSTRATIVE EXAMPLES)

**Problem 1:**

Prove that the Cosi inequality extends

Give n non-negative numbers $x_1, x_2, \dots x_n$ and n positive numbers $\alpha_1, \alpha_2, \dots \alpha_n$ so that $\alpha_1 + \alpha_2 + \dots + \alpha_n = 1$

Prove: $\alpha_1 x_1 + \alpha_2 x_2 + \dots + \alpha_n x_n \geq {x_1}^{\alpha_1}.{x_2}^{\alpha_2} \dots {x_n}^{\alpha_n}$

Equality occurs when: $x_1 = x_2 = \dots = x_n$.

*Prove:*

1) Considering $x_i > 0$ with $i = \overline{1,n}$. Consider the function $f(x) = \ln x$ on $(0, +\infty)$

We have $f'(x) = \frac{1}{x}; f''(x) = \frac{-1}{x^2} < 0, \quad \forall x \in (0, +\infty)$

So the function $f(x) = \ln x$ is convex function on (0, +∞) , should with every $x_i > 0$ với $i = \overline{1,n}$ and with every $\lambda_i > 0, i = \overline{1,n}$ we have:

$$f\left(\frac{\sum_{i=1}^{n} \lambda_i x_i}{\sum_{i=1}^{n} \lambda_i}\right) \geq \left(\frac{\sum_{i=1}^{n} \lambda f(x_i)}{\sum_{i=1}^{n} \lambda_i}\right) \quad (1)$$

Put $\alpha_i = \frac{\lambda_i}{\sum_{i=1}^{n} \lambda_i}$ we get $\alpha_i > 0$, với $i = \overline{1,n}, \sum_{i=1}^{n} \alpha_i = 1$

Inferred (1) $\Leftrightarrow \ln(\sum_{i=1}^{n} x_i \alpha_i) \geq \sum_{i=1}^{n} \alpha_i \ln x_i$

$\Leftrightarrow \sum_{i=1}^{n} x_i \alpha_i \geq {x_1}^{\alpha_1}.{x_2}^{\alpha_2} \dots {x_n}^{\alpha_n}$

Equality occurs when $x_1 = x_2 = \dots = x_n$.

2) If in $x_i$, $(i) = \overline{1,n}$ has a number equal to 0, then the inequality is obviously true.

**Comment:**

If $\lambda_1 = \lambda_2 = \dots = \lambda_n = \frac{1}{n}$ or $\alpha_1 = \alpha_2 = \dots = \alpha_n = \frac{1}{n}$

Then $\frac{1}{n}\sum_{i=1}^{n} x_i \geq \sqrt[n]{\prod_{i=1}^{n} x_i}$

**Problem 2:** Give n numbers $x_i > 0$ $(i = \overline{1, n})$. Suppose r, s are two real numbers such that $s > r > 0$. Prove that:

$$\left(\frac{1}{n}\sum_{i=1}^{n} x_i^r\right)^{\frac{1}{r}} \leq \left(\frac{1}{s}\sum_{i=1}^{n} x_i^s\right)^{\frac{1}{s}}$$

*Prove*: With $i = 1, 2, \dots n$ , put $y_i = x_i^r$ inferred $x_i^s = y_i^{\frac{s}{r}}$. Then the inequality needs to prove to be

$$\left(\frac{1}{n}\sum_{i=1}^{n} y_i\right)^{\frac{1}{r}} \leq \left(\frac{1}{n}\sum_{i=n}^{n} y_i^{\frac{s}{r}}\right)^{\frac{1}{s}}$$

Or

$$\left(\frac{1}{n}\sum_{i=1}^{n} y_i\right)^{\frac{s}{r}} \leq \frac{1}{n}\sum_{i=1}^{n} y_i^{\frac{s}{r}}$$

Due to $s \geq r > 0$ so $\frac{s}{r} \geq 1$. Consider the function $f(y) = y^{\frac{s}{r}}$ on $(0, +\infty)$

Then $f'(y) = \frac{s}{r} y^{\frac{s}{r}-1}$ ;$f''(y) = \frac{s}{r}.\left(\frac{s}{r} - 1\right) y^{\frac{s}{r}-2} \geq 0$

Inferred $f(y)$ is concave function on $(0, +\infty)$ should

$$f\left(\frac{y_1 + y_2 + \cdots + y_n}{n}\right) \leq \frac{f(y_1) + f(y_2) + \cdots + f(y_n)}{n}$$

Or $$\left(\frac{y_1 + y_2 + \cdots + y_n}{n}\right)^{\frac{s}{r}} \leq \frac{1}{n}\left(y_1^{\frac{s}{r}} + y_2^{\frac{s}{r}} + \cdots + y_n^{\frac{s}{r}}\right)$$

$$\Leftrightarrow \left(\frac{1}{n}\sum_{i=n}^{n} y_i\right)^{\frac{s}{r}} \leq \frac{1}{n}\sum_{i=n}^{n} y_i^{\frac{s}{r}}$$

Equality occurs when

$$y_1 = y_2 = \cdots = y_n \Leftrightarrow {x_1}^r = {x_2}^r = \cdots = {x_n}^r \Leftrightarrow x_1 = x_2 = \cdots = x_n$$

**Comment:**

If $s = r$ then the inequality is true for all non-negative numbers. Especially when n is non-negative numbers and $p$, $q$ is positive integers, $p \geq q$ is unequal:

$$\sqrt[q]{\frac{{x_1}^q + \cdots + {x_n}^q}{n}} \leq \sqrt[p]{\frac{{x_1}^p + \cdots + {x_n}^p}{n}}$$

**Problem 3:**

Give n positive numbers $a_1, a_2, \ldots, a_n$. Prove that:

$$({a_1}^{a_1}{a_2}^{a_2} \ldots {a_n}^{a_n})^{\frac{1}{a_1 + \cdots a_n}} \geq \frac{a_1 + a_2 + \cdots + a_n}{n} \qquad (1)$$

*Prove:*

We have:

$$(1) \Leftrightarrow {a_1}^{\frac{a_1}{a_1+a_2+\cdots+a_n}}.{a_2}^{\frac{a_2}{a_1+a_2+\cdots+a_n}} \ldots {a_n}^{\frac{a_n}{a_1+a_2+\cdots+a_n}} \geq a_1 + a_2 + \cdots + a_n$$

$$\Leftrightarrow \frac{a_1}{a_1 + a_2 + \cdots + a_n}\ln a_1 + \frac{a_2}{a_1 + a_2 + \cdots + a_n}\ln a_2 + \cdots + \frac{a_n}{a_1 + a_2 + \cdots + a_n}\ln a_n \geq \ln\frac{a_1 + a_2 + \cdots + a_n}{n}$$

Considering the function $(x) = x\ln x$ , with $x \in (0, +\infty)$

We have: $f'(x) = \ln x + 1 , f"(x) = \frac{1}{x} > 0$

Infer function $f(x)$ concave on $(0, +\infty)$. Should be with all $a_i > 0, i = \overline{1, n}$ we have:

$$f\left(\frac{a_1 + a_2 + \cdots + a_n}{n}\right) \leq \frac{f(a_1) + f(a_2) + \cdots + f(a_n)}{n}$$

Or

$$\frac{a_1 + a_2 + \cdots + a_n}{n}\ln\left(\frac{a_1 + a_2 + \cdots + a_n}{n}\right) \leq \frac{a_1\ln a_1 + a_2\ln a_2 + \cdots + a_n\ln a_n}{n}$$

$$\Leftrightarrow \ln\frac{a_1 + a_2 + \cdots + a_n}{n} \leq \frac{a_1 + a_2 + \cdots + a_n}{n}\ln a_1 + \cdots + \frac{a_1 + a_2 + \cdots + a_n}{n}\ln a_n$$

Equality only occurs when $a_1 = a_2 = \cdots = a_n$.

**Problem 4:**

Give n positive numbers $x_1, x_2, \dots x_n$ change, always satisfy the condition $x_1 + x_2 + \dots + x_n = 1$

Find $max\ y$: với y=$x_1{}^{a_1}.x_2{}^{a_2}\dots x_n{}^{a_n}$ ($a_i > 0$ for before; $i = \overline{1,n}$)

*Prove:*

Put $a = a_1 + a_2 + \dots + a_n;\ b_i = \frac{a_i}{a} \Rightarrow\ b_1 + b_2 + \dots + b_n = 1$

Applying the Cosi inequality we have:

$$\left(\frac{x_1}{a_1}\right)^{b_1}\left(\frac{x_2}{a_2}\right)^{b_2}\dots\left(\frac{x_n}{a_n}\right)^{b_n} \leq \frac{b_1}{a_1}x_1 + \frac{b_2}{a_2}x_2 + \dots + \frac{b_n}{a_n}x_n = \frac{1}{a}(x_1 + x_2 + \dots + x_n) = \frac{1}{a}$$

$$\Rightarrow \left(\frac{x_1}{a_1}\right)^{b_1}\left(\frac{x_2}{a_2}\right)^{b_2}\dots\left(\frac{x_n}{a_n}\right)^{b_n} \leq \frac{1}{a}$$

Raise both sides so the power *a* and because $a.b_i = a_i$ we get:

$$\left(\frac{x_1}{a_1}\right)^{a_1}\left(\frac{x_2}{a_2}\right)^{a_2}\dots\left(\frac{x_n}{a_n}\right)^{a_n} \leq \frac{1}{a^a}$$

Inferred $x_1{}^{a_1}.x_2{}^{a_2}\dots x_n{}^{a_n} \leq \frac{1}{a^a}a_1{}^{a_1}.a_2{}^{a_2}\dots a_n{}^{a_n}$

Equality occurs when

$$\begin{cases} \frac{x_1}{a_1} = \frac{x_2}{a_2} = \dots = \frac{x_n}{a_n} \\ x_1 + x_2 + \dots + x_n = 1 \end{cases}$$

$$\rightarrow \frac{x_1}{a_1} = \frac{x_2}{a_2} = \dots = \frac{x_n}{a_n} = \frac{x_1 + x_2 + \dots + x_n}{a_1 + a_2 + \dots + a_n} = \frac{1}{a}$$

As such: $max\ y = \frac{a_1{}^{a_1}.a_2{}^{a_2}\dots a_n{}^{a_n}}{a^a}\ with\ a = a_1 + a_2 + \dots + a_n\ khi\ x_i = \frac{a_i}{a}; i = \overline{1,n}$

**Problem 5:**

For the acute triangle ABC. Prove that:

$$(\sin A)^{\sin A}(\sin B)^{\sin B}(\sin C)^{\sin C} > \left(\frac{2}{3}\right)^{\frac{3\sqrt{3}}{2}}$$

*Prove:*

Considering $f(x) = x \ln x$ on $(0, +\infty)$. Easily proved f(x) is concave function on $(0, +\infty)$. Should have:

$$f\left(\frac{\sin A + \sin B + \sin C}{3}\right) \leq \frac{f(\sin A) + f(\sin B) + f(\sin C)}{3}$$

Or

$$\frac{\sin A + \sin B + \sin C}{3} \ln \frac{\sin A + \sin B + \sin C}{3} \leq \frac{\sin A \ln A + \sin B \ln B \sin C \ln C}{3}$$

$$\Leftrightarrow \ln\left(\frac{\sin A + \sin B + \sin C}{3}\right)^{\sin A + \sin B + \sin C} \leq \ln\left[(\sin A)^{\sin A}.(\sin B)^{\sin B}.(\sin C)^{\sin C}\right]$$

$$\Leftrightarrow \left(\frac{\sin A + \sin B + \sin C}{3}\right)^{\sin A + \sin B + \sin C} \leq (\sin A)^{\sin A}(\sin B)^{\sin B}(\sin C)^{\sin C} \quad (*)$$

Easy to see in the triangle ABC we have

$$\sin\frac{A + B + C}{3} \geq \frac{\sin A + \sin B + \sin C}{3}$$

Should $\sin A + \sin B + \sin C \leq \frac{3\sqrt{3}}{2}$

Which

$$\sin A + \sin B + \sin C > \sin^2 A + \sin^2 B + \sin^2 C > 2$$

$$\rightarrow \left(\frac{\sin A + \sin B + \sin C}{3}\right)^{\sin A + \sin B + \sin C} > \left(\frac{2}{3}\right)^{\frac{3\sqrt{3}}{2}}$$

Combined with (*) we have something to prove.

## 4. COCLUSIONS

The paper explores the concept of convex function and its basic properties to apply to solve a number of problems: Proof of Inequality or extreme problems related to Inequality.

## REFERENCES

1. Mai Thuc Ngoi (1991), *Mathematical Analysis 1,* - Scientific and technical publishing.
2. Do Van Luu and Phan Huy Khai (2000), *Convex Analysis,* - Scientific and technical publishing.
3. G. H. Hardy, J. E. Littlewood, G. Polia (1952), *Inequalities,* - Cambridge University Press.
4. Nguyen Văn Mau (2002), *Equations and inequalities,* - Scientific and technical publishing.

# HÀM LỒI VÀ ỨNG DỤNG CHỨNG MINH BẤT ĐẲNG THỨC

***Tóm tắt***: *Bài viết này, chúng tôi đề cập tới khái niệm hàm số và tính lồi (Hàm lồi) với một ứng dụng của hàm lồi trong việc giải quyết bài toán chứng minh Bất đẳng thức và Bài toán cực trị quy về bất đẳng thức.*

***Từ khóa***: *Hàm lồi, bất đẳng thức, cực trị...*

# FABRICATION AND CHARACTERIZATION OF AG PARTICLES COATED ON FE, NI DOPED $TIO_2$ USED FOR PHOTOCATALYTIC APPLICATION

**Cao Khang Nguyen**[1], **Hue Thi Tran**[1], **Tran Chien Dang**[2*]
[1] *Center for Nano Science and Technology, Hanoi national university of education*
[2] *Hanoi University of Natural Resources and Environment*

***Abstract:*** *In this paper, we fabricated Ni and Fe doped $TiO_2$ thin film with different doping percentages and fabricated Ag coated on Ni and Fe doped $TiO_2$ thin film with different doping percentages via the hydrothermal method. Characterized some physical properties of Ni and Fe doped $TiO_2$ thin film with different doping percentages and Ag coated on Ni and Fe doped $TiO_2$ thin film with different doping percentages. Photocatalytic activity of Ni and Fe doped $TiO_2$ and Ag coated on Ni and Fe doped $TiO_2$ thin films was studied by photocatalytic degradation of methylene blue (MB) in aqueous solution as a model pollutant under UV light irradiation. The result shows that 9% Fe and Ni doped $TiO_2$ have higher photocatalytic activity than other samples. We observed that as the Fe and Ni dopant level increase the photocatalytic activity of the $TiO_2$ samples increases whereas the results of degradation of MB using the Ag particles coated on Fe and Ni doped $TiO_2$ samples indicate that coating Ag particles did not prove photocatalytic activity of $TiO_2$ thin films.*

***Keywords:*** *Ag nanoparticles, phototatalytic activity, Ni and Fe doped $TiO_2$ nanorods.*

Email: dtchien@hurne.edu.vn

Received 15 October 2019
Accepted for publication 20 November 2019

## 1. INTRODUCTION

Among photocatalytic materials, titanium dioxide received a lot of interest because titanium dioxide is a n-type semiconductor material with stable structure, large band gap (about 3.2eV) so $TiO_2$ does not absorb visible light. Moreover, the high recombination rate of electron-hole pairs will also lead to its low photocatalytic efficiency [1,2]. The improvement of light harvesting proprerties of $TiO_2$ nanostructure material has become significant research topics to extend the effective operating range to visible light. Doping $TiO_2$ nanomaterials with trasition metals such as Fe, Cr and Ni [1,3,4] could extend titanium dioxide's light absorption to the visible spectrum and improve the separation efficiency of photo-induced electrons and holes.

Up to now, lots of studies about transition metal and nobel metals applied in decomposing organic substances have been reported [5-8]. Moreover, it should be noticed that $TiO_2$ doped with Fe prove higher photocatalytic activity in the experiments than that of other 3d transition metals doping [8,9]. And it shows that Fe is a good dopant for enhancing the photocatalytic activity of $TiO_2$ that has been indicated in the references through theoretical calculation.

Over the last few years, a lots of research were focused on using Ag to adjust $TiO_2$ which is applied to many kinds of photocatalytic field [8], which due to the high efficiency of electrone-hole separation by forming a Schottky barrier at the Ag-$TiO_2$, thus improving its photocatalytic activity [10]. Qui et al have proven that Ag/$TiO_2$ displayed the highest photocatalytic efficiency of degradating methylene blue (MB) under visible light irradiation in ten types of doped catalysts.

In this work, we synthesized Fe, Ni-doped titanium dioxide thin film coated Ag particle and characterized these catalytic properties by various measurements and method, and estimate the photoactivity of the samples.

## 2. EXPERIMENTAL SETUP

The synthesis of pure $TiO_2$ thin film: Firstly, 1ml TTIP was mixed with 20ml IPA then this mixture was covered by food cover film plastic and stirred at ambient air and room temperature for 60 minutes. The resultant sol after stirring should be transparent. Dropped about 7 drops of solution at the center of the FTO substrates then it was rotated at high speed in order to spread the coating materials by centrifugal force. The spin coater's parameters during the fabrication of thin films were set as: speed at 3000 rpm, acceleration is 300 rpm/s and spin time is 30 s. After spin coating, the samples were put on a hot glass plate at 80˚C for 10 mimutes (soft baking process) in order to eliminate residual solvent. Subsequent annealing was done in a mufle furnace at 400 with a heating rate of 10˚C/minute and soak time of 2 hours, followed by natural cooling. Secondly, 0.6ml TTIP was mixed with 25 ml distilled water and 25 ml hydrochloric acid HCl 36,56% to approximately reach a total volume of 50 ml in a Teflon-lined stainless steel autoclauve (50ml volume). The mixture was stirred for 45 minutes at ambient conditions (room temperature, ambient air). Two pieces of FTO which was already covered by $TiO_2$ thin fims were placed at an angle against the wall of the Teflon-liner with the thin fim side facing down. The hyrothermal synthesis was conducted at 20˚C - 165˚C for 12 hours in an electric oven. At first, the temperature was increased from 20˚C - 165˚C for 75 minutes

(2˚C/m), then the temperature was kept at 165˚C during 12 hours. After synthesis, the autoclave was cooled to room temperature naturally which took approximately 4 hours. The FTO substrate was taken out and rinsed extensively with distilled water and dried in ambient air by a hair dryer. The synthesis of Fe doping on $TiO_2$ films was conducted as following: First, similar to synthesis $TiO_2$ thin films, solution precursors were prepared using TTIP and Iron (III) nitrate: $Fe(NO_3)_3.9H_2O$ dissolved in IPA. The Fe dopant concentration was varied to 3, 6, 9 wt% Fe by adding $Fe(NO_3)_3.9H_2O$. The solution was mixed by stirring by magnetic stirrer for 60 minutes. Then Fe doping on $TiO_2$ films were fabricated by spin coating method by in the same way with pure $TiO_2$ films. Subsequent annealing was done in a mufle furnace at 400 with a heating rate of 10˚C/minute and soak time of 2 hours, followed by natural cooling. After that, 25 ml deionized water was mixed with 25 ml of concentrated hydrochloric acid (36.5% by weight). Fe also was added in this solution by adding $Fe(NO_3)_3.9H_2O$. The mixture was stirred at ambient conditions for 5 min before adding 0.6 ml of TTIP 97% then it was stirred for 45 minutes at ambient conditions (room temperature, ambient air). Two pieces of FTO which were already covered by $TiO_2$ thin films were placed at an angle against the wall of the Teflon-liner with the thin film side facing down. The hydrothermal synthesis was conducted at 20˚C - 165˚C for 12 hours in an electric oven. At first, the temperature was increased from 20˚C - 165˚C for 75 minutes (2˚C/m), then the temperature was kept at 165˚C during 12 hours. After synthesis, the autoclave was cooled to room temperature naturally which took approximately 4 hours. The FTO substrate was taken out and rinsed extensively with distilled water and dried in ambient air by hair dryer. The next heating process is carried out similarly to the heating process of synthesis of pure $TiO_2$ nanorods. The synthesis Ni doped $TiO_2$ was conducted similarly to the procedure to synthesis Fe doped $TiO_2$ with the main chemical used for sol preparation were TTIP, Nickel (II) nitrate $Ni(NO_3)_2.6H_2O$, China as a precursor of $TiO_2$ and nickel respectively and IPA as solvent. Initially, a transparent sol was prepared by mixing TTIP and IPA and then stirring $Ni(NO_3)_2.6H_2O$ for 60 minutes. The Ni dopant concentration was varied to 3, 6, 9 wt% Ni by adding different amount of $Ni(NO_3)_2.6H_2O$. Then Ni doped on $TiO_2$ films were fabricated by spin coating method by the same way with pure $TiO_2$ films. Subsequent annealing was done in a mufle furnace at 400 with a heating rate of 10˚C/minute and soak time of 2 hours, followed by natural cooling. The next step was growing the Ni doped $TiO_2$ nanorods. This step consisted of those steps which was conducted similiar to the steps which was used to grown the Fe doped $TiO_2$ nanorods. The synthesis of Ag particles coated Fe and Ni doped $TiO_2$ was made as following: Firstly, 0.12 g $AgNO_3$ was added to 1ml distilled water. This mixture was stirred for 10 minutes, then 5ml IPA was adding to it and stirred by magnetic stirrer for 45 minutes. Coating 3 layers on the FTO substrate which was cover with Fe and Ni doped $TiO_2$ nanorods. After every layer, the samples were put on a hot glass plate at

80 °C for 10 mimutes (soft baking process) in order to eliminate residual solvent. Subsequent annealing was done in a muffle furnace at 300 °C with a heating rate of 10 °C/minute and soak time of 2 hours, followed by natural cooling.

## 3. RESULTS AND DISCUSSION

### 3.1. Morphological survey of $TiO_2$ nanorods

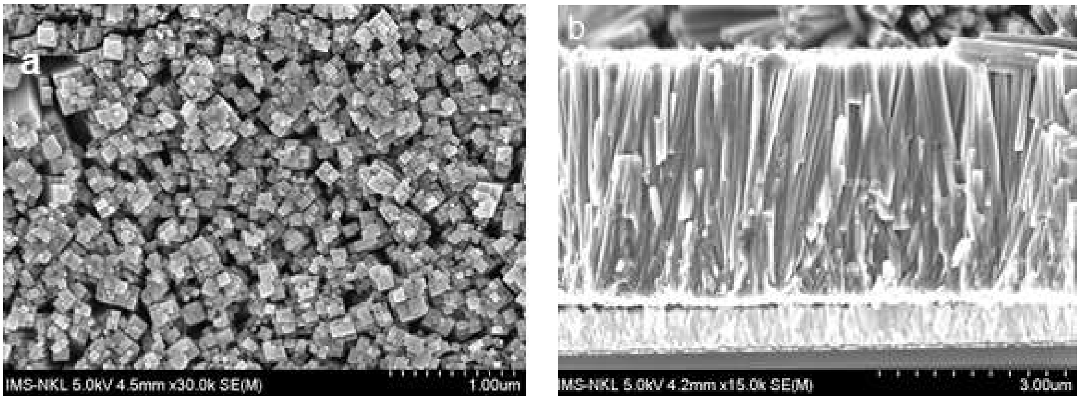

**Figure 1a:** *Top-view SEM of* $TiO_2$ *grown on FTO substrate (at 165 ˚C for 8hrs);*
**1b:** *Cross sectional view SEM image of* $TiO_2$ *thin film (nanorods).*

Figure 1a shows the SEM images of $TiO_2$ nanorods when setting hydrothermal period time for 8 hours. It can be seen that after 8 hours, the FTO surface was coated with shaped tent-like grains which may be originated due to the mismatches of Titanium dioxide crystal with FTO to minimize its surface energy [11]. M.Jithin *et al* also got the same result when they studied about $TiO_2$ nanorods and nanopillars [11].

Figure 1b shows the cross-sectional SEM image of $TiO_2$ nanorod thin film. It is clear that the nanorods are preferentially oriented normal to the substrate surface with the length of approximately 3.86 μm. Beside, the thickness of $TiO_2$ seed layers are about 1.1 μm which is quite large.

### 3.2. X-ray diffraction pattern

To study the lattice constants of the samples, we used X-ray diffraction method to analysis the structure of Fe/Ni doped $TiO_2$ thin films (nanorods) with various doping concentration 0%, 3%, 6%, 9%. Figure 2 illustrates the X- ray diffraction pattern of $TiO_2$ thin films. This XRD pattern indicates that the crystalline phase of $TiO_2$ is rutile. The rutile phase was identified at 2θ of 36.10˚ (101), 41.26˚ (111), 56.59˚ (220), 62.92˚ (002) respectively, corresponding to the standard XRD pattern (JCPCDS cards No.21-1276). A anatase phase with diffraction peaks at 37.78˚ (00) appeared. It proves that the $TiO_2$

structure is rutile and this result also demonstrates that $TiO_2$ nanorods after hydrothermal process, the structure transfer from anatase phase to rutile phase. Figure 4a shows the X ray diffraction pattern of Fe -doped $TiO_2$ with various percentage of iron 3%, 6%, 9% dopant level.

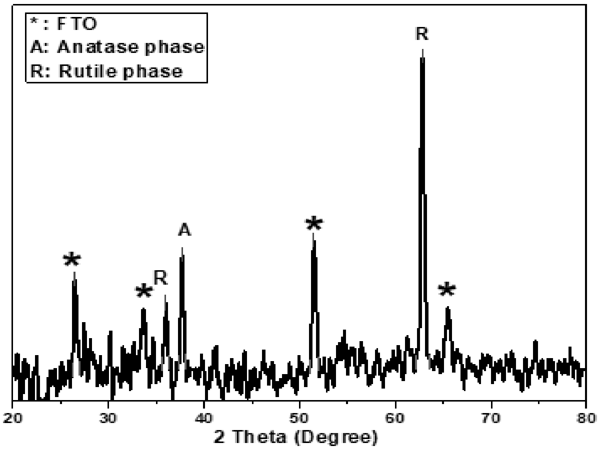

**Figure 2:** *X-ray diffraction pattern of $TiO_2$ nanorods grown on FTO substrate.*

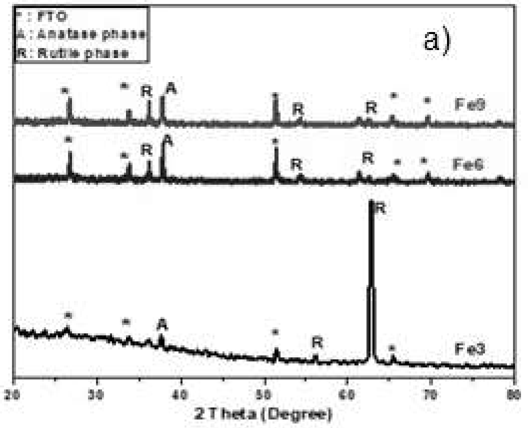

**Figure 3a:** *X-ray diffraction pattern of Fe doped $TiO_2$ grown on FTO substrate with various percentage 3%, 6%, 9% of Fe dopant level (at 165 ˚C for 12 hrs).*

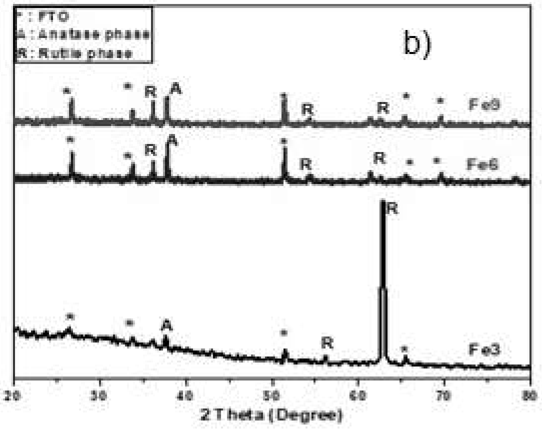

**Figure 3b:** *X-ray diffraction pattern of Ag particles coated on Fe-doped $TiO_2$ grown on FTO substrate (at 165˚C for 12hrs).*

It can obviously be seen that all samples exhibit the diffraction peaks of rutile phase 62.92˚ (002). Besides, for 3% Fe-doped $TiO_2$ thin films, the peak at 62.92 ˚ (002) got sharper and has higher intensity. For 3% Fe-doped $TiO_2$ thin films and 6% Fe-doped $TiO_2$ other peaks of rutile phase (R) were also observed clearly at 36.10˚ (101), 56.59˚ (220). For 3% Fe-doped $TiO_2$ thin films, a rutile phase with diffraction peaks at 36.10˚ (101), 54.36˚ (211) appeared, respectively, corresponding to the standard XRD pattern (JCPDS files No.21-1276).

Figure 3a shows that with increasing Fe dopant level, the rutile peaks become broader and sharper, which suggests decreasing degree of crystallinity. Since Fe was added to $TiO_2$ structure, it is clear that the accommodation of the former in the lattice, whether substitutional or interstitial, results in structural distortion and the concomitant decrease in crystallinity.

The X-ray diffraction patterns of the silver coated on Fe-doped $TiO_2$ samples shown in Figure 3b change slightly when comparing to that of Fe doped $TiO_2$ samples. The patterns show no diffraction peaks due to the silver species which might lead to the prediction that the metal particles are well substitue on the $TiO_2$ surface. Coating with Ag does not disturb the crystal structure of $TiO_2$ indicating that Silver did not covalently anchor into the Titanium dioxide lattice Ag placed on the surface. There are no diffraction pattern charactertics of the metals in the XRD patterns. Hence, these metal sites are predicted to be below the limit of visibility of X-ray measurement.

Figure 4a displays the X ray diffraction pattern of Ni-doped $TiO_2$ with various Nikel dopant level 3%, 6%, 9%. XRD shows that the $TiO_2$ films with different Ni dopant level deposited on FTO substrate are $TiO_2$ rutile. Besides, the peak of anatase phase at 37.78° (004) appeared so this result is similar to samples were doped iron.

The X-ray diffraction patterns of the silver coated on Ni-doped $TiO_2$ samples shown in Figure 4b are similar to that of Ni doped $TiO_2$ samples. To specific, it can be observed the rutile phase peaks of $TiO_2$ at 36.10° (101), 62.92° (002) and a peak at 37.78° (004) of anatase phase.

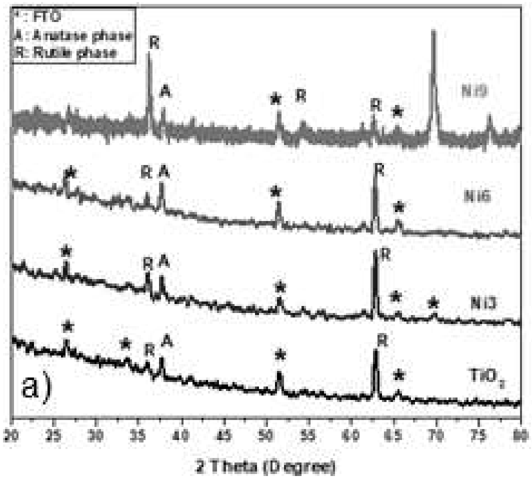

**Figure 4a:** *X-ray diffraction pattern of Ni-doped $TiO_2$ grown on FTO substrate (at 165° C for 12h) with various Ni dopant level.*

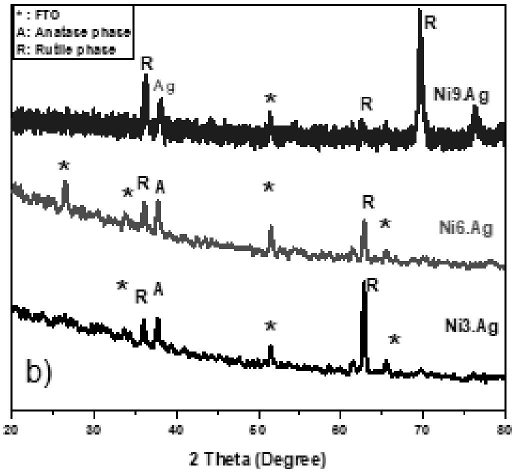

**Figure 4b:** *X-ray diffraction pattern of Ag particles coated on Ni-doped $TiO_2$ grown on FTO substrate samples (at 165 °C for 12 hrs).*

However, it can be seen that the intensity of the peak at 62.92° decreases corresponds to an increase in the concentration of Ni doping. Besides, to the 9%Ni doped $TiO_2$ samples, a characteristic peak of silver presents which means we successful coating Ag particles on thin films surface. Compared to the powder diffraction pattern, the (002) diffraction peaks were significantly changed and some diffraction peaks including (110), (111), (210) and (310) were absent, which indicates that the as-deposited film is highly oriented with respect to the substrate surface and the $TiO_2$ nanorods grow in the [001] direction with the growth axis parallel to the substrate surface. The absence of diffraction peaks often found in polycrystalline or powder samples is a strong indication that the nanorods are not only aligned but also single crystals throughout their length and these results are similar to that of the study of Bin Liu et al [12].

## 3.3. UV-VIS diffusive reflectance spectra

Figure 5a shows the corresponding UV-vis diffuse reflectance spectra of $TiO_2$ and Ni doped $TiO_2$ thin films with various Ni dopant level. The 9% Ni doped $TiO_2$ samples have an absorption in the visible region between 400 and 600nm.

At lower Ni dopant level, the optical absorption edge of synthesized samples was only shifted insignificantly, whereas when the Ni dopant level rose to higher 9%, a red- shift in the optical absorption edge of samples toward the visible light region, at 600nm was observed.

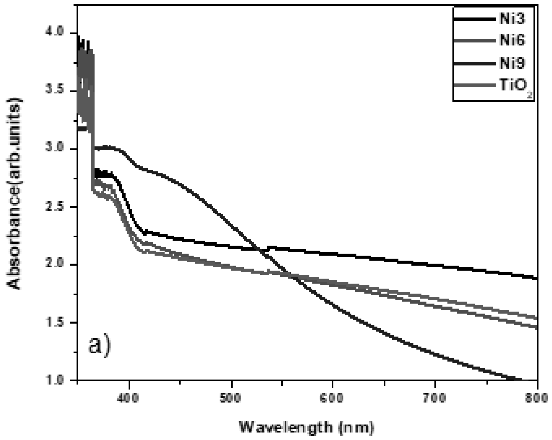

**Figure 5a:** *UV-vis diffusive reflectance spectra of $TiO_2$ thin films (nanorods) and Ni doped $TiO_2$ thin films with various level of dopant 3% (Ni3), 6% (Ni6), 9% (Ni9).*

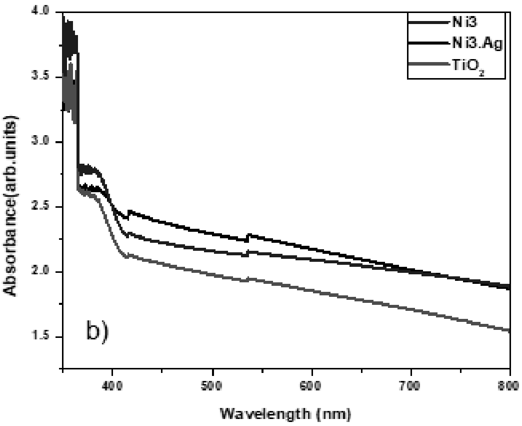

**Figure 5b:** *UV-vis diffusive reflectance spectra of $TiO_2$ thin films ($TiO_2$), 3% Ni doped $TiO_2$ (Ni3) thin films and Ag particles coated on 3% Ni doped $TiO_2$ thin films (Ni3.Ag).*

Figure 5b compares the UV-vis diffusive reflectance spectra of $TiO_2$ thin films, 3% Ni doped $TiO_2$ thin films and Ag particles coated on 3% Ni doped $TiO_2$ thin films. One can be seen that, there is no significant differences between the UV-vis diffusive reflectance spectra of 3 thin films. In addition, we can conclude that at Ni dopant level 3%, the optical absorption edge of synthesized samples Ni doped $TiO_2$ thin films and Ni doped $TiO_2$ coating Ag nanoparticles almost did not shift to visible region.

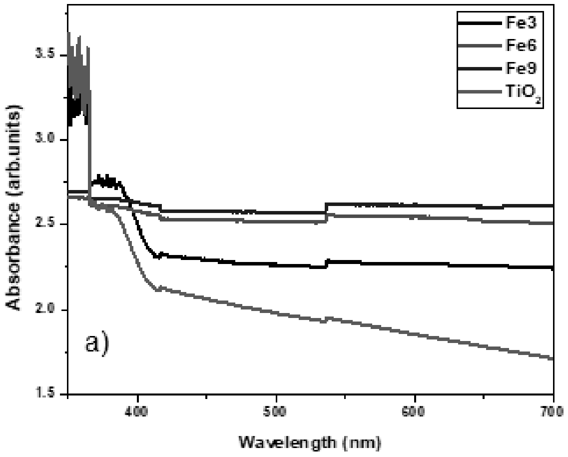

**Figure 6a:** *UV-vis diffusive reflectance spectra of $TiO_2$ thin films (nanorods) and Fe doped $TiO_2$ thin films with various level of dopant 3% (Fe3), 6% (Fe6), 9% (Fe9).*

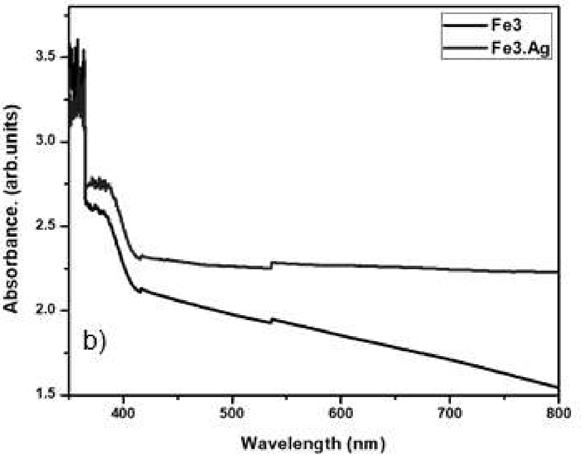

**Figure 6b:** *UV-vis diffusive reflectance spectra of 3% Fe.*

At lower Fe dopant level, the optical absorption edge of synthesized sample was only shifted insignificantly comparing to that of $TiO_2$ thin films, whereas when the Fe dopant level rose to higher 9%, a red- shift in the optical absorption edge of samples toward the visible light region, at 600nm was observed. Figure 6b compares the UV-vis diffusive reflectance spectra of 3% Fe doped $TiO_2$ thin films and Ag particles coated on 3% Fe doped $TiO_2$ thin films. One can be seen that, there is no significant differences between the UV-vis diffusive reflectance spectra of two samples.

### 3.4. Photocatalytic activity of synthesized ag particle coated on Fe/Ni doped $TiO_2$ in the degradation of methylene blue (MB)

Methylene blue (MB) was the model organic pollutant to estimate the photocatalytic activity of the samples. Photoactivites of all synthesized samples were described as above. Figure 7a shows that the MB degradation of 9% Fe doped $TiO_2$ is the best. When the Fe dopant level was increased the Fe doped $TiO_2$ samples expressed higher photocatalytic activity. In which, 3% Fe doped $TiO_2$ structure showed the worst photocatalytic results. When the Fe dopant level increased, the samples showed the better photocatalytic activity, respectively. One of the explanation of this fact is the presence of Fe which could create the amount of active sites higher due to the formation of Fe-O-Ti bonds in the $TiO_2$ crystal lattice. The consequence of formation of defects on the catalyst morphology which play the roles of a trap for preventing electron-hole recombination could be one of the reason of this phenomenon.

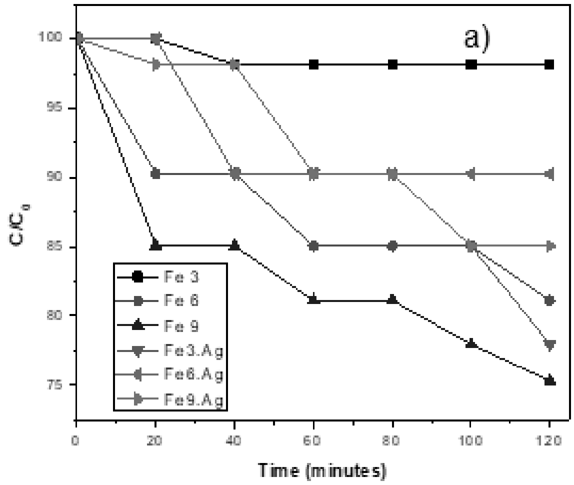

**Figure 7a:** *Decrease in MB concentration irradiation time in the presence of various photocatalysts with various Fe dopant level: 3% Fe dopant level (Fe3), 6% Fe dopant level (Fe6), 9% Fe dopant level (Fe9), Ag particles coated on 3% Fe doped on* $TiO_2$ *(Fe3.Ag), Ag particles coated on 6% Fe doped on* $TiO_2$ *(Fe6.Ag), Ag particles coated on 9% Fe doped on* $TiO_2$ *(Fe9.Ag).*

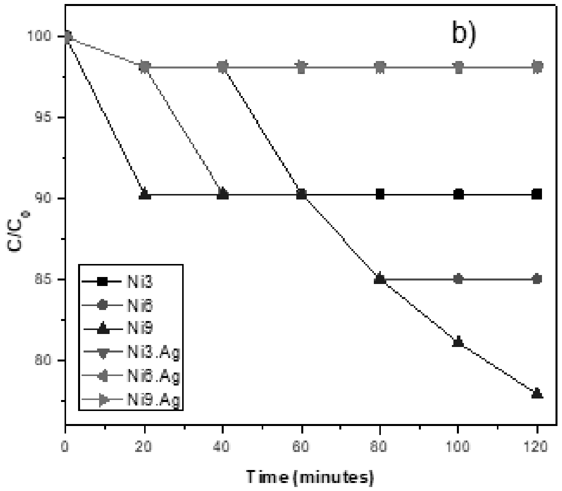

**Figure 7b:** *Decrease in MB concentration irradiation time in the presence of various photocatalyst with various Ni dopant level: 3% Ni dopant level (Ni3), 6% Ni dopant level (Ni6), 9% Ni dopant level (Ni9), Ag particles coated on 3% Ni doped on* $TiO_2$ *(Ni3.Ag), Ag particles coated on 6% Ni doped on* $TiO_2$ *(Ni6.Ag), Ag particles coated on 9% Ni doped on* $TiO_2$ *(Ni9.Ag).*

Besides, we noticed that the samples which were coated Ag particle have expressed the worse photocatalytic activity than that of the samples without Ag nano particles.

Figure 7b shows the data of the methylene blue degradation experiment under UV light in the presence of Ni-doped $TiO_2$ thin films with different Ni dopant level and Ag nano particles coated on Ni-doped $TiO_2$ thin films. It can be clearly seen that the degradation rate of MB decreased with the increase of Ni concentration in $TiO_2$ thin films. The 9% Ni doped $TiO_2$ thin film shows the highest degradation rate values under UV light. Similar to the samples which are doped Fe and coated Ag particles, the degradation rate values of the Ni doped $TiO_2$ thin films coating silver particles are low. It might prove that the concurrency of doping Ni/Fe and coating silver particles might not improve the photocatalytic activity of $TiO_2$ thin films (nanorods). Photocatalytic results of the Ag coated on Ni doped $TiO_2$ samples was not reasonable. It could be because of the inaccuracy of the equipment.

## 4. CONCLUSION

We have successfully fabricated Ni and Fe doped $TiO_2$ thin film with different doping percentages and fabricated Ag coated on Ni and Fe doped $TiO_2$ thin film with different doping percentages: 3%, 6%, 9% dopant level. Characterized some physical properties of Ni and Fe doped $TiO_2$ thin film with different doping percentages and Ag coated on Ni and Fe doped $TiO_2$ thin film with different doping percentages. Photocatalytic activity of Ni and Fe doped $TiO_2$ and Ag coated on Ni and Fe doped $TiO_2$ thin films had been studied by photocatalytic degradation of methylene blue (MB) in aqueous solution as a model pollutant under UV light irradiation. 9% Fe and Ni doped $TiO_2$ have higher photocatalytic activity than other samples. We observed that as the Fe and Ni dopant level increase the photocatalytic activity of the $TiO_2$ samples increases whereas the results of degradation of MB using the Ag particles coated on Fe and Ni doped $TiO_2$ samples indicate that coating Ag particles did not prove photocatalytic activity of $TiO_2$ thin films.

## REFERENCES

1. Dholam, R., et al., “Hydrogen Production by Photocatalytic Water-Splitting Using Cr- or Fe-Doped TiO2 Composite Thin Films Photocatalyst”, - *International Journal of Hydrogen Energy*, 2009. **34**: pp.5337-5346.
2. Khan, A., S. Woo, and O. Yang, “Hydrothermally stabilized Fe(III) doped titania active under visible light for water splitting reaction”, *International Journal of Hydrogen Energy*, 2008. 33: pp.5345-5351.
3. Niishiro, R., H. Kato, and A. Kudo, “Nickel and Either Tantalum or Niobium-Codoped TiO2 and SrTiO3 Photocatalysts with Visible-Light Response for H2 or O2 Evolution from Aqueous Solutions”, - *Physical chemistry chemical physics*: PCCP, 2005. 7: p.2241
4. Cong, Y., et al., Preparation, “Photocatalytic Activity, and Mechanism of Nano-TiO2 Co-Doped with Nitrogen and Iron (III)”, - *The Journal of Physical Chemistry C*, 2007. 111(28): pp.10618-10623.
5. Ambrus, Z., et al., “Synthesis, Structure and Photocatalytic Properties of Fe(III)-Doped TiO2 Prepared From TiCl3”, - *Applied Catalysis B: Environmental*, 2008. 81: pp.27-37.
6. Li, Z., et al., “Effect of Fe-doped TiO2 nanoparticle derived from modified hydrothermal process on the photocatalytic degradation performance on methylene blue”, - *Journal of hazardous materials*, 2008. 155: p.590-4.
7. Sun, T., et al., “High photocatalytic activity of hydrogen production from water over Fe doped and Ag deposited anatase TiO2 catalyst synthesized by solvothermal method”, - *Chemical Engineering Journal*, 2013. 228: pp.896-906.
8. Choi, W., A. Termin, and M.R. Hoffmann, “The Role of Metal Ion Dopants in Quantum-Sized TiO2: Correlation between Photoreactivity and Charge Carrier Recombination Dynamics”, - *The Journal of Physical Chemistry*, 1994. 98(51): pp.13669-13679.

9. Ma, J., et al., *Enhanced inactivation of bacteria with silver-modified mesoporous TiO2 under weak ultraviolet: irradiation*, - Microporous and Mesoporous Materials, 2011. 144: pp.97-104.

10. Mohanan Nair, J., et al., Growth, *Mechanism and Properties of TiO2 Nanorods Embedded Nanopillar: Evidence of Lattice Orientation Effect*, - Superlattices and Microstructures, 2017. 109.

11. Liu, B. and E. Aydil, "Growth of Oriented Single-Crystalline Rutile TiO2 Nanorods on Transparent Conducting Substrates for Dye-Sensitized Solar Cells", - *Journal of the American Chemical Society*, 2009. 131: pp.3985-90.

# CHẾ TẠO VÀ NGHIÊN CỨU TÍNH CHẤT CỦA VẬT LIỆU $TiO_2$ PHA TẠP SẮT VÀ NIKEN CÓ PHỦ NANO BẠC ỨNG DỤNG CHO QUANG XÚC TÁC

***Tóm tắt***: *Trong bài báo này, chúng tôi chế tạo màng mỏng titan ô xít ($TiO_2$) pha tạp niken (Ni) và sắt (Fe) với tỷ lệ pha tạp khác nhau sau đó phủ hạt nano bạc bằng phương pháp thủy nhiệt. Nghiên cứu một số tính chất vật lý của chúng. Hoạt tính quang xúc tác của $TiO_2$ pha tạp Ni và Fe có phủ Ag được nghiên cứu bằng cách phân hủy quang xúc tác dung dịch xanh methylen (MB) dưới dạng chất ô nhiễm khi chiếu tia cực tím. Kết quả cho thấy $TiO_2$ pha tạp 9% Fe và Ni có hoạt tính xúc tác quang cao hơn các mẫu khác. Chúng tôi còn nhận thấy rằng khi nồng độ Fe và Ni tăng lên thì tính chất quang xúc tác của mẫu tăng lên trong khi kết quả phân hủy MB của các mẫu có phủ nano Ag cho thấy tính quang xúc tác các mẫu này không tăng.*

***Từ khóa:*** *Hạt nano Ag, hoạt động quang xúc tác, màng $TiO_2$ tạp Ni và Fe.*

# STUDY ON THE PRODUCTION OF ODD-CP HIGGS PAIR A<sub>I</sub>A<sub>J</sub> FROM THE ANNIHILATION PROCESS OF E⁺E⁻ PAIR

**Nguyen Chinh Cuong**
*Faculty of Physics, Ha Noi National University of Education*

***Abstract:*** *In the Next Minimal Supersymmetric Standard Model (NMSSM), we obtain seven higgs, including three higgs – which are the even-CP* $h_{1,2,3}$ $(m_{h1} < m_{h2} < m_{h3})$, *two higgs – which are odd-CP* $a_{1,2}$ $(m_{a1} < m_{a2})$ *and a couple of charged higgs* $H^{\pm}$. *The decay of higgs into higgs is one of the remarkable new points of the NMSSM, which opens up hope for finding odd-CP higgs from annihilating collision of the* $e^+e^-$ *pair. In this paper, we study on the production of odd-CP higgs pair from annihilating collision of* $e^+e^-$ *pair, it's an opportunity to find new higgs in NMSSM. The numerical calculation results on the influence of CP violation are also given for discussion.*

***Keywords:*** *Higgs boson, CP violation, NMSSM.*

Email: cuongnc@hnue.edu.vn
Received 18 October 2019
Accepted for publication 20 November 2019

## 1. INTRODUCTION

The simplest version of supersymmetry is the Minimal Supersymmetric Standard Model (MSSM). This version is limited by two problems: the $\mu$ and the hierarchy [1,3,4,7]. The simple supersymmetry, which is beyond the MSSM, is the Next Minimal Supersymmetric Standard Model (NMSSM). The special characteristic of Higgs boson in the NMSSM is the decay of Higgs into Higgs. The even-CP Higgs and the heavy odd-CP Higgs can be generated at LEP in $e^+e^- \to ha$, but they may not be discovered because the dominant h decay were not searched for [2]. One simple way is to study the beyond singlet of the MSSM which contains one term $\lambda\hat{S}\hat{H}_u\hat{H}_d$ in the super-potential, this is the term that contributes $\lambda^2 v^2 \sin^2 2\beta$ at v = 174 GeV to the squared mass of even-CP Higgs [10] and therefore, it can make the mass of Higgs boson increased over the limit of independent decay state.

The neutral Higgs sector in the NMSM includes the following states: three even-CP and two odd-CP. Many analysis on Higgs sector in the NMSSM [5] have shown that, in the specific physical state of the even-CP Higgs, there is a strong mix between the doublet state and the singlet SU(2) with the reduction in the interaction of gauge boson. The study on light Higgs contributes to the discovery of one or more Higgs states at LEP, at LHC [5] and at large energy accelerators.

In the NMSSM, the terms of the super-potential W$_{\text{Higgs}}$ are dependent on superfield Higgs $\hat{H}_d, \hat{H}_u$ and $\hat{S}$:

$$\boldsymbol{W}_{\text{Higgs}} = \left(\mu + \lambda\hat{S}\right)\hat{H}_u.\hat{H}_d + \xi_F\hat{S} + \mu'\hat{S}^2 + \frac{\kappa}{3}\hat{S}^3 \tag{1}$$

with: $\lambda, \kappa$ is the non-dimension coupling Yukawa $\mu, \mu'$ is the supersymmetry mass, $\xi_F$ is the square supersymmetry mass parameter.

From (1), Yukawa interaction of quark and lepton superfield are added to

$$W_{\text{Yukawa}} = h_u\hat{H}_u.\hat{Q}\hat{U}_R^c + h_d\hat{H}_d.\hat{Q}\hat{D}_R^c + h_e\hat{H}_d.\hat{L}\hat{E}_R^c \tag{2}$$

The soft breaking supersymmetry sector is regulated in SLHA2:

$$\begin{aligned} -L_{\boldsymbol{soft}} = {} & m_{Hu}^2\left|H_u\right|^2 + m_{Hd}^2\left|H_d\right|^2 + m_s^2\left|S\right|^2 + m_Q^2\left|Q^2\right| + m_U^2\left|U_R^2\right| \\ & + m_D^2\left|D_R^2\right| + m_L^2\left|L^2\right| + m_E^2\left|E_R^2\right| \\ & + (h_uA_uQ.H_uU_R^c - h_dA_dQ.H_dD_R^c - h_eA_eL.H_dE_R^c \\ & + \lambda A_\lambda H_u.H_dS + \frac{1}{3}\kappa A_\kappa S^3 + m_3^2H_u.H_d + m_s^{2\prime}S^2 + \xi_sS + hc) \end{aligned} \tag{3}$$

As any supersymmetry theory with invariant super-potential sector (ternary), the Lagrangians, which contain the soft supersymmetry violation conditions specified by (3. The non-dimension terms in the super-potential (1) will break the symmetry $Z_3$. The model with super-potential (1) is the NMSSM. The invariant $Z_3$ Higgs sector is defined by the seven parameters $\lambda, \kappa, m_{H_d}^2, m_{H_u}^2, m_S^2, A_\lambda, A_\kappa$. The expression of Higgs mass matrix in the invariant $Z_3$ of the NMSSM shows that invariant $Z_3$ is obtained when:

$$m_3^2 = m_S^{2\prime} = \xi_S = \mu = \mu' = \xi_F = 0. \tag{4}$$

From the supersymmetry gauge interaction and soft supersymmetry breaking conditions, we obtain the Higgs potential:

$$\begin{aligned} V_{\text{Higgs}} = {} & \left|\lambda(H_u^+H_d^- - H_u^0H_d^0) + \kappa S^2 + 2\mu'S + \xi_F\right|^2 \\ & + (m_{H_u}^2 + \left|\mu + \lambda S\right|^2(\left|H_u^0\right|^2 + \left|H_u^+\right|^2) + (m_{H_d}^2 + \left|\mu + \lambda S\right|^2(\left|H_d^0\right|^2 + \left|H_d^-\right|^2) \\ & + \frac{g_1^2 + g_2^2}{8}(\left|H_u^0\right|^2 + \left|H_u^+\right|^2 - \left|H_d^0\right|^2 - \left|H_d^-\right|^2)^2 + \frac{g_2^2}{2}\left|H_u^+H_d^{0*} + H_u^0H_d^{0*}\right|^2 \\ & + m_S^2\left|S\right|^2 + (\lambda A_\lambda(H_u^+H_d^- - H_u^0H_d^0)S + \frac{1}{3}\kappa A_\kappa S^3 + m_3^2(H_u^+H_d^- - H_u^0H_d^0) \\ & + m_S'^2S^2 + \xi_SS + h.c \end{aligned} \tag{5}$$

where g$_1$ and g$_2$ present gauge interaction U(1) and SU(2).

The Higgs doublets $H_1$ and $H_2$ can be developed in the form:

$$H_1 = \begin{pmatrix} v_1 + S_1 + iA\sin\beta \\ H^{+*}.\sin\beta \end{pmatrix},$$

$$H_2 = \begin{pmatrix} H^{+}.\cos\beta \\ v_2 + S_2 + iA\cos\beta \end{pmatrix}, \tag{6}$$

$$S = (x + X + iY)$$

In case the CP violation is considered, the x parameter will be considered as the complex number.

In the year 2012, the Higgs boson was found out with the mass approximates to 125GeV, which could be considered as the $h_2$ in the NMSSM. The search for the remaining higgs such as $h_1$, $h_3$ or $a_1$ and $a_2$ is of great interest to experimental research groups and will bring us the hope of finding out these particles as well as verifying the correctness of the model [6]. In this paper, we have studied the production of odd-CP higgs pair from annihilating collision of $e^+e^-$ pair. The numerical calculation results are also presented in charts to evaluate the influence of CP violation on the cross section.

## 2. THE FEYNMAN DIAGRAMS AND CROSS SECTIONS

From the diagram of Figure 1 according to Feynman's rule, we have the scattering amplitude of this process as:

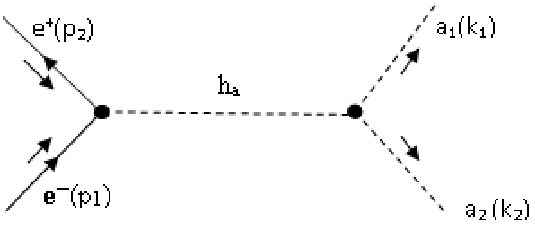

**Figure 1:** *Feyman diagram of* $e^+e^- \to a_i a_j$ *scattering process by channel s.*

$$M_1 = \bar{v}(p_2) H u(p_1) \frac{i}{(k_1 + k_2)^2 - m_h^2 + i\varepsilon} \bar{u}(k_1) M_0 (k_1 + k_2)^{\upsilon} v(k_2) \tag{7}$$

Where:

$$H = \frac{-g.m_e}{2.m_W};$$

$$\begin{aligned}
M_0 ={}& -i\frac{g^2+g^{,2}}{2\sqrt{2}}\left(v_1U^S_{a1}U^P_{\beta 1}U^P_{\gamma 1}+v_2U^S_{a2}U^P_{\beta 2}U^P_{\gamma 2}\right)\\
&+\left(i\frac{g^2+g^{,2}}{2\sqrt{2}}-\sqrt{2}\lambda^2\right)\left(v_1U^S_{a1}U^P_{\beta 2}U^P_{\gamma 2}+v_2U^S_{a2}U^P_{\beta 1}U^P_{\gamma 1}\right)\\
&-\sqrt{2}i\left(\lambda k v_1+\lambda^2 v_2\right)U^S_{a2}U^P_{\beta 3}U^P_{\gamma 3}-\sqrt{2}i\left(\lambda k v_2+\lambda^2 v_1\right)U^S_{a1}U^P_{\beta 3}U^P_{\gamma 3}\\
&-\sqrt{2}i\lambda^2 x U^S_{a3}\left(U^P_{\beta 1}U^P_{\gamma 1}+U^P_{\beta 2}U^P_{\gamma 2}\right)-i\left(2\sqrt{2}k^2x+\sqrt{2}kA_k\right)U^S_{a3}U^P_{\beta 3}U^P_{\gamma 3}\\
&+\sqrt{2}i\lambda k U^S_{a3}\left[v_1\left(U^P_{\beta 2}U^P_{\gamma 3}+U^P_{\beta 3}U^P_{\gamma 2}\right)+v_2\left(U^P_{\beta 1}U^P_{\gamma 3}+U^P_{\beta 3}U^P_{\gamma 1}\right)\right]\\
&+i\left(\sqrt{2}\lambda k x-\frac{\lambda A_\lambda}{\sqrt{2}}\right)\left[U^S_{a1}\left(U^P_{\beta 2}U^P_{\gamma 3}+U^P_{\beta 3}U^P_{\gamma 2}\right)+U^S_{a2}\left(U^P_{\beta 1}U^P_{\gamma 3}+U^P_{\beta 3}U^P_{\gamma 1}\right)\right]\\
&-i\left(\sqrt{2}\lambda k x+\frac{\lambda A_\lambda}{\sqrt{2}}\right)U^S_{a3}\left(U^P_{\beta 1}U^P_{\gamma 2}+U^P_{\beta 2}U^P_{\gamma 1}\right)
\end{aligned}$$

$U^s$ and $U^P$ are unita matrices used to diagonalize the mass matrix of higgs.

From the diagram of Figure 2 according to Feynman's rule, we have the scattering amplitude of this process as:

$$M_2=\bar{u}\left(k_1\right)H\bar{u}\left(p_1\right)\frac{i}{\left(p_1-k_1\right)^2-m_e+i\varepsilon}\bar{v}\left(p_2\right)Hv\left(k_2\right) \tag{8}$$

From the diagram of Figure 3 according to Feynman's rule, we have the scattering amplitude of this process as:

$$M_3=\bar{v}\left(k_2\right)Hu\left(p_1\right)\frac{i}{\left(p_1-k_2\right)-m_e+i\varepsilon}\bar{u}\left(p_2\right)Hv\left(k_1\right) \tag{9}$$

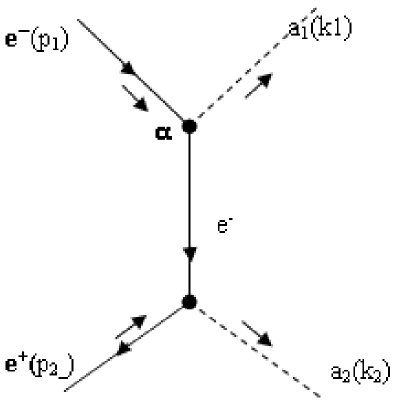

**Figure 2:** *Feyman diagram of* $e^+e^- \to a_ia_j$ *scattering process by t-channel.*

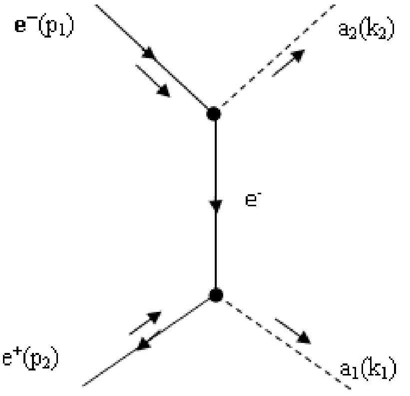

**Figure 3:** *Feyman diagram of* $e^+e^- \to a_ia_j$ *scattering process by u-channel.*

From there, we obtain the expression of the cross section, as follows:

$$\sigma = \frac{1}{8\pi}\frac{|H|^2|M_0|^2}{\left(s-m_h^2\right)^2}\left\{2(s-m_{a_i}^2-m_{a_j}^2)-m_{a_j}m_{a_i}\right\} \tag{10}$$

Where s is the square of the center of mass energy of scattering.

## 3. NUMERICAL RESULTS

To study the influence of the center of mass energy $\sqrt{s}$ and the CP violation phase $\phi$ on the cross section, we have used two set of parameters [5,6,8,9] for programming numerical calculation on the Maple version 17.0.

The selected parameter set to evaluate the change of $\sigma$ according to the center of mass energy $\sqrt{s}$ is: $\lambda = 0{,}8$; $x = 178$; $k = 0{,}1$; $\tan\beta = 3$; $\sin\alpha = -0{,}58$; $A_k = 6$; $A_\lambda = 486$; $m_{h1} = 95$GeV; $m_{h2} = 125$GeV; $m_{h3} = 498$GeV; $m_{a1} = 79$GeV and $m_{a1} = 503$GeV. From the results obtained, we have found that the influence of $\sqrt{s}$ on the cross sections of process $e^+e^- \to a_ia_j$ is relatively significant (Fig. 4-6).

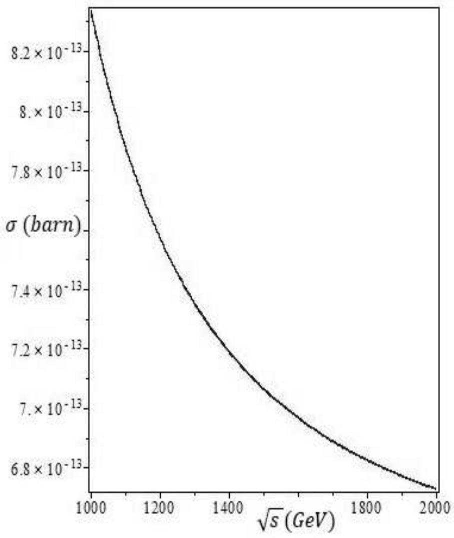

**Figure 4:** *The influence of* $\sqrt{s}$ *on the cross section of process* $e^+ + e^- \to a_1 + a_1$.

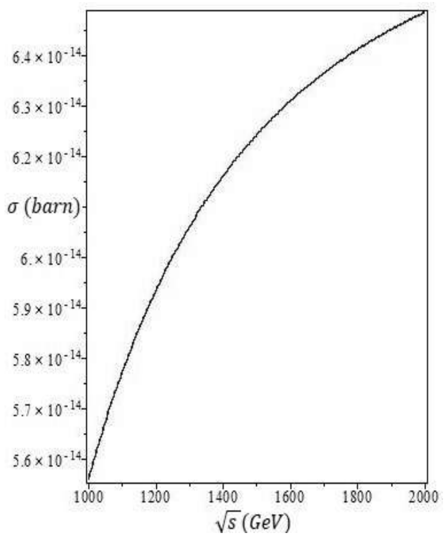

**Figure 5:** *The influence of* $\sqrt{s}$ *on the cross section of process* $e^+ + e^- \to a_1 + a_2$.

Figure 4 shows the dependence of the cross section on center of mass energy $\sqrt{s}$ in scattering $e^+ + e^- \to a_1 + a_1$. Here we consider $\sqrt{s}$ to take values in the range of

1000-2000GeV and see a cross section about $10^{-13}$ barn. The results also showed that when $\sqrt{s}$ increases, the cross section decreases and when $\sqrt{s}$ doubled, the cross section decreases by about 20%.

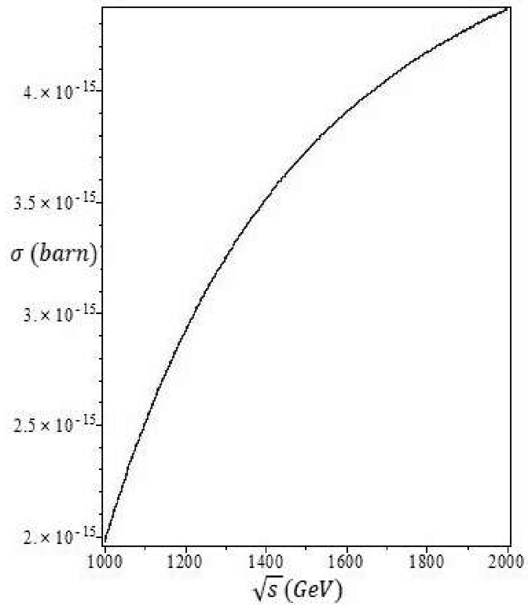

**Figure 6:** *The influence of* $\sqrt{s}$ *on the cross section of process* $e^+ + e^- \to a_2 + a_2$.

Figure 5 represents the dependence of the cross section on center of mass energy $\sqrt{s}$ in scattering $e^+ + e^- \to a_1 + a_2$. when considering center of mass energy in the range of 1000-2000GeV and we see a cross section about $10^{-14}$ barn. when center of mass energy $\sqrt{s}$ increases, the cross section increases and when $\sqrt{s}$ doubled, the cross section increases by about 18%.

Figure 6 shows the dependence of the cross section on center of mass energy $\sqrt{s}$ in scattering $e^+ + e^- \to a_2 + a_2$. when considering center of mass energy in the range of 1000-2000GeV, we see a cross section about $10^{-15}$ barn. when center of mass energy $\sqrt{s}$ increases, the result shows that the cross section increases strongly. When $\sqrt{s}$ doubled, the cross section increase over doubled.

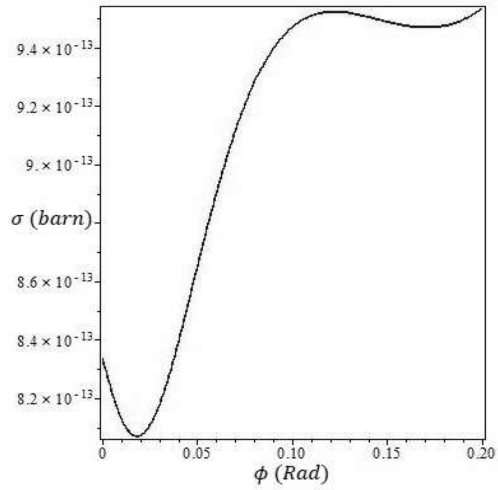

**Figure 7:** *The influence of CP violaton on process* $e^+e^- \to a_1a_1$ *with* $\sqrt{s}$ = *1000GeV.*

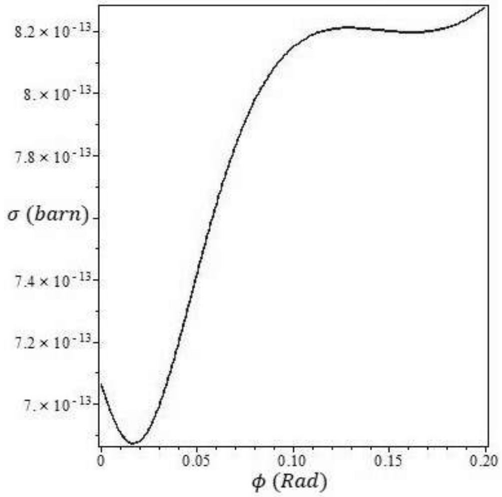

**Figure 8:** *The influence of CP violaton on process* $e^+e^- \to a_1a_1$ *with* $\sqrt{s}$ = *1500GeV.*

From the above research results, we obtain the cross section σ in the range $10^{-15}$ to $10^{-13}$ barn. On the other hand, the change of the cross section according to $\sqrt{s}$ is not too large. Therefore, when studying the influence of CP violation on the cross section of this process, we will choose the two values $\sqrt{s}$ = 1000GeV and $\sqrt{s}$ = 1500GeV to evaluate (then, x will take the complex value $x = 178e^{i\phi}$ and $\phi$ is called CP violation phase). We have obtained the results as in Fig. 7-12.

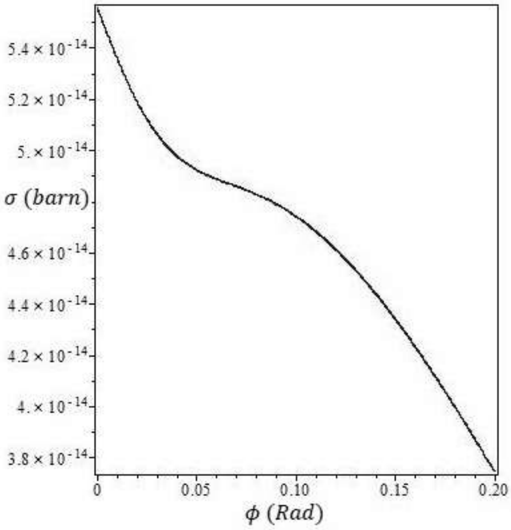

**Figure 9:** *The influence of CP violaton on process* $e^+e^- \to a_1a_2$ *with* $\sqrt{s}$ = *1000GeV.*

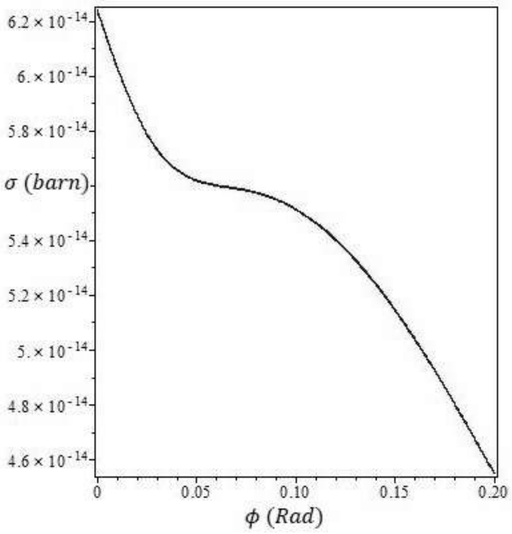

**Figure 10:** *The influence of CP violaton on process* $e^+e^- \to a_1a_2$ *with* $\sqrt{s}$ = *1500GeV.*

From Figures 7 and 8, we see that when ϕ changes from 0 to 0.2 Rad, the first cross section of $e^+ + e^- \to a_1 + a_1$ decreases a little and then suddenly increases strongly when ϕ increases from 0.02 to 0.1 Rad. In the variable range of ϕ from 0.1 to 0.2 Rad, the cross section changes insignificantly. We can see that the cross section changes (increases) about 18% in the variable range of ϕ.

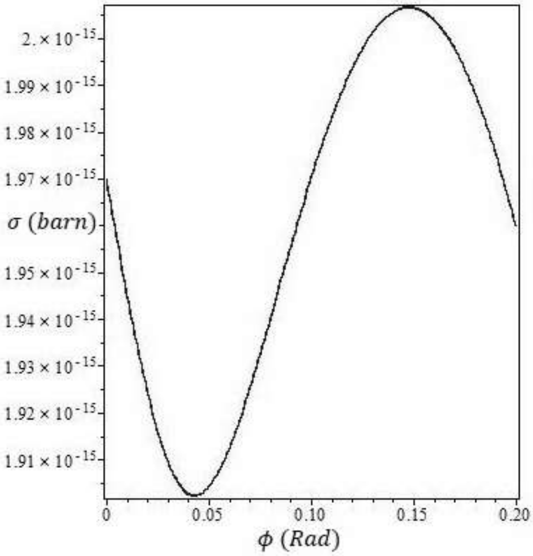

**Figure 11:** *The influence of CP violaton on process $e^+e^- \to a_2a_2$ with $\sqrt{s}$ = 1000GeV.*

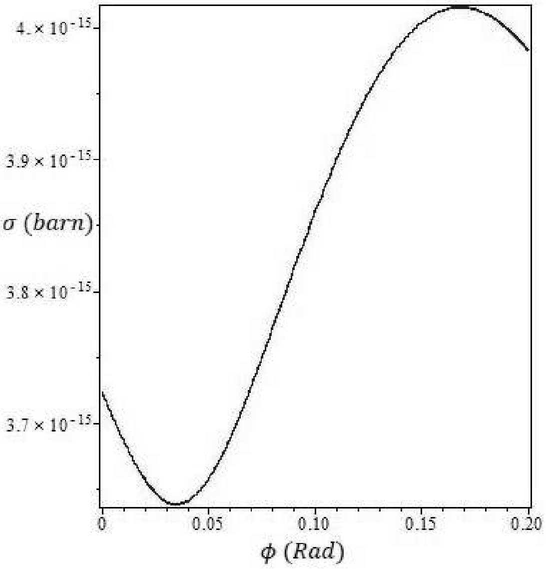

**Figure 12:** *The influence of CP violaton on process $e^+e^- \to a_2a_2$ with $\sqrt{s}$ = 1500GeV.*

Figures 9 and 10 describe the influence of CP violation on the cross section of the process $e^+ + e^- \to a_1 + a_1$. The results show that, when ϕ increases from 0 to 0.2 Rad, the cross section decreases very strongly. In the variable range of ϕ, the cross section can be change (decreases) to 40%, proving the influence of CP violation is very strong and we need to attention when studying this scattering channel.

Figures 11 and 12 describe the influence of CP violation on the cross section of the process $e^+ + e^- \to a_2 + a_2$. The results show that, when ϕ increases to from 0 Rad, the first cross section decreases, until ϕ over the value of 0.04Rad then the cross section begins to increase, when ϕ over the value of 0.16 Rad then the cross section again decreases. In the variable range of ϕ, the cross section can change from 5% to 7%, this case can be seen that the influence of CP violation is smaller than the above cases.

## 4. CONCLUSION

In the NMSSM, a single superfield is added with complex scalar field components, this leads to the appearance of seven Higgs in the NMSSM (including three even-CP Higgs $h_{1,2,3}$ ($m_{h1} < m_{h2} < m_{h3}$), two odd-CP Higgs $a_{1,2}$ ($m_{a1} < m_{a2}$) and a pair of charged Higgs $H^{\pm}$).

The numerical calculation results show that the cross section of the above processes are in the range $10^{-13}$ - $10^{-15}$ barn. In which the cross section $e^+e^- \to a_1a_1$ is the largest.

- The influence of CP violation on the cross section of the process $e^+e^- \to a_ia_j$ are also studied in detail through the changes of the CP violation phase parameter $\phi$. The evaluation was studied when choosing two values of $\sqrt{s}$ equal 1000 and 1500GeV, the results showed that the influence of CP violation on the cross section is relatively large. When $\phi$ increases from 0 to 0.2 Rad, the cross section changes as follows:

+ With scattering $e^+e^- \to a_1a_1$: cross section increases about 18%.

+ With scattering $e^+e^- \to a_1a_2$: cross section decreases to 40%.

+ With scattering $e^+e^- \to a_2a_2$: cross section can change to 5% to 7%.

This study helps to elucidate the influence of CP violation on scattering $e^+e^- \to a_ia_j$. That will not only help us become more aware of interactive unification models, but also hope to contribute to the discovery of higgs in experiment.

## REFERENCES

1. Radovan Demi’senk and John F. Gunion, hep-ph/0811.3537.
2. M.M. Almarashi anh S.moretti, hep-ph/1109.1735.
3. M.M. Almarashi anh S.moretti, hep-ph/1105.4191.
4. H. E. Haber and G.L. Kane. Phys. Rep. 117 (1985) 75.
5. Ulrich Ellwanger, hep-ph/1108.0157.
6. U. Ellwanger, C. Hugonie and A. M. Teixeira, Phys. Rept. 496 (2010) 1.
7. W. Bernrenther and M. Suzuki, Rev. Mod. Phys. 63 (1991) 3-13.
8. N. C. Cuong, P. X. Hung, L. H. Thang, Scientific Journal of HMU, 2 (2016), 22-30.
9. Radovan Dermisek (2010), hep-ph/1012.3487vl.
10. Barlt, et. al., Phys. Lett. B419 (1998) 243.

# NGHIÊN CỨU SỰ SINH CẶP HIGGS CP LẺ $a_I a_J$ TỪ QUÁ TRÌNH HỦY CẶP $e^+e^-$

***Tóm tắt:*** *Trong mô hình chuẩn siêu đối xứng gần tối thiểu (NMSSM), chúng ta thu được 7 higgs, với ba higgs vô hướng - CP chẵn* $h_{1,2,3}$ *(*$mh_1 < mh_2 < mh_3$*) cùng hai higgs giả vô hướng - CP lẻ* $a_{1,2}$ *(*$ma_1 < ma_2$*) và một cặp higgs mang điện* $H^{\pm}$*. Phân rã Higgs thành Higgs là một điểm mới đáng chú ý của NMSSM, điều đó mở ra hy vọng tìm kiếm các higgs odd-CP từ va chạm hủy cặp* $e^+e^-$*. Trong bài báo này chúng tôi nghiên cứu sự sinh cặp higgs CP lẻ* $a_i a_j$ *từ va chạm hủy cặp* $e^+e^-$*, đó là cơ hội để tìm kiếm các hạt higgs mới trong NMSSM. Các kết quả tính số về ảnh hưởng của vi phạm CP cũng được đưa ra để thảo luận.*

***Từ khóa:*** *Higgs boson, vi phạm CP, NMSSM.*

# PHOTON PAIR PRODUCTION IN $e^{-}e^{+}$ COLLISION AT ILC

**Bui Thi Ha Giang**[1], **Dang Van Soa**[2]
[1]*Hanoi National University of Education*
[2]*Hanoi Metropolitan University*

***Abstract:*** *Our work has based on the Randall-Sundrum model (RS). The total cross-section in photon pair production at* $e^{-}e^{+}$ *collision achieves the maximum value when the polarization of electron, positron beams are* $P_{e^{-}}=1, P_{e^{+}}=-1$ *or* $P_{e^{-}}=-1, P_{e^{+}}=1$ *at International Linear Colliders (ILC). The number of production events obtained for different collision energies is calculated for an integrated luminosity of* $100\ fbar^{-1}$ *yearly.*

***Keywords:*** *photon pair production, Randall-Sundrum model, ILC.*

Email: giangbth@hnue.edu.vn

Received 13 October 2019
Accepted for publication 20 November 2019

## 1. INTRODUCTION

The RS model, which was suggested in 1999, has presented the attractive phenomenology, including Dark Matter candidates [1-3]. The RS setup involves two 3-branes: UV 3-brane and IR 3-brane. Gravity is localized UV brane, while the Standard Model (SM) fields are supposed to be localized IR brane. The separation between the two 3-branes leads directly to the existence of an additional scalar called the radion ($\phi$), corresponding to the quantum fluctuations of the distance between the two 3-branes [1]. The observed boson discovered by the ATLAS and CMS collaborations in 2012 [4,5] is 125 GeV. However, it may not be the Standard model (SM) Higgs [6-9]. Therefore, in this work, the influence of the 125 GeV Higgs, radion on the photon pair production at the high energy has been studied.

In addition, at the high energy (TeV scale), the scale invariant sector has been considered as an effective theory and that if it exists, it is made of unparticle suggested by Geogri [10, 11]. Based on the Geogri's idea, unparticle physics has been mentioned with the extra dimension as the RS model [12, 13]. The effects of unparticle on properties of high energy colliders have been intensively studied in Refs. [12-22]. Recently, the possibility of the unparticle has been studied with CMS detector at the LHC [23, 24]. In the rest of work, we restrict ourselves by considering only scalar unparticle.

In this paper, we study the photon pair production, which has been proposed as an option of $e^-e^+$ collisions. The layout of this paper is as follows. Feynman rules for the particles couplings with the Higgs/radion and scalar unparticle in the RS model are reviewed in Section 2 mostly cited on [25, 26]. Section 3 is devoted to the creation of photon pair in $e^-e^+$ collision. Finally, we summarize our results and make conclusions in Section 4.

## 2. FEYNMAN RULES FOR THE PARTICLES COUPLINGS WITH THE HIGGS/RADION AND SCALAR UNPARTICLE IN THE RS MODEL

Feynman rules for the particles couplings with the Higgs/radion and scalar unparticle are showed as follows [25, 26]

$$\bar{g}_{ee\phi} = -\frac{gm_e}{2m_W}(c+\gamma a), \tag{1}$$

$$\bar{g}_{eeh} = -\frac{gm_e}{2m_W}(d+\gamma b), \tag{2}$$

$$\begin{aligned} g_{\gamma\gamma\phi} &= iC_{\gamma\phi}\left[(k_1k_2)\eta^{\mu\nu} - k_1^\nu k_2^\mu\right] \\ &= -i\frac{\alpha}{2\pi\upsilon_0}\left((\mathrm{c}+\gamma a)\sum_i e_i^2 N_C^i F_i(\tau_i) - (b_2+b_Y)\gamma a\right)\left[(k_1k_2)\eta^{\mu\nu} - k_1^\nu k_2^\mu\right], \end{aligned} \tag{3}$$

$$\begin{aligned} g_{\gamma\gamma h} &= iC_{\gamma h}\left[(k_1k_2)\eta^{\mu\nu} - k_1^\nu k_2^\mu\right] \\ &= -i\frac{\alpha}{2\pi\upsilon_0}\left((d+\gamma b)\sum_i e_i^2 N_C^i F_i(\tau_i) - (b_2+b_Y)\gamma b\right)\left[(k_1k_2)\eta^{\mu\nu} - k_1^\nu k_2^\mu\right], \end{aligned} \tag{4}$$

$$g_{eeU} = i\bar{g}_{eeU} = i\frac{\lambda_{ee}}{\Lambda_U^{d_U-1}}, \tag{5}$$

$$g_{\gamma\gamma U} = -i\bar{g}_{\gamma\gamma U}\left[(p_1p_2)\eta^{\mu\nu} - p_1^\nu p_2^\mu\right] = -4i\frac{\lambda_{\gamma\gamma}}{\Lambda_U^{d_U}}\left[(p_1p_2)\eta^{\mu\nu} - p_1^\nu p_2^\mu\right]. \tag{6}$$

## 3. THE PHOTON PAIR PRODUCTION

In this section, we consider the $e^-e^+ \to \gamma\gamma$ collision process

$$\mathrm{e}^-(p_1) + e^+(p_2) \to \gamma(k_1) + \gamma(k_2), \tag{7}$$

Here $p_i, k_i$ (i = 1,2) stand for the momentums. There are three Feynman diagrams contributing to reaction (7), representing the s, u, t-channels exchange depicted in Fig.1.

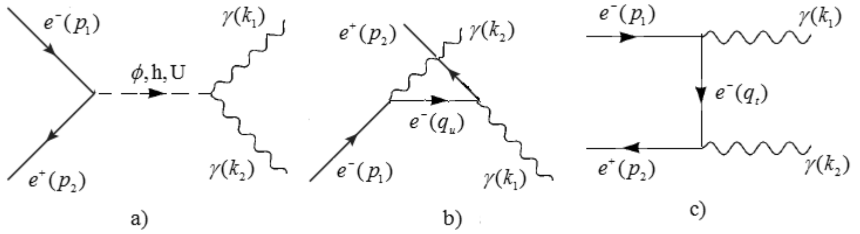

**Figure 1:** *Feynman diagrams for* $e^-e^+ \to \gamma\gamma$ *collision*

We obtain the scattering amplitude in the s, u, t-channels, respectively

$$M_s = \left( -\frac{C_{\gamma\phi}\bar{g}_{ee\phi}}{q_s^2 - m_\phi^2} - \frac{C_{\gamma h}\bar{g}_{eeh}}{q_s^2 - m_h^2} + i\frac{A_{d_U}}{2\sin(d_U\pi)}(-q_s^2)^{d_U-2}\bar{g}_{\gamma\gamma U}\bar{g}_{eeU} \right)\varepsilon_\mu^*(k_1)\left[(k_1k_2)\eta^{\mu\nu} - k_1^\nu k_2^\mu\right]\varepsilon_\nu^*(k_2)u(p_1)\bar{v}(p_2), \tag{8}$$

$$M_u = -i\frac{e^2}{q_u^2 - m_e^2}\varepsilon_\mu^*(k_1)\gamma^\mu\bar{v}(p_2)(\hat{q}_u + m_e)\varepsilon_\nu^*(k_2)\gamma^\nu u(p_1), \tag{9}$$

$$M_t = -i\frac{e^2}{q_t^2 - m_e^2}\varepsilon_\mu^*(k_1)\gamma^\mu u(p_1)(\hat{q}_t + m_e)\varepsilon_\nu^*(k_1)\gamma^\nu\bar{v}(p_2), \tag{10}$$

where

$$q_s = p_1 + p_2 = k_1 + k_2,\ q_u = p_1 - k_2 = k_1 - p_2,\ q_t = p_1 - k_1 = k_2 - p_2.$$

The expressions of the differential cross-section [27]

$$\frac{d\sigma}{d(\cos\psi)} = \frac{1}{32\pi s}\frac{|\vec{k}|}{|\vec{p}|}|M_{fi}|^2, \tag{11}$$

where $|M_{fi}|^2 = |M_s|^2 + |M_u|^2 + |M_t|^2 + 2\,\mathrm{Re}(M_s^+M_u + M_s^+M_t + M_u^+M_t)$, $\psi = (\vec{p}, \vec{k})$.

The parameters are chosen as

$$m_h = 125\ \text{GeV(CMS)}, \Lambda_\phi = 5\,\text{TeV [26]},\ m_\phi = 10\,\text{GeV [28]}, \xi = 1/6\ \text{[29]},$$
$$\Lambda_U = 1000\,\text{GeV},\ \lambda_{ee} = \lambda_{\gamma\gamma} = 1\,\text{[19]}.$$

We give some estimates for the cross-sections as follows:

As shown in [30], the cross-section is flat when $d_U > 1.6$, therefore we choose the $d_U$ as $1 < d_U < 1.5$. In case of $P_{e^-} = 1, P_{e^+} = -1, \sqrt{s} = 500$ GeV, the total cross-section decreases rapidly as $d_U$ increases.

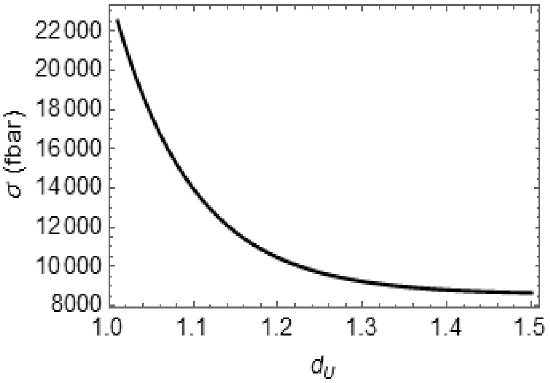

**Figure 2:** *The total cross-section in the* $e^-e^+ \to \gamma\gamma$ *collision as a function of* $\boldsymbol{d_U}$. *The parameters are taken to be* $\sqrt{s}$ *= 500 GeV,* $\boldsymbol{P_{e^-} = 1, P_{e^+} = -1}$.

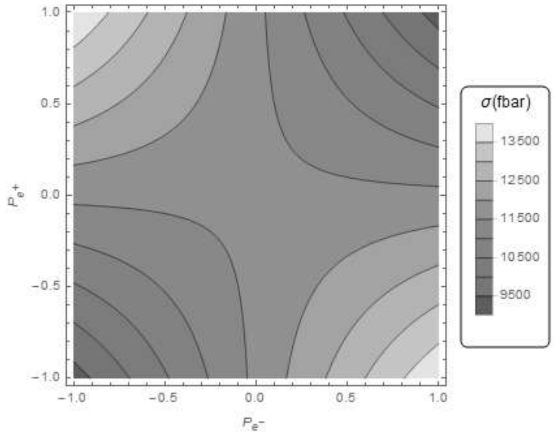

**Figure 3:** *The total cross-section in the* $e^-e^+ \to \gamma\gamma$ *collision as a function of the polarization coefficients of the* $\boldsymbol{e^-, e^+}$ *beams at ILC. The parameters are taken to be* $\sqrt{s}$ *= 500 GeV,* $\boldsymbol{d_U = 1.1}$.

**Table 1:** *The total cross-sections with some different values of the collision energy in case of* $\boldsymbol{P_{e^-} = -0.8, P_{e^+} = 0.2}$ *and* $\boldsymbol{P_{e^-} = 0.8, P_{e^+} = -0.2}$ *at the ILC.*

| $\sqrt{s}$ (GeV) | 500 | 600 | 700 | 800 | 900 | 1000 |
|---|---|---|---|---|---|---|
| σ ($10^3$ fbar) | 11.987 | 9.514 | 8.094 | 7.230 | 6.685 | 6.335 |

In Fig.3, the total cross-section is plotted as the function of $P_{e^-}, P_{e^+}$, which are the polarization coefficients of $e^-, e^+$ beams, respectively. The figure indicates that the total cross-section achieves the maximum value when $P_{e^-} = 1, P_{e^+} = -1$ or $P_{e^-} = -1, P_{e^+} = 1$ and the minimum value when $P_{e^-} = P_{e^+} = \pm 1$. We analyse the total cross-sections for two different beam polarizations $P_{e^-} = -0.8, P_{e^+} = 0.2$ and $P_{e^-} = 0.8, P_{e^+} = -0.2$ at the ILC in Table 1. In both cases of beam polarizations, the total cross-sections are same (about $10^3$ fbar).

The total cross-section is plotted as a function of the collision energy in case of $P_{e^-} = 1, P_{e^+} = -1$. The total cross-section decreases when the collision energy increases. This is because Higgs, radion and scalar unparticle propagators in the s-channel give the main contribution.

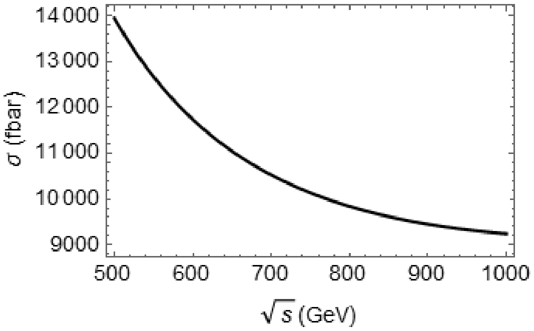

**Figure 4:** *The total cross-section in the* $e^-e^+ \to \gamma\gamma$ *collision as the function of* $\sqrt{s}$ *in case of* $P_{e^-} = 1, P_{e^+} = -1, d_U = 1.1$.

i) Some numerical values for the cross-sections are given detaily in Table 2, which shows that with the contribution of Higgs, radion, scalar unparticle propagators. With the integrated luminosity of the order of L = 100 fbar$^{-1}$ yearly [31], the radion and scalar unparticle signals can be observed at ILC in the future.

**Table 2:** *The number of events in a year with some different values of the collision energy. The parameters are chosen as* $P_{e^-} = -0.8, P_{e^+} = 0.2$ *and* $P_{e^-} = 0.8, P_{e^+} = -0.2$ , $d_U = 1.1$, *the luminosity L = 100 fb*$^{-1}$ *yearly (ILC).*

| $\sqrt{s}$ (GeV) | 500 | 600 | 700 | 800 | 900 | 1000 |
|---|---|---|---|---|---|---|
| N ($10^5$) | 11.987 | 9.514 | 8.094 | 7.230 | 6.685 | 6.335 |

## 4. CONCLUSION

In this paper, we have evaluated the contribution of Higgs, radion, scalar unparticle propagators in the photon pair production at the $e^-e^+$ collision. Due to the main contribution in the s-channel, the cross-section decreases as the collision energy increases. The total cross-section achieves the maximum value when 100% electron beam is left polarized and 100% positron beam is right polarized and vice versa. With $|P_{e^-}| = 80\%, |P_{e^+}| = 20\%$ at ILC, the total cross-section is about $10^3$ fbar and there are about $10^5$ events in a year. The existence of scalar unparticle may be discovered with the low values of the scaling dimension.

# REFERENCES

1. L. Randall and R. Sundrum, 1999, Phys. Rev. Lett. 83 3370.
2. F. Abu-Ajamieh , 2018, Int. J. Mod. Phys. A33, No.24, 1850144.
3. T. D. Rueter, T. G. Rizzo and J. L. Hewett, 2017, JHEP 10, 094.
4. G. Aad et al., 2012, ATLAS Collaboration, Phys. Lett. B716, 1.
5. S. Chatrchyan et al., 2012, CMS Collaboration, Phys. Lett. B716, 30.
6. B. Grzadkowski, J. F. Gunion, and M. Toharia, 2012, Phys. Lett. B712, 70.
7. D. Elander and M. Piai, 2013, Nucl. Phys. B867, 779.
8. K. Cheung and T-C. Yuan , 2012, Phys. Rev. Lett. 108, 141602.
9. Z. Chacko, R. Franceschini, and R. K. Mishra, 2013, JHEP 1304, 015.
10. H. Georgi, 2007, Phys. Rev. Lett. 98, 221601.
11. H. Georgi, 2007, Phys. Lett. B650, 275.

A. Friedland, M. Giannotti, M. Graesser, 2009, Phys. Lett. B678, 149.

12. E. O. Iltan, 2008, Eur. Phys. J. C 56, 105.
13. P. Mathews and V. Ravindran, 2007, Phys. Lett. B657, 198.
14. A.T. Alan and N.K. Pak, 2008, EPL Vol.84, No.1, 11001.
15. S. Majhi, 2008, Phys. Lett. B665, 44.
16. M. C. Kumar, P. Mathews, V.Ravindran and A.Tripathi, 2008, Phys. Rev. D77, 055013.
17. Sahin and B. Sahin, 2008, Eur. Phys. J. C55, 325.
18. T. Kikuchi and N. Okada, 2008, Phys. Rev. D77, 094012.
19. C. H. Chen, G. Cvetic, C. S. Kim, 2011, Phys. Lett. B694, 393.
20. S. Khatibi, M. M. Najafabadi, 2013, Phys. Rev. D87, No.3, 037701.
21. T. M. Aliev, S. Bilmis, M. Solmaz and I. Turan, 2017, Phys. Rev. D95, No.9, 095005.
22. CMS Collaboration, 2015, Eur. Phys. J. C75, 235.
23. CMS Collaboration, 2016, Phys. Rev. D93, 052011.
24. K. Cheung, W. Y. Keung and T. C. Yuan, 2007, Phys. Rev. Lett. 99, 051803.
25. D. Dominici, B. Grzadkowski, J. F. Gunion and M. Toharia, 2003, Nucl.Phys. B671, 243.
26. M. E. Peskin and D. V. Schroeder, 1995, An Introduction to Quantum Field Theory, Addision-Wesley Publishing.
27. C. Csaki, M. L. Graesser, G. D. Kribs, 2001, Phys.Rev. D63, 065002.
28. G. F. Giudice, R. Rattazzi and J. D. Wells, 2001, Nucl. Phys. B595, 250.
29. D. V. Soa, B. T. H. Giang, 2018, Nucl. Phys. B936, 1.
30. N. Sonmaez, 2014, Phys. Rev. D91, 085021.

# SỰ SINH CẶP PHOTON TỪ TÁN XẠ $e^{-}e^{+}$ Ở ILC

***Tóm tắt:*** *Bài báo được nghiên cứu dựa trên mô hình Randall-Sundrum. Tiết diện tán xạ toàn phần trong sự tạo cặp photon từ tán xạ* $e^{-}e^{+}$ *nhận giá trị lớn nhất khi hệ số phân cực của chùm electron và chùm positron là* $P_{e^{-}} = 1, P_{e^{+}} = -1$ *hoặc* $P_{e^{-}} = -1, P_{e^{+}} = 1$ *ở máy gia tốc ILC. Chúng tôi cũng tính số sự kiện xảy ra đối với một số giá trị năng lượng tán xạ khi độ trưng của máy bằng 100 fbar*$^{-1}$*/ năm.*

***Từ khóa:*** *Sinh cặp photon, mô hình Randall-Sundrum, ILC*

# THE PHENOMENA OF CHARGE INVERSION AND EFFECTIVE ATTRACTION BETWEEN THE SPHERICAL MACROMOLECULES IN ELECTROLYTE SOLVENT

**Nguyen Vu Nhan**[1], **Nguyen Viet Duc**[2], **Toan T. Nguyen**[2]
*[1]Hanoi Metropolitan University*
*[2]Key Laboratory for Multiscale Simulation of Complex Systems,*
*VNU University of Science, Vietnam National University*

***Abstract:*** *The phenomena of charge inversion and effective attraction between the like - charged spherical macromolecules in electrolyte solvent has been studied by using Poisson - Boltzmann mean-field theory, alongside the assumption that counterions condense on the surface of macromolecules to form a strongly correlation liquid. This oversimplified model is able to capture many important features of these phenomena, provide essential understanding of electrostatics in strong interaction regime in biological and soft matter systems.*

***Keywords:*** *Charge inversion, like-charged attraction, polyelectrolyte solution, Poisson - Boltzmann equation, biological macromolecule.*

Email: nvnhan@hnmu.edu.vn
Received 16 October 2019
Accepted for publication 15 November 2019

## 1. INTRODUCTION

In recent years, the there are many researches on physical properties of biological and soft maters macro-molecules, such as colloidal particles, vesicles, micelles, proteins, DNA… Insightly knowledge about structure and also interaction of biological molecules is essential to understand biological processes [1]. Most of these systems function in aqueous solution in the presence of many electrolytes such as NaCl, $MgCl_2$… Standard theoretical and computational approaches to understand the electrostatics of these system has been mostly based on the Poisson-Boltzmann self-consistence mean field theory [2]. Since this is a mean field theory, its validity is limited to electrolyte solution with weak electrostatic interaction. When the counterion concentration in the solution is too large, or the solution contain highly valent ions, there are effects that the mean field theory cannot explain, such as the effect of the inversion of charges, the like - charge attraction between macromolecules... [3]. Strongly correlated liquid theory and similar theories have been employed to investigate electrostatics in these systems [3,4]. In many cases, one can understand the essential physics by separating the mobile ions into two populations, a condensed counterion population on the surface of macroions which can be treated in the strong interaction limit, and a diffuse counterion population further away into the aqueous solution which can be treated using conventional weak interaction electrostatic theories [3]. In this paper, we gave a brief overview of these approaches and applying it to calculate the attraction among spherical macroions in electrolyte solution. Our results can contribute to understand electrostatics in microemulsion systems, protein solutions, or other soft matter and biological systems with charged macromolecules.

## 2. BRIEF REVIEW ON POISSON-BOLTZMANN MEAN FIELD THEORY

Consider the Poisson equation of electrostatics:

$$\nabla\vec{\mathrm{E}} = \frac{\rho}{\varepsilon\varepsilon_0}, \tag{1}$$

in which, $\rho$ is the electric charge density, and $\vec{E}$ is electric field, $\varepsilon$ and $\varepsilon_0$ are dielectric constant of air and relative dielectric constant of medium (water in our case) equivalently. The latter is related to the electrostatic potential by the formula:

$$\vec{E} = -\nabla \quad \phi. \tag{2}$$

In electrolyte solution containing ions with valence $Z_+$ and $Z_-$, the electric charge density can be written in the following form:

$$\rho(\vec{r}) = Z_+ e n_+(\vec{r}) - Z_- e n_-(\vec{r}) \tag{3}$$

where $n_+(\vec{r})$ và $n_-(\vec{r})$ are the densities of ions with the charge of $Z_+$ và $Z_-$, given by:

$$n(\vec{r}) = \sum_{i=1}^{N} \delta(\vec{r} - \vec{r_i}) \tag{4}$$

Because the density of ions is represented by Dirac delta function in Eq. (4), the explicit form of electric charge density $\rho$ is dependent implicitly on time. The statistical investigation of electrostatics of electrolyte solution requires averaging of the ion concentration over time, and is generally a non-tractable analytically, and simulation methods are usually employed [5]. Even so, the Coulomb interaction is long range so the computational approaches require many difficult manipulations to make the system tractable such as Ewald summations and similar approaches [6]. Therefore, we need to use approximation to make the system tractable analytically. The most common approach is the use of Boltzmann distribution for the charge density of the mobile ions [2]. In this approach, we use the distribution:

$$n_{\pm}(\vec{r}) = n_{0\pm}e^{-\frac{E_{\pm}}{k_BT}} = n_{0\pm}e^{\mp Z_{\pm}e\phi(\vec{r})/k_BT}, \tag{5}$$

Or:

$$n_{+}(\vec{r}) = n_{0+}e^{-Z_{+}e\phi(\vec{r})/k_BT}, \tag{6}$$

$$n_{-}(\vec{r}) = n_{0-}e^{+Z_{-}e\phi(\vec{r})/k_BT}. \tag{7}$$

Here $n_{0\pm}$ are the charge density at the location where the electrostatic potential is zero (usually at infinity). Using Eq. (6) and Eq. (7), the charge density $\rho$ can be replaced by its mean density:

$$\rho(\vec{r}) = Z_{+}en_{0+}e^{-Z_{+}e\phi(\vec{r})/k_BT} - Z_{-}en_{0-}e^{Z_{-}e\phi(\vec{r})/k_BT} \tag{8}$$

And Laplace equation leads to:

$$\frac{e}{\varepsilon\varepsilon_0}\left[Z_{+}n_{0+}e^{-Z_{+}e\phi(\vec{r})/k_BT} - Z_{-}n_{0-}e^{Z_{-}e\phi(\vec{r})/k_BT}\right] = -\nabla^2\phi(\vec{r}) \tag{9}$$

Eq. (9) is called the self – consistent mean field Poisson - Boltzmann equation. It is a mean-field equation because in the standard Poisson equation, but in which charge density $\rho$ is replaced by its average over Boltzmann distribution of ions. This equation called the self-consistence equation due to electric charge density $\rho$ depends on electric potential $\phi(\vec{r})$ which is what we are trying to solve. Note that replacing the explicit density by its averages, one has ignored the positional correlation of ions, and therefore it is valid when this correlation is weak, meaning a weak electrolyte solution.

## 3. LINEAR DEBYE - HÜCKEL APPROXIMATION

Due to the exponential functions, the Poisson - Boltzmann equation is highly non-linear equation. Except for the case of simple geometries, this equation can only be solved by numerical methods such as finite difference method or finite element method [7]. Further approximations are needed for analytical tractability. One of them is based on the fact that if electric potential energy $e\phi(\vec{r})$ is much less than thermal energy $k_B T$, one could linearize the Poisson - Boltzmann equation. Indeed, expand the exponential function by Taylor series in powers of $e\phi(\vec{r})/k_B T << 1$ and keep only the lower meaningful terms (first order terms):

$$e^{\mp Z_\pm e\phi(\vec{r})/k_B T} \simeq 1 \mp Z_\pm e\phi(\vec{r})/k_B T \tag{10}$$

Using Eq. (9) and Eq. (10), we find:

$$\nabla^2\phi(\vec{r}) = \frac{e}{\varepsilon\varepsilon_0}\left[Z_+ n_{0+}\left(1 - \frac{Z_+ e\phi(\vec{r})}{k_B T}\right) - Z_- n_{0-}\left(1 + \frac{Z_- e\phi(\vec{r})}{k_B T}\right)\right]. \tag{11}$$

At $\infty$ there is the neutrality condition $\rho_+(\infty) = \rho_-(\infty)$, therefore $Z_+ n_{0+} = Z_- n_{0-}$. One has:

$$\nabla^2\phi(\vec{r}) = -\frac{e^2}{\varepsilon\varepsilon_0 k_B T}[Z_+^2 n_{0+} + Z_-^2 n_{0-}]\phi(\vec{r}) \tag{12}$$

Let $I = n_{0+}(eZ_+)^2 + n_{0-}(eZ_-)^2$ is the ionic strength of the solution,

$$\nabla^2\phi(\vec{r}) = -\frac{I}{\varepsilon_0\varepsilon\, k_B T}\phi(\vec{r}) = -\kappa^2\phi(\vec{r}) \tag{13}$$

with $\kappa^2 = \frac{I}{\varepsilon\varepsilon_0 k_B T} = \frac{1}{r_s^2}$, where $r_s$ called Debye – Hückel screening radius. So, we have:

$$\nabla^2\phi(\vec{r}) = -\kappa^2\phi(\vec{r}) = -\frac{1}{r_s^2}\phi(\vec{r}) \tag{14}$$

This is the Debye - Hückel solution [2]. It is a linear solution so it is much easier to solve either analytically or numerically. For example, for a fixed point-charge, q, lies at the origin, Eq. (14) has the solution for the electrostatic potential:

$$\phi(\vec{r}) = \frac{q}{4\pi\varepsilon\varepsilon_0 r} e^{-\frac{r}{r_s}} \tag{15}$$

If $r \gg r_s$, $e^{-\frac{r}{r_s}} \rightarrow 0$, leads to $\phi(\vec{r}) = 0$. Henceoutside the range $r_s$, the electric field is negligible.

If $r \ll r_s$, $e^{-\frac{r}{r_s}} \rightarrow 1$, $\phi(\vec{r}) = \frac{q}{4\pi\varepsilon\varepsilon_0 r}$, the electric field is similar to that of Coulomb potential of a point charge in a dielectric medium of relative dielectric constant $\varepsilon$, no mobile ions.

Due to this, one can see the physical meaning of the screening radius $r_s$. Specifically, at the lower approximation, the meaning of Debye - Hückel screening radius is the range that charges outside the Debye screening radiuswillnot experience the electric field produced by one on another. On the other hand, inside this range, the interactions among charges are standard unscreened Coulomb interactions.

One notices that:

$$r_s^2 = \frac{\varepsilon\varepsilon_0\, k_B T}{I} \sim \frac{1}{n} \tag{16}$$

Or the screening radius is inversely proportional to the electrolyte salt concentration:

$$r_s \sim \frac{1}{\sqrt{n}} \tag{17}$$

For example, NaCl salt is composed of $\mathrm{Na}^+$ and $\mathrm{Cl}^-$ ions with $Z_+ = 1$, $Z_- = 1$. In aqueous solution of salt concentration of$= 1\mathrm{M}$, at room temperature of T=300K, then$r_s \cong 3\acute{A}$. Or at concentration$n = 100\mathrm{mM}$ then$r_s \cong 10\acute{A}$; in biological systems at physiologicalNaCl salt concentration of about 150mM we have$r_s \sim 7.8\acute{A}$. This is typical range of electrostatics in the cell.

Poisson - Boltzmann and Debye - Hückel equations all lead to the solutions that the potential everywhere have the same sign with electric charged macro molecule. The mean field theory ignored position correlation interaction, and it is only correct for the situations where the entropy is much greater than interaction energy of electric charges. For the opposite case of strong interactions, we can observe many counterion intuitive effects which can not be explained by these mean-field theories such as the charge inversion phenomenon and the like-charge attraction [3].

## 4. OVERCHARGE EFFECT AND ATTRACTIVE INTERACTION BETWEEN BIOLOGICAL MACRO MOLECULES

### 4.1. The effect of overcharging of macro molecules by high valence counteions

Consider a charged plane with surface charge density $\sigma$ in solution, containing difference valent counterions and coions. One has to solve the Poisson - Boltzmann of plane:

$$\nabla^2\phi(\vec{r}) = -\kappa^2\phi(\vec{r}) \tag{18}$$

with $\kappa^2 = \frac{1}{r_s^2}$, and the boundary conditions:

$$\frac{\partial\phi(z)}{\partial z}\Big|_{z\to 0_+} - \frac{\partial\phi(z)}{\partial z}\Big|_{z\to 0-} = \vec{E} \tag{19}$$

Because $\vec{E} = 4\pi\sigma r_s$, one infers $\phi(z) = 4\pi\sigma r_s^2 e^{-\frac{z}{r_s}}$, so $\phi(z)$ has the same sign as $\sigma$.

If $Z_+$ is large then counterions would condense on the surface $\sigma$ at $z = 0$. At the same time, also due to large $Z_+$, the interaction energy amongcounter-ions condensed on the surface of macro molecules is much greater than thermal energy $k_BT$, condensed counterions can be consider as a two-dimensional strongly correlated liquid or, in the lowest approximation, to form a Wigner crystal (see Fig.1).

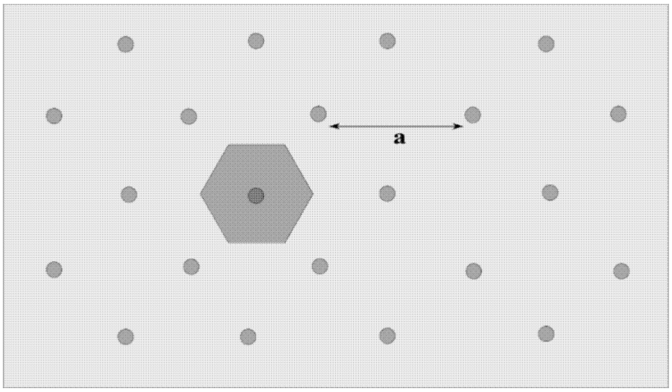

**Fig.1:** *High valance counter-ionscondense on the surface of charged macro molecule to form Wigner crystal with lattice constant a. A typical Wigner-Seitz unit cell is shown.*

In this crystal, each ion occupies a unit Wigner-Seitz cell as shown on Fig.1. The lattice constant is denoted by $a$. It is trivial to calculate the area of the Wigner-Seitz cellto be$\frac{\sqrt{3}}{2}a^2$ on the surface. Therefore, the surface density of charge:

$$\sigma \sim \frac{Z_+ e}{\frac{\sqrt{3}}{2}a^2} \tag{20}$$

Or inversely,

$$a = \sqrt{\frac{2Z_+ e}{\sqrt{3}\sigma}} \tag{21}$$

Typical interaction energy between two neighboring counter-ions which are separated by a distance $a$ is

$$U = \frac{(Z_+ e)^2}{4\pi\varepsilon_0\varepsilon a} = \frac{Z_+^2 e^2}{4\pi\varepsilon\varepsilon_0\sqrt{\frac{2}{\sqrt{3}}\cdot\frac{Z_+ e}{\sigma}}} \sim Z_+^{3/2}\sigma^{1/2}\ . \tag{22}$$

Consider negatively charged biological macromolecules in electrolyte solution with charge density -1e/nm$^2$, surroundedby positive ions have valent $Z_+ = 2$or 3. Then this interaction energy is approximately$U \cong 4\ or\ 9k_BT \gg k_BT$, the thermal energy. Therefore, if $Z_+ \geq 2$, interactions in condensed counter-ions layer dominates over entropy. Therefore, the condensed counterion layer on the macro surface isactually a strong correlated liquid on the surface of biological macro molecules. Approximating it as a Wigner crystal, the chemical potential $\mu$ in this liquid is easily shown to be negative:

$$\mu \approx \frac{\partial U(N)}{\partial N} \approx -\frac{(Z_+ e)^2}{4\pi\varepsilon\varepsilon_0 a} < 0 \tag{23}$$

This means that, from energy point of view, it is more beneficial for the counterions to condensed on the macroion surface to lower the potential energy. As we will see soon, this is the main driving force leading to over-condensation (or overcharging) of the macroion. To actually find out the limit of overcharging at given ion concentration, one needs to balance the electrochemical potential of the counterions on the surface and in the bulk. At equilibrium, equality of electrochemical potentials is written as:

$$\mu + \frac{1}{\varepsilon\varepsilon_0}\sigma^* r_s Z_+ e = k_B T \ln(n v_0) \tag{24}$$

Here, $\sigma^*$ is the net charge of the macroion surface and the condensed counterions, $v_0$ is the molecular volume of one ions. The first term in Eq. (24) is the chemical potential of the counterion in the Wigner crystal, the second term is the electrostatic potential energy of a ion of charge $Z_+e$ on a charged surface $\sigma^*$ screened by mobile ions in linear Debye - Hückel theory. The term on the RHS of Eq. (25) is the chemical potential of ions in the bulk which is approximated as the entropy of an ideal gas of concentration n.

$$\sigma^* = \varepsilon\varepsilon_0 \frac{k_B T}{r_s\ Z_+ e} \ln\left(n v_0 e^{\frac{-\mu}{k_B T}}\right) \tag{25}$$

Because $\mu \gg k_B T n_0 = \frac{1}{v_0 e^{\frac{-\mu}{k_B T}}}$is quite small. So, if $n > n_0$then$\sigma^* > 0$, opposite to the bare surface charge of the macroions. This is the counter-intuitive effect of inversion of charges of macromolecules in electrolyte solution at high enough high valence counterion concentration. It is driven by the negative chemical potential of the condensed counterions, and clearly cannot be described by mean field theories.

## 4.2. The effect of like-charge interaction among macro molecules in the presence of high valence counterions

In addition to the phenomenon of charge inversion, there is the effective attraction between spherical macromolecules also caused by the strong correlation of condensed counterions.

From Eq. (21) and Eq. (23), we infer:

$$\mu \approx -\frac{0.931}{4\pi\varepsilon\varepsilon_0} e^{3/2}\left(Z_+^{\frac{3}{2}} \sigma^{\frac{1}{2}}\right) \tag{26}$$

The higher charge density is, the more negative chemical potential become, so two charged macro molecules attract them together at small distance because at the place of contact, the density of the counterions doubles leading to lower chemical potential of the condensed counterions (see Fig.2). As the macro molecule approaches each other, within distance a at the place of contact, the ions share common surfaces of *two* macroions instead of *one*. This means that at this contact region, the "effective" surface charge is $2\sigma$ instead of $\sigma$. As a result, each ion in this contact region gains an amount of energy:

$$\mu(2\sigma) - \mu(\sigma) \cong 0.41\,\mu(\sigma) \tag{27}$$

This is again a negative energy for high valence counterions. This means that total energy is gained when macroion surface comes closer to within the distance a. In other words, the two macro ions would experience a short-range attraction due to the correlation of condensed high valence counterions. This is the phenomenon of like-charge attraction, another counter-intuitive phenomenon caused by high valence counterion that can't be described by standard mean-field theories.

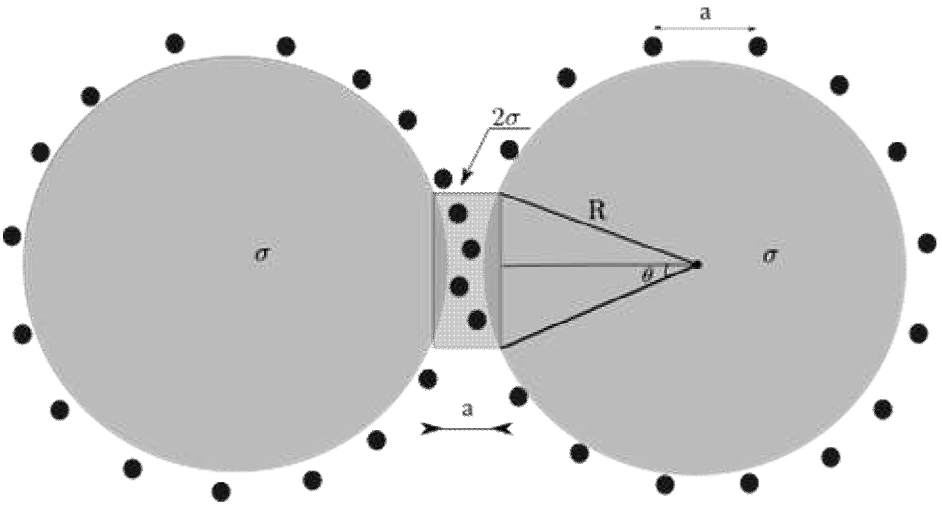

**Fig.2:** *Like - charged attraction between spherical macromolecules.*

Let us next estimate the strength of this interaction at close contact for the case of two spherical macroions. Consider two spherical negative charge macromolecules with radii $R$, in electrolyte solvent contains counterions $Z_+$, both molecules approach to each other. Counterions condense on the surfaces to form 2D Wigner Seitz lattice (Fig. 2), but density of charge in the contact region is $2\sigma$. Interaction energy between two macromolecules can be determinedas:

$$\Delta E = [(\mu(2\sigma) - \mu(\sigma)] \cdot n_{ion} \tag{28}$$

Because of spherical shapes of molecule, we used spherical coordinates for convenience. The area of the contact region can be trivial calculated in the following formula:

$$\Delta S = 2\int R^2 \sin\theta \, d\varphi \, d\theta = 2R^2 \int_0^{2\pi} d\varphi \int_0^{\theta_0} \sin\theta \, d\theta = 4\pi R^2 (1 - \cos\theta_0) \tag{29}$$

$$\Delta S = 4\pi R^2 \left(1 - \frac{R - a/2}{R}\right) = 2\pi a R \tag{30}$$

where $\Delta S$ is the surface interaction region, $R$ is the radii of macromolecules.

We also calculate the number of ions which are inside the contact region.

$$n_{ion} = \frac{\Delta S}{S_{WS}} = \frac{2\pi a R}{\frac{\sqrt{3}a^2}{2}} = \frac{4\pi R}{\sqrt{3}a} \tag{31}$$

where $S_{WS}$ is Wigner-Seitz area of the 2D strong correlation liquid of condensed ions on the surface of the molecule.

We infer from Eq. (28) and Eq. (31)

$$\Delta E \cong -3 \cdot 10^8 \, Z_+ \, \sigma \quad e \, R \tag{32}$$

The interaction energy is small than zero, therefore, macromolecules attractive together.

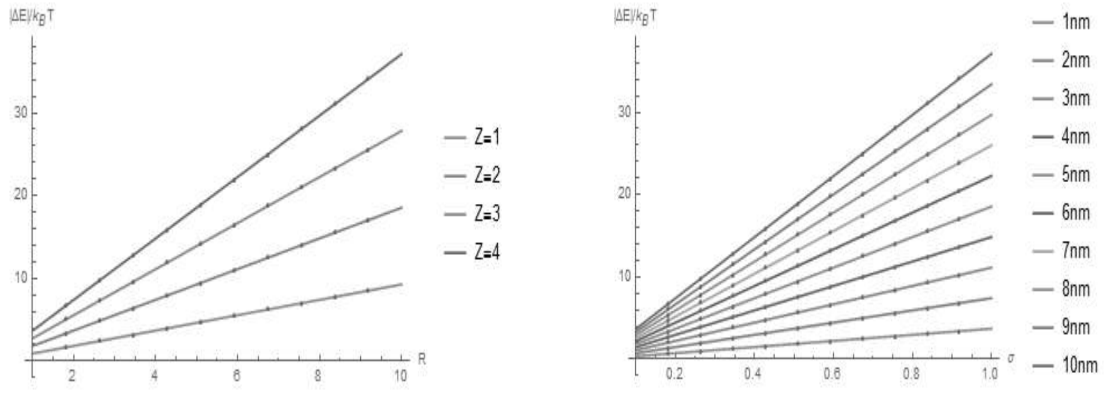

(a) ( b)

**Fig.3:** *Energy –charged attraction between spherical macromolecules as a function of radius of spherical macromolecules (a) at difference valence of counterions and* $\sigma = 0.5e/nm^2$*; and as a function of charge density at difference values of radius of macromolecules (b).*

On Fig.3, we plot the dependence of interaction energy on radius of macromolecule and the charge density to explore various behaviors of the like-charge attraction energy, where $\varepsilon = 78$ is dielectric constant of water,$\sigma$ is the density of charge of molecule, $\Delta E$ is interaction energy. As one can see, the interaction energy of macromolecule is about ten times as much as thermal energy at radii of molecule approximate 3nm and greater as increasing the radii, alongside interaction energy also is about ten times as much as thermal energy when the density of charge of molecule is 0.3e/nm$^{-2}$, and increasing linearly as the density of charge.

The results are in line with the fact that in colloidal solution, or biological solution, macro molecules tend to attract together, because the attractive interaction is more greater then thermal energy in such a solution.

## 5. CONCLUSION

In this article, we have briefly reviewed the mean field theories and Poisson - Boltzmann equation, and its linearized form Debye - Hückel equations. The mean field theories cannot explain the situation where the counterions have high valence and the interactions among them can be much higher than thermal energy at the surface of highly charged macro molecules.In these cases, new effects come about such as the overcharge phenomenon and the like-charge attraction phenomenon at small distance. Both effects have origins from the negative chemical potential of the condensed counterions on the macroion surfaces. We estimate the strength of the effect for spherical macroions and explore its behaviors for different surface charge density, ion concentrations, macroion radius… Our numerical estimates show that these effects are rather strong for strongly charged surface. Our results provide insight into strongly correlated liquid pictures of molecules of biological systems and soft matter systems.

## REFERENCES

1. Bruce Alberts, Alexander Johnson, Julian Lewis, Julian Lewis, Martin Raff, Keith Roberts, Peter Walter (2007), "Molecular Biology of the Cell, Garland Science", 5th edition.
2. L. D. Landau, E. M. Lifshits (1980), "Statistical Physics, Butterworth-Heinemann", 3 edition.
3. Yu. Grosberg, T. T. Nguyen, and B. I. Shklovskii (2002), "Colloquium: The physics of charge inversion in chemical and biological systems", - Reviews Of Modern Physics, Volume: 74, Issue: 2, pp. 329-345.
4. Naji, A., Arnold, A., Holm, C., Netz, R.R.(2004), "Attraction and unbinding of like-charged rods", - Eur. Phys. Lett., Volume: 67, pp.130-136.

5. M. P. Allen, D. J. Tildesley (1989), “Computer Simulation of Liquids”, Clarendon Press.

6. Ewald P. P. (1921), “Evaluation of optical and electrostatic lattice potentials”, - Ann. Phys. Volume: 64, p.253.

7. Todd J. Dolinsky, Jens E. Nielsen, J. Andrew Mc Cammon and Nathan A. Baker (2004), “PDB2PQR: An automated pipeline for the setup of Poisson - Boltzmann electrostatics calculations”, - Nucleic Acids Research, Volume: 32.

# HIỆN TƯỢNG ĐẢO DẤU ĐIỆN TÍCH VÀ TƯƠNG TÁC HÚT HIỆU DỤNG GIỮA CÁC ĐẠI PHÂN TỬ SINH HỌC TRONG DUNG DỊCH ĐIỆN PHÂN

***Tóm tắt:*** *Trong bài báo này chúng tôi trình bày về hiện tượng đảo dấu điện tích và tương tác hút hiệu dụng giữa các đại phân tử sinh học trong dung dịch điện phân. Nghiên cứu bằng cách sử dụng lý thuyết trường trung bình Poisson - Boltzmann, có tính tới tương quan vị trí của các ion, giả thiết rằng các ion ngưng tụ trên bề mặt đại phân tử thành một mạng tinh thể 2D Wegner - Seitz… Các tính toán của chúng tôi cho kết quả phù hợp với các thí nghiệm quan sát đã quan sát được.*

***Từ khóa:*** *Đảo dấu điện tích, dung dịch điện phân, tương tác hút của điện tích cùng dấu, phương trình Poisson - Boltzmann, đại phân tử sinh học.*

# EFFECT OF EXTERNAL STATIC ELECTRIC FIELD ON SOME PROPERTIES OF IRON THIN FILM

**Nguyen Van Hung**[1], **Tran Van Quang**[2]
[1]*Falcuty of KTCN, Hong Duc University, Thanh Hoa*
[2]*Department of Physics, University of Transport and Communications*

***Abstract:*** *The effect of external electric field on magnetic properties has attracted great attention due to potential applications for advanced magnetic and electronic devices. In this paper, we employed density function theory to examine the effect of an external static electric field on some properties of iron thin film with the field strength varied up to 0.1V/Å. In the presence of the electric field, the Fe ions are relaxed to the equilibrium positions which increases the computational time. The critical change of convergence occurs at the 10th iteration.*

***Keywords:*** *Magnetoelectrics, magnetic moments, thin film, density functional theory, pseudopotential.*

Email: tkuangv@gmail.com
Received 21 August 2019
Accepted for publication 10 November 2019

## 1. INTRODUCTION

The coupling between electric and magnetic orders in thin-film heterostructures is an interesting problem in nanoscience. Physics behind this intriguing properties is magnetoelectric effects (ME). This phenomenon involves magnetization of materials under electric field and/or electric polarization under an external magnetic field [1-5]. The mechanism of the ME effects might stem from the fact that the external electric field displaces the ions away from their equilibrium positions, thereby altering the exchange-correlation interaction thus altering the electron spin interaction that leads to the change of magnetism of materials [6].

In this report, we employed first-principles density functional theory to study the direct effect of an external electric field on some basic properties of iron nano-thin films. We show calculation results and discuss about the convergence of some physical quantities which will spur further studies on the control of magnetism of nano thin film in future technologies.

## 2. CRYSTAL STRUCTURE AND COMPUTATIONAL DETAILS

The crystal structure of iron is body centered cubic (FCC) with space symmetry group No. 229, i.e. Im-3m. The thin film is formed by cutting the crystal along the plane (001) which includes atomic layers as shown in Fig.1. The applied external electric field is perpendicular to the thin film which varies from 0 to 0.1V/Å. The ground states electrons in the crystal determines the magnetism of the thin film.

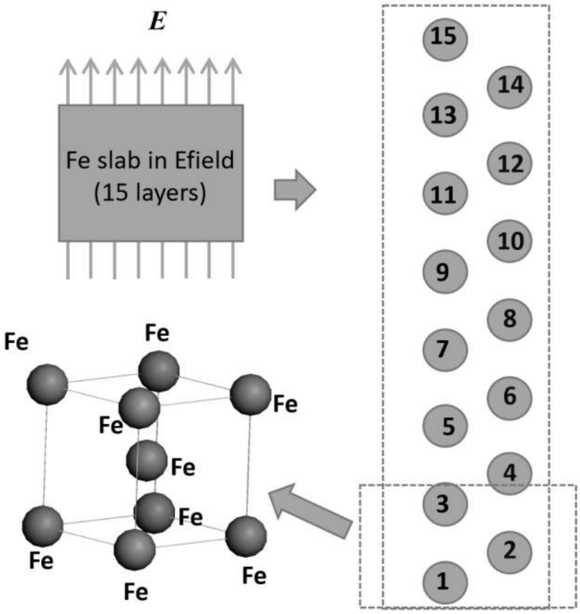

**Fig.1:** *Nanocrystal of Fe in bulk and in thin film*

Such the ground states are determined by the lowest total energy, $E[\rho]$ [7–9]

$$E[\rho]=T[\rho]+V_{ee}[\rho]+\int v(\vec{r})\rho(\vec{r})d\vec{r}\,. \tag{1}$$

The electron density can be found via internal products of Kohn-Sham orbitals, which is obtained by solving Kohn-Sham equation consistently [7, 10],

$$\left[-\frac{\Delta}{2}+v(\vec{r})+\int\frac{\rho(\vec{r}\,')}{|\vec{r}-\vec{r}\,'|}d\vec{r}\,'+v_{xc}[\rho(\vec{r})]\right]\psi_i=\varepsilon_i\psi_i\,, \tag{2}$$

where $\rho(\vec{r})=\sum_{i=1}^{N}n_i\langle\psi_i|\psi_i\rangle$ is electron density and $n$ is the occupied number, and the exchange potential is $v_{xc}[\rho]=\delta E_{xc}[\rho]/\delta\rho$. Solving this equation leads to the gound states of electrons in the crystal, which can be done by starting from a trial density to calculate Halminton in Eq. (2). The next step is solving Eq. (2) to obtain the eigeinvector $\psi$ and the eigienvalues $\varepsilon$. The self-consistently solving scheme can be illustrated in Fig. 2.

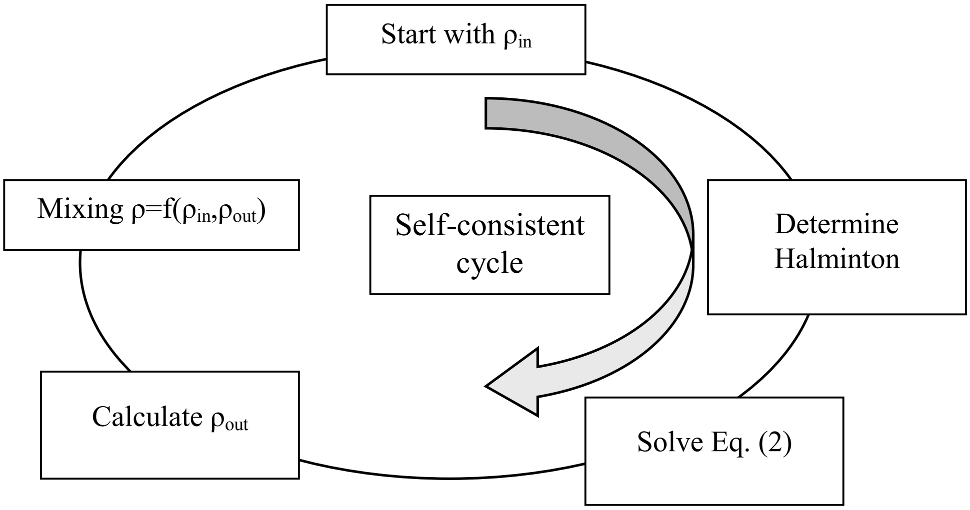

**Fig.2:** *Scheme of solving Kohn-Sham equation self-consistently*

To perform the task, the plane wave method has been used [11,12]. Accordingly, the Kohn-Sham orbital is expanded to the basis of plane waves, i.e. [13],

$$\psi_n(\vec{r}) = \sum_{\vec{G}} c_{n,(\vec{k}+\vec{G})} e^{i(\vec{k}+\vec{G})\vec{r}} , \tag{3}$$

where $c_{n,(\vec{k}+\vec{G})}$ are the coefficients defining the orbirals.

Electrons in the region near the nuclei are driven by strong Coulomb interaction from nuclei and the iner electrons. Thus, the associate wave functions vary rapidly. This demands a large number of plane waves to fully describe their properties. To overcome, one introduces pseudopotential which is chosen such that the wave functions are exactly same to those of all-electron wave function outside the defined core. Inside the core, the potential is replaced by a smoother equivalent potential, called pseudopotential [11, 13, 14]. The task has been done by using The Vienna Ab initio Simulation Package (VASP) [11, 12]. The use of ultra-soft pseudopotentials leads to significant reduction of the size of the basis set without effecting to the calculated results [11].

## 3. RESULTS AND DISCUSSIONS

The calculation has been done for both bulk and thin film. In both cases, solving equations (2) is same in principle. After each iteration, the total energy of the system determined by (1) will converge to a certain value. The larger the number of k-point grid in the first Brillouin zone [18], the more accurate the calculation. The convergence of total energy and magnetic moment versus the number of grid points for Fe bulk is carried out and presented in Fig. 3. We find that when increasing the number of k-point grid in the BZ region, these two quantities gradually converge to a value. From here, we can see that, with the number of 10x10x10 k-point grid, the total energy and the magnetic moment are well converged.

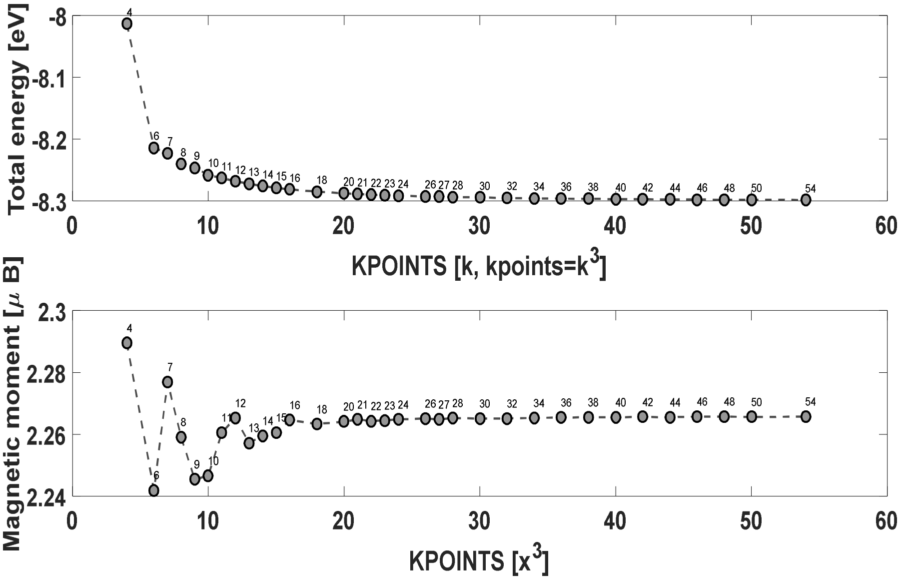

**Fig.3:** *Convergence of total energy and magnetic moment as a function of k-grid*

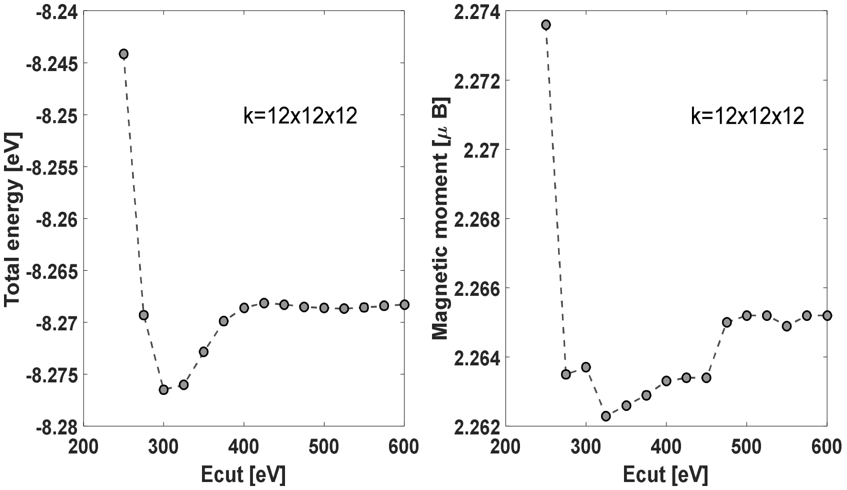

**Fig.4:** *Convergence of total energy and magnetic moment as a function of cut off energy, Ecut*

The next problem is the size of the basis set used to expand Kohn-Sham orbital which is determined by cutoff energy, *Ecut*. This value will limit *G* values in equation (3). Similar to the number of the k-point grid, the larger the *Ecut* value, the more accurate the result. Nevertheless, the more computational time is demanded. The dependences of total energy and magnetic moment on *Ecut* are presented in Fig. 4. As can be seen, the total energy converges rapidly while the magnetic moment converges more slowly. When the *Ecut* reaches 500 eV, both quantities are converged well. As can be seen, the obtained values are consistent with previous published values, e.g. mangtic moment of $2.26\mu_B$ [15]. The results of these calculations show that for this system the values of k-point grid of $10\times10\times10$ and *Ecut* of 500 eV can be used for further calculation.

Next, we use these parameters to continue the calculation for the thin film. The pseudopotential here is PAW_PBE [12]. Some information is as following:

VRHFIN =Fe: d7 s1
LEXCH = PE
EATOM = 594.3153 eV, 43.6809 Ry
IUNSCR = 1 unscreen: 0-lin 1-nonlin 2-no
RPACOR = 2.000 partial core radius
POMASS = 55.847; ZVAL = 8.000 mass and valenz
RCORE = 2.300 outmost cutoff radius
RWIGS = 2.460; RWIGS = 1.302 wigner-seitz radius (au A)
ENMAX = 267.882; ENMIN = 200.911 eV
RCLOC = 1.701 cutoff for local pot
EAUG = 511.368
RMAX = 2.356 core radius for proj-oper
RAUG = 1.300 factor for augmentation sphere
RDEP = 2.442 radius for radial grids
RDEPT = 1.890 core radius for aug-charge
And the energy levels in Fe atoms are
n l j E occ.
1 0 0.50 -6993.8440 2.0000
2 0 0.50 -814.6047 2.0000
2 1 1.50 -693.3689 6.0000
3 0 0.50 -89.4732 2.0000
3 1 1.50 -55.6373 6.0000
3 2 2.50 -3.8151 7.0000
4 0 0.50 -4.2551 1.0000
4 1 1.50 -3.4015 0.0000
4 3 2.50 -1.3606 0.0000

Thus, electrons 3d4s are used as valence electrons. The remaining electrons are the core. As the input converged parameters, i.e. *Ecut* and k-grid, above, the maximum number of plane wave included is 8167. Performing the calculation, we obtained the following results

*(i) Convergence of computational time versus iterations*

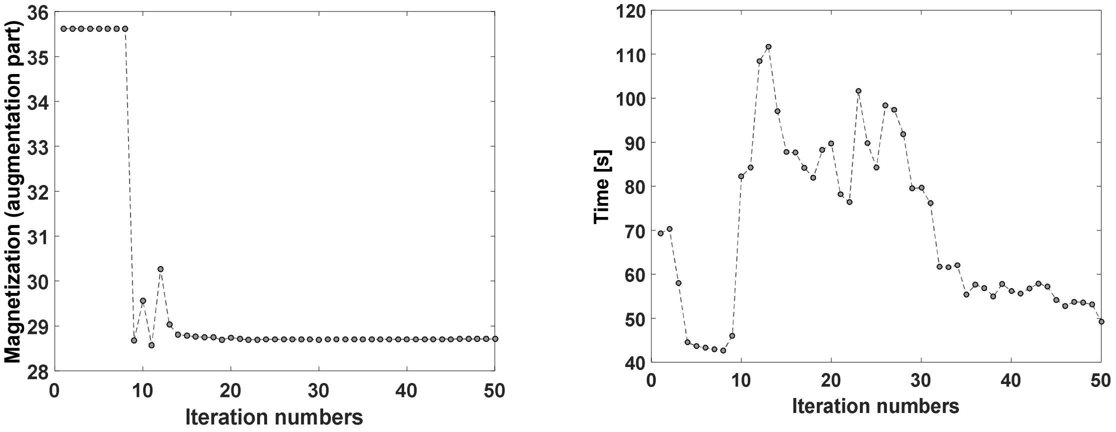

**Fig.5:** *Convergence of magnetization and computational time of an iteration versus iteration orders for the case of E=0 V/Å*

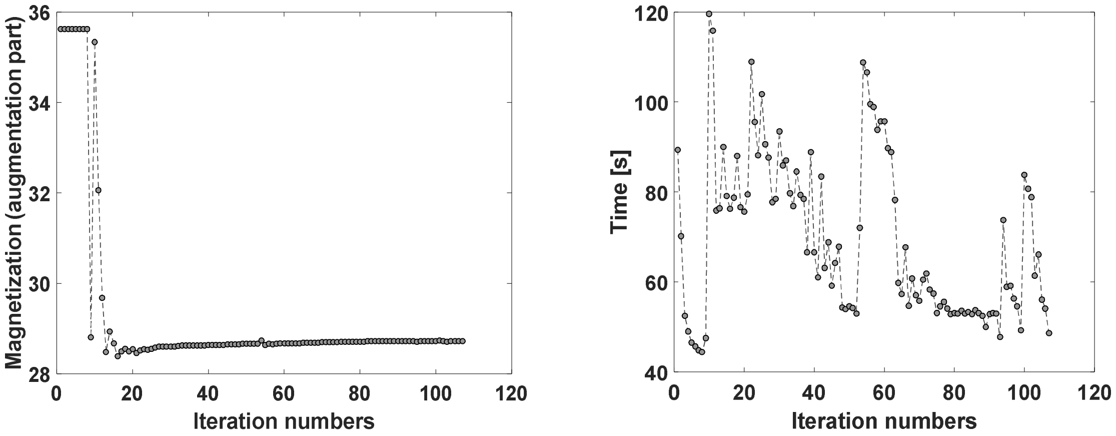

**Fig.6:** *Convergence of magnetization and computational time of an iteration versus iteration orders for the case of E=0.1 V/Å.*

Fig. 5 and 6, respectively, describe the dependences of magnetization (augmentation part) and time consumed of an iteration on the iteration order for both cases, i.e. the absence of electric field, i.e. E = 0 V/Å, and the presence of electric field, i.e. E = 0.1 V/Å. In both cases, it can be seen that the convergence of magnetization has a sudden jump at the 10th iteration. It is also the most time-consuming iteration. For the case of E ≠ 0, the number of iteration to achieve convergence is many times greater. The reason is the relaxation of Fe ions at lattice sites to achieve their equilibrium states. When the electric field is applied, the system including Fe ions and electrons is under the external field, which increases its total energy. In the calculation, each iteration after achieving convergence will have finite total energy. This value depends on the position of Fe ion in the electric field. Fe ions is shifted in the direction of the field and the calculation continues until the forces exerting on Fe ions reaches to a defined criterion. As a result, the energy of the system is minimum at the final step. Therefore, the total number of iterations in this case is significantly increased.

*(ii) Effect of electric field*

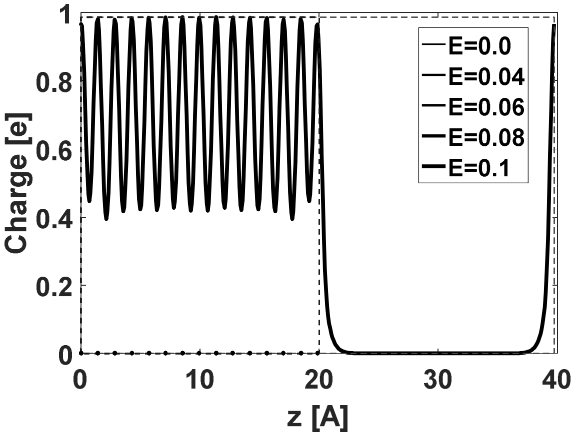

**Fig.7:** *(Color online) Charge distribution for the external electric field E= 0; 0.04; 0.06; 0.08; and 0.1 V/Å*

When an electric field is applied, according to the classical model, the electrons in the thin film will be exerted and distributed on the surface of the thin film. The electrons will be redistributed in the entire thin film. Fig. 7 describes the calculated charge of the thin-film system depending on the position for various electric fields. As can be seen, the variation in this scale is negligible, the lines show the overlap and we cannot distinguish the difference. However, the small change might lead to delicate change in stable energy and magnetic properties. This essue will be studied in our forthcoming studies.

## 4. CONCLUSION

By employing first-principles calculation within density functional theory, we find that total energy and magnetic moment of Fe ion are well converged at k-point grid of $10\times10\times10$ and *Ecut* of 500 eV in pseudopotential method using PAW_PBE. The calculation for the thin film show that the magnetic moment is rapidly converged whereas the total energy is converge more slowly. In both cases, without and with electric field, the convergence achieves critical convergence at the 10th iteration. The computational time for the latter case is significantly slower due to the relaxation of Fe ions to the equilibrium positions. The external electric field induces a minor change in charge density in the scale of total valence charge.

***Acknowledgments:*** *The authors thank Prof. Miyoung Kim and Prof. Hanchul Kim at Sookmyung Women's Univeristy for their supervision at very early stage of this research.*

## REFERENCES

1. S. Kanai, M. Yamanouchi, S. Ikeda, Y. Nakatani, F. Matsukura, H. Ohno, Electric field-induced magnetization reversal in a perpendicular-anisotropy CoFeB-MgO magnetic tunnel junction, Appl. Phys. Lett. 101 (2012). DOI:10.1063/1.4753816.
2. Tran Van Quang, Electric-field modification of magnetism in a free-standing palladium ultrathin film, 42th Natl. Conf. Theor. Physics, Can Tho, Vietnam. (2017).
3. C.G. Duan, J.P. Velev, R.F. Sabirianov, Z. Zhu, J. Chu, S.S. Jaswal, E.Y. Tsymbal, Surface magnetoelectric effect in ferromagnetic metal films, Phys. Rev. Lett. 101 (2008) 137201. DOI:10.1103/PhysRevLett.101.137201.
4. M.K. Niranjan, C.G. Duan, S.S. Jaswal, E.Y. Tsymbal, Electric field effect on magnetization at the Fe/MgO(001) interface, Appl. Phys. Lett. 96 (2010) 222504. DOI:10.1063/1.3443658.
5. C.G. Duan, J.P. Velev, R.F. Sabirianov, W.N. Mei, S.S. Jaswal, E.Y. Tsymbal, Tailoring magnetic anisotropy at the ferromagnetic/ferroelectric interface, Appl. Phys. Lett. 92 (2008) 1–4. DOI:10.1063/1.2901879.
6. T. Van Quang, H. Kim, K. Miyoung, Ab initio investigation on the magnetization of Pd thin films, Int. Symp. Magn. Magn. Mater. (2014).
7. W. Kohn, L.J. Sham, Self-Consisten Equations Including Exchange and Correlation Effects, Phys. Rev. 140 (1965) A1134–A1138. DOI: Http://dx.doi.org/10.1103/PhysRev.140.A1133.
8. P.C. Hohenberg, W. Kohn, L.J. Sham, The beginnings and some thoughts on the future, Adv. Quantum Chem. 21 (1990) 7–26. DOI:10.1016/S0065-3276(08)60589-4.
9. R.G. Parr, W. Yang, Density-functional theory of atoms and molecules, Density-Functional Theory Atoms Mol. 65 (1989) 1–352. DOI:10.1016/0306-4549(89)90016-9.
10. P. Hohenberg, W. Kohn, Inhomogeneous Eelectron gas, Phys. Rev. 136 (1964) B864-871. DOI:10.1103/PhysRev.136.B864.
11. G. Kresse, J. Furthmüller, Efficient iterative schemes for *ab initio* total-energy calculations using a plane-wave basis set, Phys. Rev. B. 54 (1996) 11169–11186. DOI:10.1103/PhysRevB.54.11169.
12. G. Kresse, D. Joubert, From ultrasoft pseudopotentials to the projector augmented-wave method, Phys. Rev. B. 59 (1999) 1758–1775. DOI:10.1103/PhysRevB.59.1758.

13. R. Martin, Electronic Structure: Basic Theory and Practical Methods, 2004.

14. W. Kohn, A.D. Becke, R.G. Parr, Density Functional Theory of Electronic Structure, J. Phys. Chem. 100 (1996) 12974–12980. DOI:10.1021/jp960669l.

15. P. Janthon, S. Luo, S.M. Kozlov, F. Viñes, J. Limtrakul, D.G. Truhlar, F. Illas, Bulk properties of transition metals: A challenge for the design of universal density functionals, J. Chem. Theory Comput. 10 (2014) 3832–3839. DOI:10.1021/ct500532v.

# MỘT SỐ TÍNH CHẤT CỦA MÀNG MỎNG Fe DƯỚI TÁC DỤNG CỦA ĐIỆN TRƯỜNG TĨNH NGOÀI

***Tóm tắt:*** *Tác động của điện trường ngoài lên tính chất các tính chất từ điện của màng mỏng nói chúng là một bài toán thời sự, hàm ý nhiều ý tưởng phát triển công nghệ hiện đại trong tương lai. Trong bài báo này, chúng tôi đã sử dụng lý thuyết phiếm hàm mật độ để nghiên cứu ảnh hưởng của điện trường tĩnh ngoài lên một số tính chất của màng mỏng sắt với cường độ trường thay đổi lên đến 0,1 V/Å. Các kết quả tính toán cho trường hợp tinh thể khối không đặt trong điện trường ngoài đã được thu lại. Với sự có mặt của điện trường, các ion Fe trong màng mỏng bị di dời đến các vị trí cân bằng mới. Điều này là một trong những nguyên nhân làm thời gian tính toán của chương trình máy tính tăng lên. Sự hội tụ của mô men từ diễn ra nhanh hơn so với sự hội tụ năng lượng toàn phần. Thay đổi quan trọng của sự hội tụ xảy ra ở lần lặp thứ 10.*

***Từ khóa:*** *tính chất từ điện, điện tích cảm ứng, màng mỏng, lý thuyết phiếm hàm mật độ, giả thế.*

# THE SYNTHESIS OF $CU_2O$ NANOPARTICLES BY A BIPOLAR ELECTROLYSER APPLIED FOR BACTERICIDAL

**Vu Thi Hong Nhung**[1], **Bui Thi Thuy Linh**[1], **Tran Dang Khoa**[2] **and Pham Van Vinh**[1]
[1]*Faculty of Physics, Hanoi National University of Education*
[2]*Faculty of Agricultural Technology, VNU University and Technology,*
*Vietnam National University, Hanoi*

***Abstract:*** *$Cu_2O$ nanoparticles were successfully synthesized using bipolar electrolytic method from an electrolyte solution containing $Cu(CH_3COO)_2.H_2O$ (99.99%; Sigma Aldrich) and PVP (99.999%; Sigma Aldrich) with different ratios. The effect of PVP concentration on the properties of samples was investigated. The phase analysis by XRD showed the presence of $Cu_2O$ crystals corresponding to face-centered cubic structure. SEM images also showed the cubic shape of $Cu_2O$ with morphology that modified by PVP concentration. The finest particles were found on the samples prepared with the PVP $45.50_{\mu M}$. The presence of plasmon peak around the wavelength of 500nm on the absorption spectrum reconfirmed the presence of $Cu_2O$ nanoparticles. $Cu_2O$ nanoparticles could disperse well in $H_2O$ and exhibited their bactericidal action by inhibiting the growth of E.coli bacteria on agar plates.*

***Keywords:*** *$Cu_2O$, bipolar electrolysis, bactericidal, E.coli*

Email: nhungvu910@gmail.com

Received 24 October 2019
Accepted for publication 20 November 2019

## 1. INTRODUCTION

The development of new resistant strains of bacteria to current antibiotics has become a serious problem in public health. So there is a strong incentive to develop new bactericides. This makes current research in bactericidal nanomaterials particularly timely. The emergence of nanoscience and nanotechnology in the last decade presents opportunities for exploring the bactericidal effect of metal and metal oxide nanoparticles. The bactericidal effect of nanoparticles has been attributed to their small size and high surface to volume ratio, which allows them to interact closely with microbial membranes [1]. Among all the metal oxides, cuprous oxide ($Cu_2O$) nanoparticles are one of the promising semiconductors with a direct band gap of 2.17 eV comprising suitable photo catalysis [2], CO oxidation [3], gas sensing [4], antibacterial and antifungal properties [5]. They have cheaper price than other metal oxide nanoparticles. The antimicrobial activity of cuprous oxide has long been recognized. Considering the increasing of diseases in the world, the biocidal characteristics of cuprous oxide nanoparticles are very important specifically for application in medical fields including bed sheets, medical and protective clothing [5].

$Cu_2O$ has been prepared by several different methods, such as electro deposition [6], sonochemical method [7], thermal relaxation [8], liquid phase reduction [9] and vacuum evaporation [10]. However, now it is highly desirable to develop a simple and effective method to synthesize structurally $Cu_2O$ over a large range. The electrolysis method has been preferred to use because it's an economically feasible, simple, non-polluting process and cost effective. The DC electrolysis method is common to be used. However, the use of DC current in electrolyzing process results in creating the large size of particles, usually in microscale [11]. To solve the grain size issue, a bipolar electrolyser is expected to synthesize $Cu_2O$ particles in nanoscale. With bipolar electric current, the current will be inverted direction for each cycle, resulting in interrupting the ions agglomerating process thereby decreasing the grain size. So in this study, instead of using a conventional electrolyser, a bipolar electrolyser was used to synthesize $Cu_2O$ nanoparticles. We focused on preparing $Cu_2O$ nanoparticles by a bipolar electrolyser and studying the effect of PVP concentration on $Cu_2O$ nanoparticles' properties. The finest particles were used to an antibacterial test against E.coli bacteria.

## 2. EXPERIMENTAL

0.16g $Cu(CH_3COO)_2$ (99.99%; Sigma Aldrich) powders were dissolved into 80ml of dehydrated water containing different concentrations of PVP surfactant (polyvinylpyrrolidon - 99.999%; Sigma Aldrich) under the assistance of ultrasonic. The solution was placed inside ultrasonic cleaner tank during the electrolyzing process with Cu electrodes. The synthesized parameters were controlled by a computer. The electrolyzing process took up 1h with period was fixed at 20s, the distance between two electrodes was 1cm and the pulse intensity was 13V. The sample was washed with dehydrated water. The $Cu_2O$ products were dried in vacuum for 1 hour. The analysis methods XRD, SEM, UV-Vis were used to investigate the structure, morphology and absorption of samples. Agar well diffusion method was use to an antibacterial test against E.coli bacteria. To evaluate the antibacterial ability of $Cu_2O$ nanoparticles, other antimicrobial agents including Ag nano-compound and ampicillin were used as the references samples. The E.coli bacteria were inoculated on the agar plate surface. Then, five wells with a diameter of 6 mm were punched aseptically on the surface of the agar plate. The antimicrobial agents were dispersed separately in water and introduced to the wells. The agar plates were incubated under suitable conditions. The antimicrobial agents diffused in the agar medium and inhibited the growth of the microbial strain tested. The bactericidal action was evaluated through the black area zone that spread around the wells.

## 3. RESULT AND DISCUSSION

It has been so many researches about $Cu_2O$ nanoparticles so far. In previous research [12], we have found out that the current cycles and voltages used in electrolysis process significantly affect the particle size while nanoscience applications requires the particles to have small size (nm). Among voltages, current cycles that were studied, the voltage 13V and current cycle 20s are selected to synthesize $Cu_2O$ nanoparticles for further investigations. In this study, the effect of different concentration surfactant (PVP) on $Cu_2O$ nanoparticles'properties was studied. The volume of solution, electrolyte mass unchanged during the experiment and the distance between two electrodes was kept 1 cm.

### 3.1. The effect of PVP concentration on $Cu_2O$ crystal structure

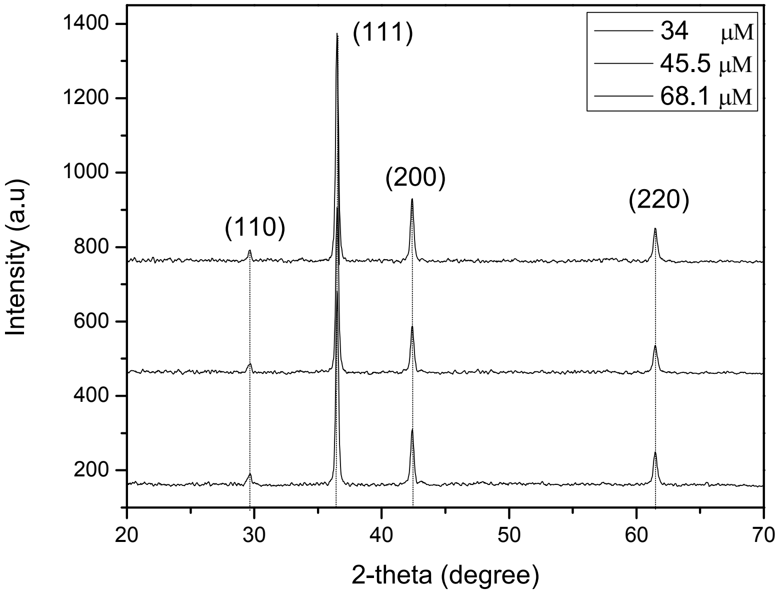

**Figure 3.1:** *XRD patterns of $Cu_2O$ nanoparticles synthesized at different PVP concentration: 34 μM; 45.5 μM and 68.1 μM*

Fig.3.1 is the XRD patterns of $Cu_2O$ nanoparticles prepared with different PVP concentration in the range from 34μM to 68.1 μM. The results demonstrated that $Cu_2O$ nanoparticles have face-centered cubic lattice structure (fcc). The peaks with 2θ values of $29.62^0$, $36.45^0$; $42.48^0$ and $61.49^0$ correspond to the crystal planes of (110), (111), (200) and (220) respectively, of crystalline $Cu_2O$ [JCPDS card, no. 05-0667].

The interplane spacing d was calculated using the Bragg's law with n=1 for (111) plane showed that the lattice constant was equal to 0.427 nm. This reconfirmed the formation of $Cu_2O$ crystal.

The crystallite sizes were estimated using Scherrer's formula:

$$D = \frac{0.9\lambda}{\beta \cos\theta}$$

Where D: the average particle size

λ: the wavelength of X-ray (λ = 1.540560 Å)

β: FWHM (rad)

θ: the angle of peak position.

The crystalline size was calculated at $2\theta = 36.45^0$

**Table 3.1:** *The average crystalline size at different PVP concentration*

| β (rad) | 0.0026 | 0.0023 | 0.0015 |
|---|---|---|---|
| Concentrations (μM) | 34 | 45.5 | 68.1 |
| D (nm) | 56 | 63 | 97 |

The results show that the intensity of peaks increases and FWHM also tends to reduce with the increase in PVP concentration. The crystallite sizes in the range from 56 to 97nm.

## 3.2. The effect of PVP concentration on the morphology of $Cu_2O$ particles

Fig.3.2 shows the SEM images of synthesized $Cu_2O$ nanoparticles at different PVP concentration. The results showed that particle size is strongly influenced by the PVP concentration in the electrolyte solution. The sample prepared with 45.5 μM PVP has the finest particles with an average particle size of 60 nm. This is an impressive result because Cu particles prepared by conventional electrolytic method are quite large (mostly micro size) [11]. This proves that the bipolar electrolytic method has ability to reduce particle size.

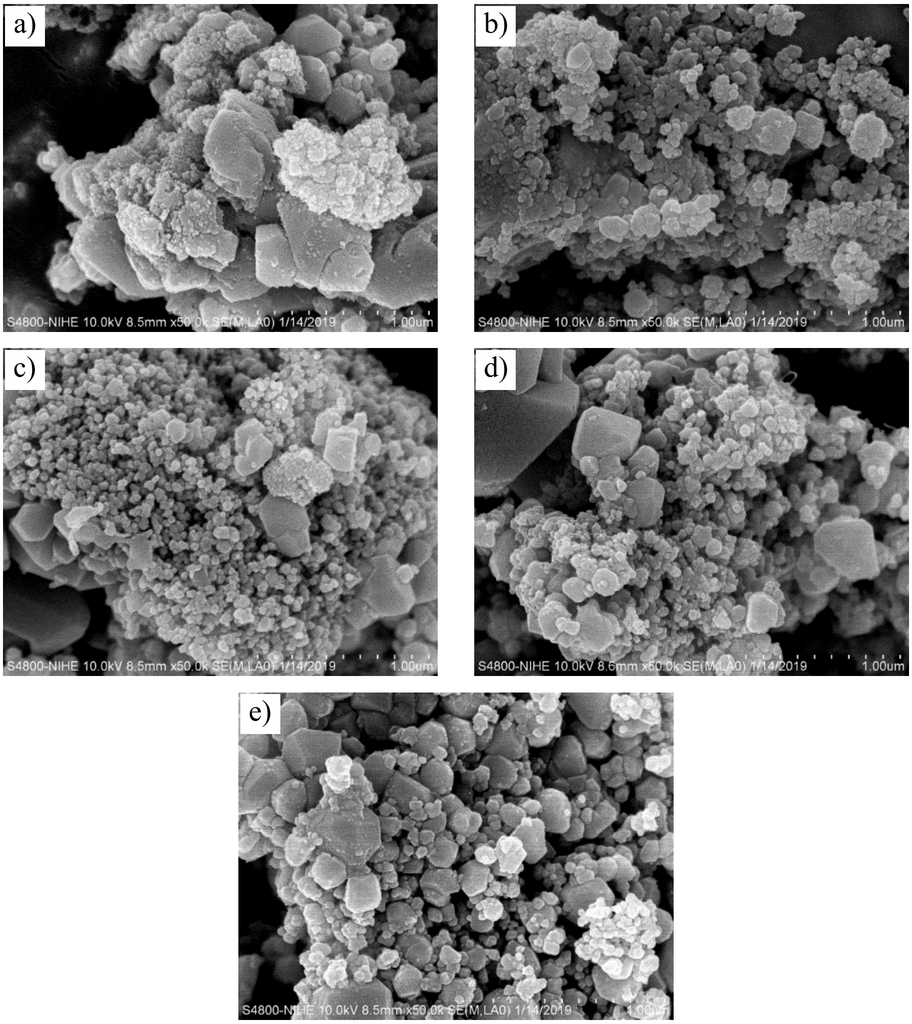

**Figure 3.2:** *SEM images of $Cu_2O$ nanoparticles synthesized at different PVP concentration: a- 11.4 μM PVP; b- 34 μM PVP; c- 45.5 μM PVP; d- 56.9 μM PVP; e- 68.1 μM PVP*

## 3.3. UV-Vis spectrum of $Cu_2O$ nanoparticles

Fig.3.3 shows UV-Visible spectra of $Cu_2O$ nanoparticles. There was a plasmon resonance absorption peak at wavelength about 490 nm were found. In general, the optical absorption peak of $Cu_2O$ nanoparticles around the wavelength of 500nm. The shift of the absorption peak could occur due to the effects of shape and size of the particles. According to recent studies, the plasmon absorption peak of nanoparticles change was attributed to quantum size effects for small enough particles (≤14nm), scattering effects in larger particles, and crystal defects created during synthesis ($Cu^+$ or $O^{2-}$ vacancies, or other impurities), interparticle distance (interconnection), and more [13]. The broad absorption peak from 380 nm to 500 nm was reported for flower-like $Cu_2O$ nanocrystals with the inhomogeneous size of wires [14]. Therefore, the present of the plasmon peak was agreed well with other results. This indicated that $Cu_2O$ nanocrystals were successfully prepared by the bipolar electrolytic method.

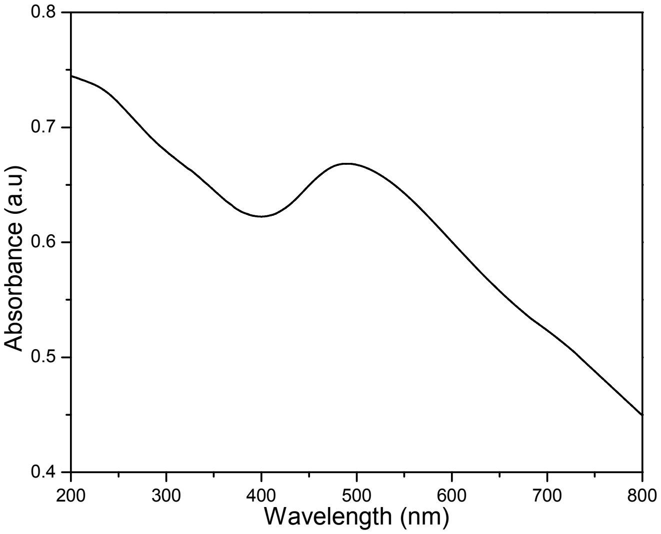

**Figure 3.3:** *UV-Vis spectrum of* $Cu_2O$ *nanoparticles*

## 3.4. Antibacterial test

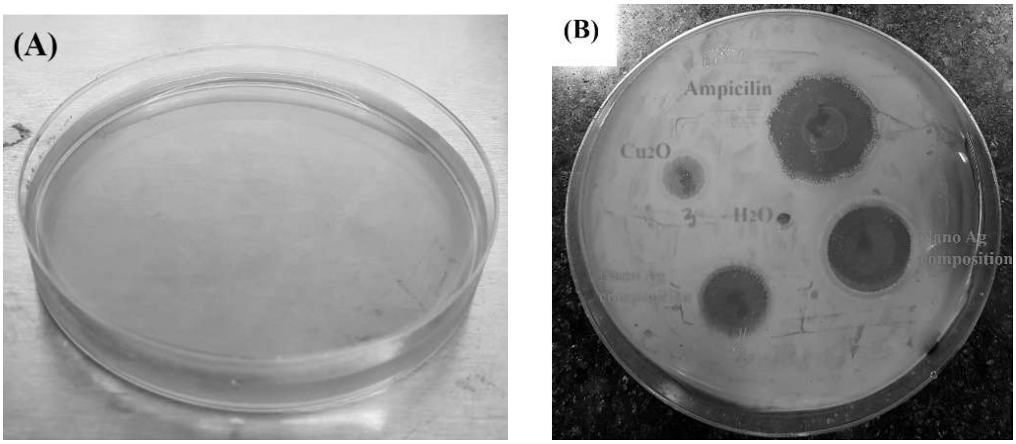

**Figure 3.4:** *Antibacterial test results against by agar well diffusion method (A): agar plate without bacterial; (B): agar plate inoculated with bacterial*

Fig 3.4 is antibacterial test results against E.coli bacteria. There is no black zone around the well containing water (located at the center of the plate). The black zone starts appearing around the wells containing antimicrobial agents indicated their antibacterial activity. Compared to Ag nano compound and ampicillin, $Cu_2O$ nanoparticle did not show better antibacterial activity. This is indicated by the size of the circle for each well in Fig. 3.4 B. In spite of this, $Cu_2O$ is low cost material. Therefore, it has the potential applications in medicine and agriculture.

The antibacterial mechanism of $Cu_2O$ nanoparticles is currently controversial [15, 16, 17]. The interaction between copper ions and the cell wall of bacterial is an acceptable hypothesis. In this case, copper ions are produced by the dispersion of $Cu_2O$ nanoparticles in water. The groups of amines and carboxyl in the cell wall of E.coli bacteria have caused a great affinity toward copper ions that are released from oxide nanoparticles. These ions bind easily with the negative charged cell wall in the gram-negative bacteria and damage its cell wall. The permeability of the cell membrane is altered so that the cytoplasm is flowed out, resulting in the cell death. Therefore, it can be seen that after entering the cell, the oxide nanoparticles will bind to the bacterial DNA and disrupt its helical structure by forming cross links within and between DNA molecules. Moreover, it will also disrupt the biochemical process inside bacteria. Bacterial growth is further inhibited by the indirect effect of changing the bacterial environment by releasing Cu ions from the nanoparticles.

## 4. CONCLUSION

$Cu_2O$ nanoparticles were successfully synthesized by the bipolar electrolytic method. The size of $Cu_2O$ nanoparticles prepared by the bipolar electrolytic method was significantly reduced comparing to that prepared by conventional electrolytic method. The PVP concentration of the electrolyte solution influenced on the morphology of $Cu_2O$ nanoparticles. $Cu_2O$ nanoparticles exhibited antibacterial activity against E.coli bacteria.

***Acknowledgments:*** *This research was supported by Hanoi National University of Education.*

## REFERENCES

1. Morones JR, Elechiguerra JL, Camacho A, Holt K, Kouri JB, Ramírez JT, & Yacaman M J, The bactericidal effect of silver nanoparticles, - Nanotechnology (2005) p.2346.
2. JianPan and GangLiu, Facet Control of Photocatalysts for Water Splitting, Semiconductors and Semimetals (2017), pp.349-391.
3. Michael O'keeffe and Walter J. Moore, Thermodynamics of the formation and migration of defects in cuprous oxide, The Journal of Chemical Physics, (1962), pp.3009-3013.
4. Yongming Sui, Yi Zeng, Weitao Zheng, Bingbing Liu, Bo Zou, Haibin Yang, Synthesis of polyhedron hollow structure Cu2O and their gas-sensing properties, Sensors and Actuators B: Chemical (2012), pp.135-140.
5. Sungki Lee, Chen-Wei Liang, Lane W. Martin, Synthesis, control, and characterization of surface properties of Cu2O nanostructures, ACS Nano (2011), pp.3736-3743.
6. P. E. De Jongh, D.Vanmaekelbergh and J.J.Kelly, Cu2O: electrodeposition and characterization. Chemistry of materials (1999), pp.3512-3517.

7. R Vijaya Kumar, Y Mastai, Y Diamant, A Gedanken, Sonochemical synthesis of amorphous Cu and nanocrystalline Cu2O embedded in a polyaniline matrix. Journal of Materials Chemistry (2001), pp.1209-1213.

8. Shigehito Deki, Kensuke Akamatsu, Tetsuya Yano, Minoru Mizuhata, Akihiko Kajinami, Preparation and characterization of copper (I) oxide nanoparticles dispersed in a polymer matrix, Journal of Materials Chemistry (1998), pp.1865-1868.

9. W.Z. Wang, G.H. Wang, X.S. Wang, Y.J. Zhan, Y.K. Liu, C.L. Zheng, Synthesis and characterization of Cu2O nanowires by a novel reduction route, Advanced Materials (2002), pp.67-69.

10. Hiroshi Yanagimoto, Kensuke Akamatsu, Kazuo Gotoh and Shigehito Deki, Synthesis and characterization of Cu2O nanoparticles dispersed in NH2-terminated poly (ethylene oxide). Journal of Materials Chemistry (2001), pp.2387-2389.

11. Gökhan Orhan and Gizem Güzey Gezgin, Effect of electrolysis parameters on the morphologies of copper powders obtained at high current densities, Serbian Chemical Society Journal (2012), pp.651-665.

12. Pham Van Vinh, Dang Duc Dung, Nguyen Bich Ngan and Tran Xuan Bao, The Combination of Bipolar Electrolytic and Galvanic Method to Synthesize CuPt Nano-Alloy Electrocatalyst for Direct Ethanol Fuel Cell, Journal of Electronic Materials (2019), pp.6176-6182.

13. Mariano D. Susman, Yishay Feldman, Alexander Vaskevich, Israel Rubinstein, Chemical Deposition of Cu2O Nanocrystals with Precise Morphology Control. ACS Nano (2014), pp.162-174.

14. Liang Chen, Yu Zhang, Pengli Zhu, Fengrui Zhou, Wenjin Zeng, Daoqiang Daniel Lu, Rong Feng Sun, Chingping Wong, Copper salts mediated morphological transformation of Cu2O from cubes to hierarchical flower-like or microspheres and their supercapacitors performances, Scientific reports (2015), p.9672.

15. K. Gopalakrishnan C.Ramesh, V.Ragunathan, M.Thamilselvan, *Antibacterial activity of Cu2O nanoparticles on E Coli synthesized from Tridax Procumbens leaf extract and surface coating with polyaniline*, Digest Journal of Nanomaterials and Biostructures (2012), pp.833-839.

16. C. S. Liyanage, S. N. T. De Silva and C. A. N. Fernando, Green Synthesis, *Characterization and Antibacterial Activity of Cuprous Oxide Nanoparticles Produced from Aloe Vera Leaf Extract and Benedict's Solution*, International Journal of Nanoelectronics and Materials (2018), pp.129-136.

17. Wenting Wu, Wenjie Zhao, Yinghao Wu, Chengxu Zhou, Longyang Li, Zhixiong Liu,

18. Jianda Dong, Kaihe Zhou, Antibacterial behaviors of $Cu_2O$ particles with controllable morphologies in acrylic coatings, Applied Surface Science (2019), pp.279-287.

# CHẾ TẠO HẠT NANO $Cu_2O$ ỨNG DỤNG DIỆT KHUẨN BẰNG PHƯƠNG PHÁP ĐIỆN PHÂN SỬ DỤNG DÒNG LƯỠNG CỰC

***Tóm tắt:*** *Hạt nano oxit đồng (I) đã được chế tạo thành công bằng phương pháp điện phân sử dụng dòng lưỡng cực từ dung dịch chứa* $Cu(CH_3COO)_2.H_2O$ *(99.99%; Sigma Aldrich) và PVP (99.999%; Sigma Aldrich) với tỉ lệ khác nhau. Ảnh hưởng của nồng độ PVP lên các tính chất của mẫu đã được nghiên cứu. Phép phân tích thành phần pha cấu trúc của vật liệu bằng giản đồ nhiễu xạ tia X đã cho thấy sự xuất hiện pha tinh thể* $Cu_2O$ *tương ứng với cấu trúc lập phương tâm mặt. Ảnh SEM cũng cho thấy hình khối lập phương của* $Cu_2O$ *với hình thái bề mặt thay đổi theo nồng độ của PVP. Với nồng độ PVP 45.5 µM, mẫu có phân bố kích thước hạt đồng đều nhất. Sự xuất hiện đỉnh plasmon ở vùng bước sóng khoảng 500nm trên phổ hấp thụ đã tái khẳng định sự hình thành cấu trúc tinh thể* $Cu_2O$*. Hạt nano* $Cu_2O$ *có thể phân tán tốt trong nước và đã chứng tỏ khả năng diệt khuẩn đối với vi khuẩn E.coli bằng cách ức chế sự phát triển của vi khuẩn nằng trên đĩa thạch.*

***Từ khóa:*** $Cu_2O$*, điện phân lưỡng cực, kháng khuẩn, E.coli*

# THE CORRECTIONS TO THE HIGH ENERGY SCATTERING IN THE FRAMEWORK OF MODIFIED PERTURBATION THEORY

**Vu Toan Thang**
*University of Science – Hanoi Intenational University*

***Abstract***: *In the linearized gravitational theory, we follow up the lead to eikonal amplitude for two scalar particles at high energies with fixed momentum transfers based on quasi-potential equation in the framework of the modified perturbation theory. The scattering amplitude is calculated in detail with the Yukawa interaction potential. The results are also discussed and reviewed with Wallace calculations.*

***Keywords***: *Eikonal scattering, quantum gravity, quasi-potential equation*

Email: vuthang76@gmail.com

Received 10 October 2019
Accepted for publication 10 November 2019

## 1. INTRODUCTION

In the papers [1, 2, 11], the first correction to the leading eikonal amplitude of two scalar nucleons scattering are found by means of solving the Logunov-Tavkhelidze quasi-potential equation [2, 9, 10] and basing on modified perturbation theory. These corrections play a crucial role in such problems as strong gravitational forces near the black hole, string modification of the gravitational theory and some other effects of quantum gravity [1, 4].

The purpose of this paper is to continue to find the next correction term of the leading eikonal amplitude, and calculate the differential scattering cross section of these two particles that interact gravitationally with each other by exchanging graviton with $\mu$ mass, corresponding to the Yukawa interaction potential.

This paper is organized as follows. In the second section, the solution of the Logunov-Tavkhelidze quasi-potential equation is introduce briefly by using the modified perturbation method. The asymptotic equation of amplitude scattering at high energies and fixed momentum transfer is also considered systematically. We also derive the analytical formulas for the leading term, the first and second corrections terms for the scattering amplitude. Section 3 is devoted to compute the scattering amplitude for the Yukawa potential in the linearized gravity in the effective radius region R. Note that, the collision parameters which were selected here are less than the Compton wavelength of the scattering particle and the effective radius R, graviton mass $\mu$, gravity constant $\kappa$ are determined by analytical expression of the scattering amplitude [12]. Finally, we discuss the results obtained and compare them with Wallace's results for this problem [13].

## 2. THE LEADING EIKONAL SCATTERING AMPLITUDE AND ITS CORRECTIONS

The scattering amplitude of two scalar nucleons by exchanging scalar mesons is found from the Logunov-Tavkhelidze equation with local quasi – potential on the mass shell [9]:

$$T\left(\vec{p},\vec{p}';s\right)=gV\left(\vec{p}-\vec{p}';s\right)+g\int d\vec{q}K\left(\vec{q}^{\,2};s\right)V\left(\vec{p}-\vec{q};s\right)T\left(\vec{q},\vec{p}';s\right), \quad (2.1)$$

where $K\left(\vec{q}^{\,2};s\right)=\left(1\big/\sqrt{\vec{q}^{\,2}+m^2}\right)\left[1\big/\left(\vec{q}^{\,2}+m^2-s\big/4-i\varepsilon\right)\right]$ is the kernel,

$$s=4E^2=4\left(\vec{p}^{\,2}+m^2\right)=4(\vec{p}'^2+m^2)$$

is the total energy and $\vec{p}$, $\vec{p}\,'$ are the relativistic momentums of two particles in the center of the mass reference frame in the initial and final states respectively. Equation (2.1) is one of the possible generalizations of the Lippman-Schwinger equation for the case of relativistic quantum field theory. The quasi-potential $V$ in Eq. (2.1) is a complex function of the energy and relativistic momenta. The quasi-potential equation simplifies considerably if $V\left(r,s\right)$ is a function that depends only of the relative momenta and the total energy i.e. if the quasi-potential is local.

Performing the Fourier transformations and defining the pseudo-differential operator, $\hat{L}_r=K\left(-\nabla_r^2;s\right)$, Eq (2.1) is rewritten in an operator form as

$$F\left(\vec{r},\vec{r}\,';s\right)=\delta^{(3)}\left(\vec{r}-\vec{r}\,'\right)+g\hat{L}_r\left[V\left(\vec{r};s\right)F\left(\vec{r},\vec{r}\,';s\right)\right] \quad (2.2)$$

Within the framework of the quasi-potential approach, the potential is defined by expanding it into infinite series in order of the g – coupling constant. It corresponds to the expansion of perturbation amplitude on the mass shell. Using this method, the relativistic eikonal expression of the scattering amplitude was found in quantum field theory with large energy and small momentum transfer.

On the other hand, we can strengthen the above perturbation theory by the modified perturbation theory proposed by Fradkin[1] [6, 7], that was based on a combination of functional integral method and covariant perturbation theory.

The solution of eq. (2.2) is written in the symbolic form:

$$F\left(\vec{r},\vec{r}\,';s\right)=\frac{1}{\left(2\pi\right)^3}\int d\vec{k}\,\exp\left[W(\vec{r},\vec{k};s)\right]\ e^{-i\vec{k}(\vec{r}-\vec{r}\,')} \tag{2.3}$$

Substitute Eq.(2.3) into Eq.(2.2), we obtain an equation for the function $W\left(\vec{r},\vec{k};s\right)$

$$\exp\left[W\left(\vec{r},\vec{k};s\right)\right]=1+g\hat{L}_r\left[V\left(\vec{r};s\right)\mathrm{e}^{W\left(\vec{r},\vec{k};s\right)-i\vec{k}\vec{r}}\right]e^{i\vec{k}\vec{r}\,'} \tag{2.4}$$

Using the idea of the modified perturbation theory in exponent function we can write the function $W\left(\vec{r},\vec{k};s\right)$ as an expansion in series in the coupling constant $g$, we can obtain a system of equations connected with each other in successive approximations.

Restricting the treatment to only $W_1\left(\vec{r},\vec{k};s\right)$ instead of $W\left(\vec{r},\vec{k};s\right)$ in Eq. (2.2) we obtain approximate expression for the scattering amplitude

$$T_1\left(\vec{p},\vec{p}\,';s\right)=\frac{g}{\left(2\pi\right)^3}\int d\vec{r}\,e^{i(\vec{p}-\vec{p}\,')\vec{r}}\,V\left(\vec{r};s\right)e^{gW_1\left(\vec{r};\vec{p};s\right)}\,. \tag{2.5}$$

Take the $z-$ axis along the $\left(\vec{p}+\vec{p}\,'\right)$ momentum of the incident particles and use Mandelstam variables, we find asymptotic behavior of the scattering amplitude at high energy and fixed momentum transfers.

Making calculations in the limit of high energies $s\to\infty$ and fixed $t$ - momentum transfers, we finally obtain

---

[1] In quantum field theory, two methods are commonly used to find the scattering amplitude i/ The covariant perturbation theory: The theory based on the expansion of the coupling constant g; ii/ Functional integral method: do not expand according to the coupling constant, but use the inverse operator representation according to Fock [14], Feynman [15] in exponential form $Z^{-1}=i\int_0^\infty e^{iZs}...ds$, closed form expression of two-particle scattering amplitude is represented by the path integrals, in which the interaction is done through the exchange of virtual quanta (scalar or vector, or tensor with mass $\mu$) including quantum linear gravity [4].

$$
\begin{aligned}
T(s,t)\Big|_{\substack{s\to\infty;\\ t-fixed}} = &-\frac{is}{2(2\pi)^3}\int d^2\vec{r}_\perp dz e^{i\vec{\Delta}_\perp\vec{r}_\perp}\left\{\exp\left[\frac{2ig}{s}\int_{-\infty}^{\infty}dzV\left(\sqrt{\vec{r}_\perp^{\,2}+z^2};s\right)\right]-1\right\}\\
&-\frac{6g^2}{(2\pi)^3 s\sqrt{s}}\int d^2\vec{r}_\perp e^{i\vec{\Delta}_\perp\vec{r}_\perp}\exp\left[\frac{2ig}{s}\int_{-\infty}^{\infty}dz'V\left(\sqrt{\vec{r}_\perp^{\,2}+z'^2};s\right)\right]\times\int_{-\infty}^{\infty}dzV^2\left(\sqrt{\vec{r}_\perp^{\,2}+z^2};s\right)
\end{aligned}
$$

$$
\begin{aligned}
&-\frac{ig}{(2\pi)^3\sqrt{s}}\int d^2\vec{r}_\perp e^{i\vec{\Delta}_\perp\vec{x}_\perp}\int_{-\infty}^{\infty}dz\left\{\exp\left[\frac{2ig}{s}\int_{z}^{\infty}dz'V\left(\sqrt{\vec{r}_\perp^{\,2}+z'^2};s\right)\right]-\exp\left[\frac{2ig}{s}\int_{-\infty}^{\infty}dz'V\left(\sqrt{\vec{r}_\perp^{\,2}+z'^2};s\right)\right]\right\}\\
&\qquad\times\left\{\int_{-\infty}^{\infty}dz''V\left(\sqrt{\vec{r}_\perp^{\,2}+z''^2};s\right)-\frac{2ig}{s}\left[\int_{z}^{\infty}dz'\vec{\nabla}_\perp V\left(\sqrt{\vec{r}_\perp^{\,2}+z'^2};s\right)\right]^2\right\}\\
&-\frac{ig}{(2\pi)^3\sqrt{s}}\vec{\Delta}_\perp^2\times\int d^2\vec{r}_\perp e^{i\vec{\Delta}_\perp\vec{r}_\perp}\int_{-\infty}^{\infty}zdzV\left(\sqrt{\vec{r}_\perp^{\,2}+z^2};s\right)\exp\left[\frac{2ig}{s}\int_{z}^{\infty}dz'V\left(\sqrt{\vec{r}_\perp^{\,2}+z'^2};s\right)\right]+\ldots \qquad (2.6)
\end{aligned}
$$

In Eq. (2.6), the first term describes the leading eikonal behavior of scattering amplitude, while the remaining terms determine the corrections of relative magnitude $1/\sqrt{s}$. Due to the smoothness of the potential $V$ at high energy $s\to\infty$ the change of the particle momentum $\vec{\Delta}_\perp$, is relatively small. Therefore, the terms proportional to $\vec{\nabla}_\perp^2 V$ in Eq. (2.6) can be neglected, now we have:

$$
T^{(0)}(s;t) = -\frac{is}{2(2\pi)^3}\int d^2\vec{r}_\perp e^{i\vec{\Delta}_\perp\vec{r}_\perp}\left\{\exp\left[\frac{2ig}{s}\int_{-\infty}^{\infty}dzV\left(\sqrt{\vec{r}_\perp^{\,2}+z^2};s\right)\right]-1\right\} \qquad (2.7)
$$

$$
\begin{aligned}
T^{(1)}(s;t) = &-\frac{12g^2}{(2\pi)^3 s\sqrt{s}}\int d^2\vec{r}_\perp e^{i\vec{\Delta}_\perp\vec{r}_\perp}\exp\left[\frac{2ig}{s}\int_{-\infty}^{\infty}dzV\left(\sqrt{r_\perp^2+z^2};s\right)\right]\\
&\times\int_0^{\infty}dz\left(\frac{4}{3}+\frac{r}{3}\frac{d}{dr}\right)V^2\left(\sqrt{r_\perp^2+z^2};s\right)
\end{aligned} \qquad (2.8)
$$

$$
\begin{aligned}
T^{(2)}(s;t) = &\frac{24g^3}{(2\pi)^3 s^3}\int d^2\vec{r}_\perp e^{i\vec{\Delta}_\perp\vec{r}_\perp}\exp\left[\frac{2ig}{s}\int_{-\infty}^{\infty}dzV\left(\sqrt{r_\perp^2+z^2};s\right)\right]\\
&\times\int_0^{\infty}dz\left(5+2r\frac{d}{dr}\right)V^3\left(\sqrt{r_\perp^2+z^2};s\right)
\end{aligned} \qquad (2.9)
$$

The correction terms (2.8), (2.9) are equivalent to Wallace's corrections [13] (see Appendix).

For the first term from Eq. (2.6) in the limit of high energies s → ∞ and for fixed $t$ - momentum transfers, with the assumption of smooth behavior the smooth behavior of the quasipotential as a function of the relative coordinate of two "nucleons", in the framework of quantum field theory we find the leading eikonal of the high energy scattering amplitude

$$T^{(0)}(s;t) = -\frac{is}{2(2\pi)^3}\int d^2\vec{r}_\perp e^{i\vec{\Delta}_\perp \vec{r}_\perp}\left[e^{i\chi_0(r_\perp;s)}-1\right] \tag{2.10}$$

with $\chi_0(|r_\perp|;s) = -\frac{g^2}{(2\pi)^2 s}K_0(\mu|r_\perp|)$; $K_0(\mu|\vec{r}_\perp|) = \frac{1}{2\pi}\int d^2k_\perp \frac{e^{-i\vec{k}_\perp \vec{r}_\perp}}{k_\perp^2+\mu^2}$, where $|\vec{r}_\perp|$ is a two-dimensional vector perpendicular to the "nucleons" – collision direction (the impact parameter), $K_0(\mu|\vec{r}_\perp|)$ is Mac Donald function of zeroth order, $\mu$ is a graviton mass which serves as an infrared cut-off , and $\chi_0(|r_\perp|;s)$ is the eikonal phase function.

In the framework of the quasipotential approach and the modified perturbation theory a systematic scheme of finding the leading eikonal scattering amplitudes and its corrections are developed and constructed in quantum field theory including the linearized gravity. The first and second correction to leading eikonal amplitude is found.

## 3. THE ASYMPTOTIC TERMS OF THE SCATTERING AMPLITUDE IN THE YUKAWA POTENTIAL

In this section, the interaction of two "nucleon" with the Yukawa interaction potential in linearized gravity is considered. It is the result of the exchange of gravitons with mass $\mu$.

In case of tensor model[2] the quasi-potential Yukawa increases with energy

$$V(r,s) = \frac{\kappa^2 s}{2\pi}\frac{e^{-\mu r}}{r} \tag{3.1}$$

---

[2] The model of interaction of a scalar "nucleons" with a gravitational field in the linear approximation to $h_{\mu\nu}(x)$ $L(x) = L_{0,\varphi}(x) + L_{0.grav}(x) + L_{\text{int}}(x)$ where:

$$L_{0,\varphi}(x) = \frac{1}{2}\left[\partial^\mu\varphi(x)\partial_\mu\varphi(x) - m^2\varphi^2(x)\right];\ L_{\text{int}}(x) = -\frac{\kappa}{2}h^{\mu\nu}(x)T_{\mu\nu}(x);$$

$T_{\mu\nu}(x) = \partial_\mu\varphi(x)\partial_\nu\varphi(x) - \frac{1}{2}\eta_{\mu\nu}\left[\partial^\mu\varphi(x)\partial_\mu\varphi(x) - m^2\varphi^2(x)\right]$; and $T_{\mu\nu}(x)$ is the energy momentum tensor of the scalar field. The coupling constant $\kappa$ is related to Newton's constant of gravitation $G$ by $\kappa^2 = 32\pi G = 32\pi l_{PL}^2$. $l_{PL} = 1,6.10^{-33}cm$ is the Planck length.

The leading eikonal behavior and the first correction terms of the scattering amplitude have been calculated in the paper [1, 2]

$$T^{(0)}_{Tensor}(s;t)\Big|_{\substack{s\to\infty \\ t-fixed}} = \frac{\kappa^2 s}{(2\pi)^4}\cdot\left[\frac{1}{\mu^2 - t} - \frac{\kappa^4}{2(2\pi)^2}F_1(t) + \frac{\kappa^7}{3(2\pi)^5}F_2(t)\right] \tag{3.2}$$

$$T^{(1)}_{Tensor}(s;t)\Big|_{\substack{s\to\infty \\ t-fixed}} = \frac{3i\kappa^6\sqrt{s}}{(2\pi)^6}\left[F_1(t) + \frac{2\kappa^4}{(2\pi)^3}F_2(t)\right] \tag{3.3}$$

where
$$F_1(t) = \frac{1}{t\sqrt{1-\frac{4\mu^2}{t}}}\ln\left|\frac{1-\sqrt{1-4\mu^2/t}}{1+\sqrt{1-4\mu^2/t}}\right| \tag{3.4}$$

$$F_2(t) = \int_0^1 dy \frac{1}{(ty+\mu^2)(y-1)}\ln\left|\frac{\mu^2}{y(ty+\mu^2-t)}\right| \tag{3.5}$$

We know that one of specific characteristics of gravitational force is too large at the Planck scale [4]. These forces exist only in some region with a finite radius in contrast with the Coulomb force which decreases slowly with distance squared. This is connected with the fact that the Coulomb force between charged particles appear as a result of the exchange of photon – massless particles, while the gravitational forces arise from the exchange of massive particle.

Due to the analytic nature of the scattering amplitude in the high energy region and fixed momentum transfer, Nguyen Van Hieu [12] has shown the effective interaction radius $R$ for gravitons with the same mass $\mu$ ($R$ can be considered as the effective radius in the region where the nuclear force is still active)

$$R = \frac{1}{\mu}\ln\left|\frac{\kappa^2 s}{2\pi}\right| \tag{3.6}$$

Here, we note that, the potential $V(r,s)$ is very small and can be ignored at a distance greater than $R$. And for each determined value of s, the effective radius $R$ is finite so the scattering amplitude is finite. Therefore the addition of terms contained in the scattering expression (3.2), (3.3) is that we have not considered the loop corrections for the scattering amplitude. The scattering process is equivalent to the following ladder diagrams

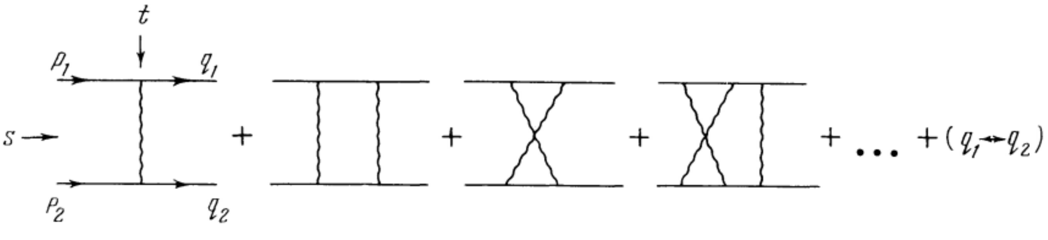

If we ignore the loop corections (ie only taking into account the ladder diagrams), we can ignore the terms that contain $F_2(t)$ function and keep the terms that contain $F_1(t)$ function.

It should be noted that, according to the formula (C.4), (C.5) in Appendix C of paper [1], the expression of the $F_1(t)$ function is:

$$F_1(t)=2\int d|\vec{r}_\perp||\vec{r}_\perp|J_0\left(\Delta_\perp|\vec{r}_\perp|\right)K_0^2\left(\mu|\vec{r}_\perp|\right) \tag{3.7}$$

We consider the collision parameters are small compared to the Compton wavelength of the scattering particle $|x_\perp|\le\lambda=\frac{1}{p_0};p_0=\left(\sqrt{s}/2\right)\to\infty$ and use the approximation [11]:

$$K_0\left(\mu|r_\perp|\right)\Big|_{|r_\perp|\to0}\approx\ln^2\frac{s}{\mu^2} \tag{3.8}$$

Substitute (3.8) into (3.7), we get:

$$F_1(t)=2\ln^2\frac{s}{\mu^2}\int d|\vec{r}_\perp||\vec{r}_\perp|J_0\left(\Delta_\perp|\vec{r}_\perp|\right)K_0\left(\mu|\vec{r}_\perp|\right)=2\ln^2\frac{s}{\mu^2}.\frac{1}{\Delta_\perp^2+\mu^2}=2\ln^2\frac{s}{\mu^2}.\frac{1}{\mu^2-t} \tag{3.9}$$

We obtain the leading term and first correction of the high energy scattering amplitude

$$T_{Tensor}^{(0)}(s;t)=\frac{\kappa^2 s}{(2\pi)^4}.\frac{1}{\mu^2-t}\left[1-\frac{\kappa^4}{(2\pi)^2}\ln^2\frac{s}{\mu^2}\right] \tag{3.10}$$

$$T^{(1)}(s;t)=\frac{6i\kappa^6\sqrt{s}}{(2\pi)^6}\frac{1}{\mu^2-t}\ln^2\frac{s}{\mu^2} \tag{3.11}$$

The second correction term in the eq.(2.9) is further calculated by using eq.(3.8) . We have:

$$K_1\left(3\mu|r_\perp|\right)\Big|_{|r_\perp|\to0}\approx\frac{\sqrt{s}}{3\mu}\ln\frac{s}{9\mu^2} \tag{3.12}$$

Then, we derive the final expression of the second correction term

$$T^{(2)}(t;s)=-\frac{48\kappa^9\sqrt{s}}{(2\pi)^5\sqrt{-t}}\ln\left(\frac{s}{9\mu^2}\right) \tag{3.13}$$

And now the expression of the eikonal scattering amplitude to the second order approximation has form:

$$T_{Tensor}(s;t)=\frac{\kappa^2 s}{(2\pi)^4}\frac{1}{\mu^2-t}\left[1-\frac{\kappa^4}{(2\pi)^2}\ln^2\frac{s}{\mu^2}\right]+\frac{6i\kappa^6\sqrt{s}}{(2\pi)^6\left(\mu^2-t\right)}\ln^2\frac{s}{\mu^2}-\frac{48\kappa^9\sqrt{s}}{(2\pi)^5\sqrt{-t}}\ln\left(\frac{s}{9\mu^2}\right) \tag{3.14}$$

The scattering amplitude at the second order is:

$$\begin{aligned}\frac{d\sigma}{d\Omega}=&\left[\frac{\kappa^2 s}{(2\pi)^4\left(\mu^2-t\right)}-\frac{\kappa^6 s}{(2\pi)^6\left(\mu^2-t\right)}\ln^2\frac{s}{\mu^2}-\frac{48\kappa^9\sqrt{s}}{(2\pi)^5\sqrt{-t}}\ln\left(\frac{s}{9\mu^2}\right)\right]^2\\&+\frac{36\kappa^{12}s}{(2\pi)^{12}\left(\mu^2-t\right)^2}\ln^4\frac{s}{\mu^2}\end{aligned} \tag{3.15}$$

All considerations here are restricted to the case masses of two particles are equal $m_1 = m_2 = m$. We have in the s-channel (c.m system) with Mandelstam variables:

$$s=4(m^2+p^2);t=-\Delta_{\perp}^2=-4p^2\sin^2\frac{\theta}{2}\Rightarrow t_{\min}=-4p^2=4m^2-s\geq -s \tag{3.16}$$

Comparing the relative magnitude of both correction terms from eqs.(3.11) and (3.13) we see that:

$$\left|T^{(1)}(s;t)\right|\approx\left|\frac{6\kappa^6\sqrt{s}}{(2\pi)^6}\frac{1}{\mu^2-t}\ln^2\frac{s}{\mu^2}\right|\approx\frac{6\kappa^6}{(2\pi)^6}\frac{\sqrt{s}}{\mu^2+s}\ln^2\frac{s}{\mu^2} \tag{3.17}$$

$$\left|T^{(2)}\left(t;s\right)\right|\approx\frac{48\kappa^9\sqrt{s}}{(2\pi)^5\sqrt{-t_{\min}}}\ln\left(\frac{s}{9\mu^2}\right)=\frac{48\kappa^9}{(2\pi)^5}\ln\left(\frac{s}{9\mu^2}\right) \tag{3.18}$$

From eqs. (3.11), (3.13), we see obviously the first and second correction terms in the scattering amplitude increasing with total energy $\sqrt{s}$. However, at the high energy limit according to the eqs.(3.17) and (3.18), the first correction term decreases with energy and gives a small contribution to the scattering amplitude, while the second correction term gives significant contribute to the scattering amplitude at extremely high energies (if total energy has a relative magnitude when compared to the gravitational coupling constant).

## 4. CONCLUSION

In the framework of the modified perturbation theory and the quasi – potential equation, a systematic scheme of finding the leading eikonal scattering amplitudes and its corrections [1] are developed and constructed. The first and second non-leading corrections to leading eikonal amplitude are found.

In the linearized gravity, the interaction between of scattered “nucleons” by exchanging graviton corresponds to the smooth quasi-potential of the Yukawa type. The new results in this paper are that we have found the second correction term for the scattering amplitude and clarify the dependence of the differential scattering section on total energy in the linearized gravitational theory. The contributions of the correction terms for the scattering amplitude are determined at the Compton wavelength distance of scattering particles, at high energy and low momentum transfer.

Note that, the analytical terms of the leading term and the correction terms of the scattering amplitude obtained in this paper coincide with those obtained by Wallace on this issue.

***Acknowledgements:*** *The author is grateful to Prof. Nguyen Suan Han for his suggestions of the problem and many useful comments. This work was supported in part by Vietnam National Foundation for Science and Technology Development (NAFOSTED) under grant number 103.01-2018.42.*

## Appendix. WALLACE’S CORRECTION

The amplitude for the scattering of a particle with momentum $\vec{p}$ to $\vec{p}'$ is

$$T(\vec{p},\vec{p}') = \int d^3\vec{r} e^{-i\vec{p}'\vec{r}} T e^{i\vec{p}\vec{r}} \tag{A.1}$$

The Wallace’s correction is derived from an expansion of the scattering $T$ matrix whose exact form reads [13]:

$$T = (V + VGV) \tag{A.2}$$

where $G$ is the exact propagator defined by $G^{-1} = k^2\big/2m - p^2\big/2m - V + i\eta$ (A.3)

This propagator can be expressed in terms of the eikonal propagator $g$ and a corrective term $N$ accounting for the deviations of the momentum from the average momentum:

$$G = g + gNG \tag{A.4}$$

The eikonal propagator can be derived by expanding the momentum $\vec{p}$ around the average momentum and neglecting the quadratic terms

$$g^{-1} = \vec{v}.(\vec{k} - \vec{p}) - V + i\eta \tag{A.5}$$

and its correction is defined by $N = \left(1 - \cos\theta\big/2\right)\left(g^{-1} + V\right) + \frac{\hbar^2}{2m}\left(\vec{p} - \vec{k}_f\right).\left(\vec{p} - \vec{k}_i\right),$ (A.6)

where $\vec{v}$ is the average velocity.

Wallace has obtained an expansion of the $T$ matrix by inserting iteratively the relation Eq. (A.4) into Eq. (A.2)

$$T = \left(V + VgV\right) + VgNgV + VgNgNgV + VgNgNgNgV + \ldots \tag{A.7}$$

Substitute (A.6) into (A.1), the scattering amplitude can be expressed as:

$$T\left(\vec{p}, \vec{p}'\right) = \int d^3\vec{r} e^{-i\vec{p}'\vec{r}} \left[\left(V + VgV\right) + VgNgV + VgNgNgV + \ldots\right] e^{i\vec{p}\vec{r}} \tag{A.8}$$

Because of the rotational invariance of the potential, the correction terms depending explicitly on the scattering angle $\theta$ cancel. The zeroth order $T^{(0)}$ corresponds to the leading eikonal model:

$$T^{(0)} = \int d^3\vec{r} e^{-i\vec{p}'\vec{r}} \left(V + VgV\right) e^{i\vec{p}\vec{r}} = vi \int d^2\vec{r}_\perp e^{i\vec{\Delta}_\perp \vec{r}_\perp} \left[e^{i\chi_0\left(r_\perp\right)} - 1\right] \tag{A.9}$$

where
$$\chi_0\left(r_\perp\right) = -\frac{1}{v} \int_{-\infty}^{\infty} dz V\left(r\right). \tag{A.10}$$

Wallace has derived the corrections of the scattering amplitude:

$$T^{(1)} = \frac{1}{vk} \int d^2\vec{r}_\perp e^{i\vec{\Delta}_\perp \vec{r}_\perp} e^{i\chi_0\left(r_\perp\right)} \int_0^{\infty} dz \left(2 + r\frac{d}{dr}\right) V^2\left(r\right) \tag{A.11}$$

$$\begin{aligned} T^{(2)} = -iv \int d^2\vec{r}_\perp e^{i\vec{\Delta}_\perp \vec{r}_\perp} e^{i\chi_0\left(r_\perp\right)} \Bigg\{ & \frac{i}{v^3k^2} \int_0^{\infty} dz \left(\frac{8}{3} + \frac{7}{3} r\frac{d}{dr} + \frac{1}{3} r^2 \frac{d^2}{dr^2}\right) V^3\left(r\right) + \\ & + \frac{ir_\perp \left[\chi_0'\left(r_\perp\right)\right]^3}{24k^2} + \frac{r_\perp \chi_0'\left(r_\perp\right) \nabla^2 \chi_0\left(r_\perp\right)}{8k^2} \Bigg\} \end{aligned} \tag{A.12}$$

If $\chi_0\left(r_\perp\right)$ is a fast function, we can skip the term that contain $\nabla^2\chi_0\left(r_\perp\right)$, we obtain:

$$T^{(2)} = \frac{1}{v^2k^2} \int d^2\vec{r}_\perp e^{i\vec{\Delta}_\perp \vec{r}_\perp} e^{i\chi_0\left(r_\perp\right)} \int_0^{\infty} dz \left(\frac{8}{3} + \frac{7}{3} r\frac{d}{dr} + \frac{1}{3} r^2 \frac{d^2}{dr^2}\right) V^3\left(r\right) \tag{A.13}$$

## REFERENCES

1. Nguyen Suan Han, Do Thu Ha, Nguyen Nhu Xuan (2019), "The contribution of effective quantum gravity to the high energy scattering in the framework of modified perturbation theory and one loop approximation", - *Eur. Phys. J. C*, 79:835.

2. Nguyen Suan Han, Le Thi Hai Yen, Nguyen Nhu Xuan (2012), "High Energy Scattering in the Quasipotential Approach", - *Int. J. Mod. Phys. A*, Vol. 27, 1250004-19.

3. Nguyen Suan Han (2000), “Straight-line path approximation for high energy elastic and inelastic scattering in quantum gravity”, - *Eur. Phys. J. C*, 16, pp.547-553.
4. Nguyen Suan Han and Nguyen Nhu Xuan (2002), “Planck scattering beyond the eikonal approximation in the functional approach”, - *Eur. Phys. J. C*, 24, pp.643-651.
5. R. J. Glauber (1959), “High-Energy Collision Theory”, - *Lectures in Theoretical Physics*, Vol. 1, pp.315-414.
6. E.S. Fradkin (1966), “Application of functional methods in quantum field theory and quantum statistics (II)”, - *Nuclear Physics*, Vol. 76, pp.588-624.
7. E.S. Fradkin, U. Esposito and S. Termini (1970), “Functional Techniques in Physics”, - *La Rivista del Nuovo Cimento*, Vol. II, No. 4, pp.498-560.
8. Nguyen Suan Han, Le Anh Dung, Nguyen Nhu Xuan and Vu Toan Thang (2016), “High Energy Scattering of Dirac Particles on Smooth Potentials”, - *Int. J. Mod. Phys. A*, Vol. 31, No. 23, pp.1650126-18.

A. Logunov and A. N. Tavkhelidze (1963), “Quasipotential approach in quantum field theory”, - *Nuovo Cimento.*, Vol. 29, pp.380-399.

9. Nguyen Van Hieu and R. N. Faustov (1964), “Quasi-Optical Potential in Quantum Field Theory”, - *Nuclear Physics*, Vol. 53, pp.337-344.
10. Nguyen Suan Han, Nguyen Nhu Xuan, Vu Toan Thang (2017) “Applying the Modified Perturbation Theory to High Energy Scattering in the Quasi-Potential Approach”, - *J. Phys. Sci. Appl*, Vol. 7(4), pp.47-58.
11. Nguyen Van Hieu (1970), “Analytical Properties of the Scattering Amplitude and Asymptotic Theorems”, - *Proceedings of the International Conference on High Energy Physics*, Kiev, pp.564-593.
12. S. J. Wallace (1973), “Eikonal Expansion”, - *Annals of Physics,* Vol. 78, pp.190-257.
13. V. A. Fock (1961), Fizmatgiz, Moscow.
14. R. P. Feynman (1951), “An Operator Calculus Having Applications in Quantum Electrodynamics”, - *Phys. Rev.,* Vol. 84, pp.108-128.

# BỔ CHÍNH CHO BIÊN ĐỘ TÁN XẠ NĂNG LƯỢNG CAO TRONG KHUÔN KHỔ LÝ THUYẾT NHIỄU LOẠN CẢI BIẾN

***Tóm tắt:*** *Trong lý thuyết hấp dẫn tuyến tính, chúng tôi đã thu được biên độ eikonal cho tán xạ hai hạt vô hướng ở năng lượng cao và xung lượng truyền không đổi, dựa trên phương trình chuẩn thế trong khuôn khổ lý thuyết nhiễu loạn cải biến. Biên độ tán xạ được tính toán chi tiết với thế tương tác Yukawa. Kết quả được thảo luận và so sánh với tính toán của Wallace.*

***Từ khóa:*** *Tán xạ Eikonal, hấp dẫn lượng tử, phương trình chuẩn thế*

# EXPLOITATION OF THE ROLE OF MESON DELTA IN ANOTHER NUCLEAR NUTRITION

**Le Huy Son, Bui Thi Phuong Thuy, Ta Anh Tan**
*Hanoi Metropolital Univesity*

***Abstract:*** *By expanding the calculations [7] we investigated a four-nucleon model of the nucleus which takes into account the delta meson. The main results show that without the addition of Goguta-Bodmer, the expected compression value* $K_0 = 240\ MeV$ *is still obtained, and the slope and curvature of the symmetrical energy are also consistent with the experiment. It should be further emphasized that, in the approximation of the Lagrangian 2.2 mean field, the equivalent of the Lagrangian of the Waleka model is the one that gave an inappropriate value of the compression* $K_0 = 540\ MeV$*. This suggests that the contribution of the loop schema has increased the porosity of the nucleus, thus again confirming the important role of the loop [8]. Therefore, the study of a four-nucleon model at a higher approximation than the average field approximation would be most suitable for examining many fundamental phenomena of both nuclear and cosmological physics.*

***Keywords:*** *Meson delta, sigma, omega ...*

Email: tatan@hnmu.edu.vn

Received 10 October 2019
Accepted for publication 10 November 2019

## 1. INTRODUTION

The use of collisions between heavy ions, especially the nuclear reactions caused by radioactive beams, is important for studying many nuclear phenomena and their applications in cosmology. Theoretically, the survey of nuclear properties just stopped at the approximate average field and symmetric nucleus. So one of the urgent requirements is to extend the higher approximation and examine the asymmetric nuclei. Solving this problem could help detect new physical effects generated in asymmetric nuclei. In the work [8] with the calculation of $\sigma$, $\omega$ and $\rho$ mesons in the four-nucleon interaction model, the authors calculated the energy of the symmetrical nucleus and found that the approximate Hartree-Fock the dependence on the density of energy is in good agreement with recent empirical data. However, the value of the compression ratio (incompressibility) is too large compared to the accepted values. To overcome this shortcoming, we proceeded to add delta meson to the considered model.

## 2. EXPERIMENTAL

Learn about quantum field theory methods at finite temperature and density, in which we delve into the effective acting method CJT (introduced by J. M. Cornwall, R. Jackiw and E. Tomboulis in 1974).

Applied to nuclear research described by Lagrangien density:

$$\mathcal{L} = \bar{\psi}\big(i\widehat{\partial - M}\big)\psi + \frac{G_\sigma}{2}(\bar{\psi}\psi)^2 - \frac{G_\omega}{2}(\bar{\psi}\gamma^\mu\psi)^2 + \frac{G_\rho}{2}(\bar{\psi}\vec{\tau}\gamma^\mu\psi)^2 + \frac{G_\delta}{2}(\bar{\psi}\vec{\tau}\psi)^2$$

Here $\psi$(x) is the nucleon field, $\vec{\tau}$ is the isotopic spin matrix, $G_\sigma$, $G_\omega$, $G_\rho$ and $G_\delta$ are the interaction constants.

Thus, by summarizing the effective method for composite operators, we have come to the final goal: Presentation of the effective form of quantum field theory at finite temperatures. Presentation of the effective formalism of quantum field theory at finite temperatures. Through the presentation, we also focus more on the NJL model and the NJL Gauge for low energy phenomena. These models are favored for research because they describe quite well the low-energy Hadron world both qualitatively and quantitatively. From here we will have a useful tool for investigating phenomena occurring in Hadron with finite temperature and density, it is also an effective tool to investigate phase transitions.

The use of collisions between heavy ions, especially the nuclear reactions caused by the radiation beam, is important for studying many nuclear phenomena and their applications in cosmology. It should be emphasized that the symmetric energy of the nucleus is determined by the expression

$$E_{sym}(\rho_B) = \frac{1}{2}\left(\frac{\partial^2 \epsilon_{bind}(\rho_B, \alpha)}{\partial \alpha^2}\right)_{\alpha=0} \tag{2.1}$$

together with related quantities plays a key role in understanding the dynamics of heavy ion interactions [1] and the structure of nucleon rich nuclei [3]. In Equation (3.1) $\epsilon_{bind}$ is the binding energy of asymmetric nucleus, $\rho_B = \rho_p + \rho_n$ *and* $\alpha = (\rho_n - \rho_p)/\rho_B$ with $\rho_p$

and $\rho_n$ are proton and neutron density, respectively. In the work [7] taking into account the mesons σ; ω; ρ in the 4-nucleon interaction model, the authors calculated the energy of the symmetric nucleus and found that in the approximate Hartree-Fock (HF) the dependence of the symmetric energy $E_{sym}(\rho_B)$ fits well with Recent empirical data. However, the value of the compression ratio (incompressibility) $K_0$ = 547,56 MeV is too large compared with the accepted values. To overcome this shortcoming, we have added meson δ to the model under consideration. Specifically, a system of properties of asymmetric nuclei was described by the following Lagrangian density.

$$\mathcal{L} = \bar{\psi}\left(i\widehat{\partial - M}\right)\psi + \frac{G_\sigma}{2}(\bar{\psi}\psi)^2 - \frac{G_\omega}{2}(\bar{\psi}\gamma^\mu\psi)^2 + \frac{G_\rho}{2}(\bar{\psi}\vec{\tau}\gamma^\mu\psi)^2 + \frac{G_\delta}{2}(\bar{\psi}\vec{\tau}\psi)^2 \qquad (2.2)$$

Here $\psi$(x) is the nucleon field, $\vec{\tau}$ is the isotopic spin matrix, $G_\sigma$, $G_\omega$, $G_\rho$ and $G_\delta$ are the interaction constants.

Proceed to bosonization of the Lagrangian density (3.2) by placing

$$\breve{\sigma} = \frac{g_\sigma}{m_\sigma^2}\bar{\psi}\psi, \breve{\omega}_\mu = \frac{g_\omega}{m_\omega^2}\bar{\psi}\gamma_\mu\psi$$

$$\vec{\breve{b}}_\mu = \frac{g_\rho}{m_\rho^2}\bar{\psi}\vec{\tau}\gamma_\mu\psi, \vec{\breve{d}} = \frac{g_\delta}{m_\delta^2}\bar{\psi}\vec{\tau}\psi$$

We obtained:

$$\mathcal{L} = \bar{\psi}\left(i\widehat{\partial - M}\right)\psi + g_\sigma\bar{\psi}\breve{\sigma}\psi - g_\omega\bar{\psi}\gamma^\mu\vec{\tau}\psi + g_\sigma\bar{\psi}\gamma^\mu\vec{\tau}\vec{\breve{b}}_\mu\psi + g_\delta\bar{\psi}\vec{\tau}\vec{\breve{d}}\psi - \frac{m_\sigma^2}{2}\breve{\sigma}^2 + \frac{m_\omega^2}{2}\breve{\omega}^\mu$$
$$- \frac{m_\rho^2}{2}\breve{b}^\mu\vec{\breve{b}}_\mu - \frac{m_\delta^2}{2}\vec{\breve{d}}\vec{\breve{d}} \qquad (2.3)$$

Where $G_{\sigma,\omega,\rho,\delta} = g_{\sigma,\omega,\rho,\delta}^2/m_{\sigma,\omega,\rho,\delta}^2$ and N and P are the masses of the corresponding mesons.

Where $G_{\sigma,\omega,\rho,\delta} = g_{\sigma,\omega,\rho,\delta}^2/m_{\sigma,\omega,\rho,\delta}^2$; $m_\sigma, m_\omega, m_\rho$ and $m_\delta$ are the masses of the mesons, respectively.

Note that the bosonization technique above ensures that the binding states of nucleons and antiparticles have quantum numbers (spin, isotope spin and products) of mesons σ; ω; ρ; δ. At the energy scale considered here, hadrons are just ordinary degrees of freedom and therefore the density of their associated states is corresponding to high energy $N\bar{N}$.

By directly expanding the results obtained in [7], an expression for the CJT effective potential in HF approximation, with the corresponding two-loop schemes, is shown in Figure (2.1) (where $M_{\sigma,\omega,\rho,\delta} = m_{\sigma,\omega,\rho,\delta}$) specific expression of the effective potential. in this case it is:

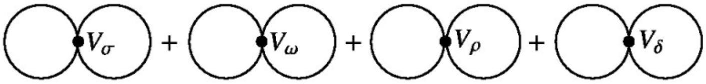

**Figure 2.1:** *Graphs corresponding to approximate HF*

$$V(M^*,\mu,T) = \frac{m_\sigma^2}{2}\sigma^{2-}\frac{m_\omega^2}{2}\omega^2 + \frac{m_\rho^2}{2}b^2\frac{m_\delta^2}{2}d^2 +$$

$$+\frac{N_c}{\pi^2}\int_0^\infty q^2dq\left[Tln\left(n_q^{p*-}n_q^{p*+}\right)Tln\left(n_q^{n*-}n_q^{n*+}\right)\right] +$$

$$+\frac{N_c}{8\pi^4}\left(G_\sigma - 2G_\omega - \frac{G_\rho + G_\delta}{2}\right)\left[\int_0^\infty q^2dq\left(n_q^{p*-} - n_q^{p*+}\right)\right] +$$

$$+\frac{N_c}{8\pi^4}\left(G_\sigma - 2G_\omega - \frac{G_\rho + G_\delta}{2}\right)\left[\int_0^\infty q^2dq\left(n_q^{n*-} - n_q^{n*+}\right)\right] +$$

$$+\frac{N_c}{8\pi^4}\left(G_\sigma + 4G_\omega + G_\rho + G_\delta\right)\left[\int_0^\infty q^2dq\frac{M^{p*}}{E_q^{p*}}\left(n_q^{p*-} + n_q^{p*+}\right)\right] +$$

$$+\frac{N_c}{8\pi^4}\left(G_\sigma + 4G_\omega - G_\rho - G_\delta\right)\left[\int_0^\infty q^2dq\frac{M^{p*}}{E_q^{p*}}\left(n_q^{n*-} + n_q^{n*+}\right)\right] =$$

$$= \frac{N_c^2 G_\sigma}{2}\rho_s^2 - \frac{N_c^2 G_\omega}{2}\rho_B^2 + \frac{N_c^2 G_\rho}{2}\rho_3^2 + \frac{N_c^2 G_\delta}{2}\rho_\delta^2 +$$

$$+\frac{N_c}{\pi^2}\int_0^\infty q^2dq\left[Tln\left(n_q^{p*-}n_q^{p*+}\right) + Tln\left(n_q^{n*-}n_q^{n*+}\right)\right] +$$

$$+\frac{N_c}{8}\left(G_\sigma - 2G_\omega - \frac{G_\rho}{2} - \frac{G_\delta}{2}\right)\rho_{B_p}^2 + \frac{N_c}{8}\left(G_\sigma - 2G_\omega + \frac{G_\rho}{2} + \frac{G_\delta}{2}\right)\rho_{B_n}^2 +$$

$$+\frac{N_c}{8}\left(G_\sigma + 4G_\omega + G_\rho + G_\delta\right)\rho_{s_p}^2 + \frac{N_c}{8}\left(G_\sigma + 4G_\omega - G_\rho - G_\delta\right)\rho_{s_n}^2 \qquad (2.4)$$

In it

$$\mu^{p*} = \mu^{p} - \Sigma_0^{p} \quad =$$

$$= \mu^{p} - \frac{1}{4\pi^2}\begin{bmatrix} -G_\sigma + 2(2N_c+1)G_\omega - (2N_c-1)\dfrac{G_\rho}{2} \\ -\dfrac{G_\delta}{2} \end{bmatrix}\int_0^\infty q^2 dq\left(n_q^{p*-} - n_q^{p*+}\right) -$$

$$-\frac{N_c}{\pi^2}\left[G_\omega + \frac{G_\rho}{4}\right]\int_0^\infty q^2 dq\left(n_q^{n*-} - n_q^{n*+}\right) \tag{2.5}$$

$$\mu^{n*} = \mu^{n} - \sum\nolimits_0^{p} \quad =$$

$$= \mu^{p} - \frac{1}{4\pi^2}\left[-G_\sigma + 2(2N_c+1)G_\omega - (2N_c+1)\frac{G_\rho}{2} + \frac{G_\delta}{2}\right]\int_0^\infty q^2 dq\left(n_q^{n*-} - n_q^{n*+}\right) -$$

$$-\frac{N_c}{\pi^2}\left[G_\omega + \frac{G_\rho}{4}\right]\int_0^\infty q^2 dq\left(n_q^{p*-} - n_q^{p*+}\right) \tag{2.6}$$

$$M^{p*} = M + \sum\nolimits_s^{p} =$$

$$= M - \frac{1}{4\pi^2}\left[(4N_c+1)G_\sigma + 4G_\omega + G_\rho + (2N_c+1)G_\delta\right]\int_0^\infty q^2 dq\frac{M^{p*}}{E_q^{p*}}\left(n_q^{p*-} + n_q^{p*+}\right) -$$

$$-\frac{N_c}{\pi^2}\left[G_\sigma - \frac{G_\delta}{2}\right]\int_0^\infty q^2 dq\frac{M^{p*}}{E_q^{p*}}\left(n_q^{n*-} + n_q^{n*+}\right) \tag{2.7}$$

$$M^{n*} = M + \sum\nolimits_s^{n} =$$

$$= M - \frac{1}{4\pi^2}\left[(4N_c+1)G_\sigma + 4G_\omega - G_\rho - (2N_c+1)G_\delta\right]\int_0^\infty q^2 dq\frac{M^{p*}}{E_q^{p*}}\left(n_q^{n*-} + n_q^{n*+}\right) -$$

$$-\frac{N_c}{\pi^2}\left[G_\sigma + \frac{G_\delta}{2}\right]\int_0^\infty q^2 dq\frac{M^{p*}}{E_q^{p*}}\left(n_q^{p*-} + n_q^{p*+}\right) \tag{2.8}$$

From the effective acting (2.4) We have:

a) Thermodynamic potential

$$\Omega = (V - V_{vac})_{min} \tag{2.9}$$

With $V_{vac} = V(M, \rho = 0, T = 0)$

b) Energy density

$$\varepsilon = \Omega + \mu_p \rho_p + \mu_n \rho_n \tag{2.10}$$

c) Binding energy

$$\epsilon_{bind} = -M + \varepsilon / \rho_B \tag{2.11}$$

d) Pressure

$$P = N_c \left( \rho_{B_p} \mu_p^* + \rho_{B_n} \mu_n^* \right) - \varepsilon = N_c (\rho_B \mu_B^* + \rho_3 \mu_3^*) - \varepsilon$$

$$= -\frac{N_c^2 G_\sigma}{2} \rho_S^2 - \frac{N_c^2 G_\omega}{2} \rho_B^2 + \frac{N_c^2 G_\rho}{2} \rho_3^2 + \frac{N_c^2 G_\delta}{2} \rho_\delta^2$$

$$-\frac{N_c}{\pi^2} \int_0^\infty q^2 dq \left[ T ln\left(n_q^{p*-} n_q^{p*+}\right) + T ln\left(n_q^{n*-} n_q^{n*+}\right) \right] +$$

$$+\frac{N_c}{8} \left( G_\sigma - 2G_\omega - \frac{G_\rho}{2} - \frac{G_\delta}{2} \right) \rho_{B_p}^2 + \frac{N_c}{8} \left( G_\sigma - 2G_\omega + \frac{G_\rho}{2} + \frac{G_\delta}{2} \right) \rho_{B_n}^2 -$$

$$-\frac{N_c}{8} (G_\sigma + 4G_\omega + G_\rho + G_\delta) \rho_{s_p}^2 - \frac{N_c}{8} (G_\sigma + 4G_\omega - G_\rho - G_\delta)\, \rho_{s_n}^2 \tag{2.12}$$

Equations (2.9), (2.10), (2.11) and (2.12) are the equations of the asymmetric nucleus material considered in the model, they contain all the physical processes they have. can occur in the nuclear substance investigated in the model. As the initial comment, the focus here is on the examination of the nuclear properties described by the model.

## 3. RESULTS AND DISCUSSION

At T = 0 equation (2.4) to (2.8) returns:

$$(M, \mu, 0) = \frac{N_c^2}{8\pi^4} G_\sigma \begin{bmatrix} M^{p*} \left( \mu^{p*} \sqrt{\mu^{p*2} - M^{p*2}} - M^{p*2} \ln \left| \dfrac{\mu^{p*} + \sqrt{\mu^{p*2} - M^{p*2}}}{M^{p*}} \right| \right) \\ +M^{n*} \left( \mu^{n*} \sqrt{\mu^{n*2} - M^{*2}} - M^{p*2} \ln \left| \dfrac{\mu^{*} + \sqrt{\mu^{p*2} - M^{p*2}}}{M^{p*}} \right| \right) \end{bmatrix}^2 +$$

$$+\frac{N_c^2}{8\pi^4} G_\delta \begin{bmatrix} M^{p*} \left( \mu^{p*} \sqrt{\mu^{p*2} - M^{p*2}} - M^{p*2} \ln \left| \dfrac{\mu^{p*} + \sqrt{\mu^{p*2} - M^{p*2}}}{M^{p*}} \right| \right) \\ -M^{n*} \left( \mu^{n*} \sqrt{\mu^{n*2} - M^{*2}} - M^{p*2} \ln \left| \dfrac{\mu^{*} + \sqrt{\mu^{p*2} - M^{p*2}}}{M^{p*}} \right| \right) \end{bmatrix}^2 +$$

$$+\frac{N_c^2}{18\pi^4}G_\omega\left(k_{F_p}^3+k_{F_n}^3\right)^2-\frac{N_c^2}{72\pi^4}G_\rho\left(k_{F_p}^3+k_{F_n}^3\right)^2-\frac{N_c^2}{72\pi^4}(G_\sigma-2G_\omega)\left(k_{F_p}^6+k_{F_n}^6\right)+$$

$$+\frac{N_c^2}{72\pi^4}\frac{G_\rho}{2}\left(k_{F_p}^6-k_{F_n}^6\right)+\frac{N_c^2}{72\pi^4}\frac{G_\delta}{2}\left(k_{F_p}^6-k_{F_n}^6\right)+$$

$$+\frac{N_c^2}{8\pi^2}\left[\begin{array}{c}\mu^{p*}(2\mu^{p*2}-M^{p*2})\sqrt{\mu^{p*2}-M^{p*2}}\\ -M^{p*4}\ln\left|\frac{\mu^{p*}+\sqrt{\mu^{p*2}-M^{p*2}}}{M^{p*}}\right|+\mu^{n*}(\mu^{n*}-M^{n*2})\sqrt{\mu^{n*2}-M^{n*2}}\\ -M^{n*4}\ln\left|\frac{\mu^{n*}+\sqrt{\mu^{n*2}-M^{n*2}}}{M^{n*}}\right|\end{array}\right]^2+$$

$$+\frac{N_c}{32\pi^4}(G_\sigma+4G_\omega+G_\rho+G_\delta)$$
$$\times M^{p*}\left(\mu^{p*}\sqrt{\mu^{p*2}-M^{p*2}}-M^{p*2}\ln\left|\frac{\mu^{p*}+\sqrt{\mu^{p*2}-M^{p*2}}}{M^{p*}}\right|\right)+$$

$$+\frac{N_c}{32\pi^4}(G_\sigma+4G_\omega-G_\rho-G_\delta)$$
$$\times M^{n*}\left(\mu^{n*}\sqrt{\mu^{n*2}-M^{*2}}-M^{n*2}\ln\left|\frac{\mu^{n*}+\sqrt{\mu^{n*2}-M^{n*2}}}{M^{n*}}\right|\right)-$$

$$-N_c\left(\mu^p\rho_{B_p}+\mu^n\rho_{B_n}\right) \tag{3.1}$$

$$\mu^{p*}=\mu^p-\frac{1}{4\pi^2}\left[2(2N_c+1)G_\omega-G_\sigma-(2N_c-1)\frac{G_\rho}{2}-\frac{G_\delta}{2}\right]\frac{(\mu^{p*2}-M^{p*2})^{\frac{3}{2}}}{3}$$
$$-\frac{N_c}{\pi^2}\left[G_\omega+\frac{G_\rho}{4}\right]\frac{(\mu^{n*2}-M^{n*2})^{\frac{3}{2}}}{3} \tag{3.2}$$

$$\mu^{n*}=\mu^n-\frac{1}{4\pi^2}\left[2(2N_c+1)G_\omega-G_\sigma-(2N_c+1)\frac{G_\rho}{2}+\frac{G_\delta}{2}\right]\frac{(\mu^{n*2}-M^{n*2})^{\frac{3}{2}}}{3}$$
$$-\frac{N_c}{\pi^2}\left[G_\omega+\frac{G_\rho}{4}\right]\frac{(\mu^{p*2}-M^{p*2})^{\frac{3}{2}}}{3} \tag{3.3}$$

$$M^{p*} = M - \frac{1}{8\pi^2}\left[(4N_c + 1)G_\sigma + 4G_\omega + G_\rho + (2N_c + 1)G_\delta\right]$$
$$\times M^{p*}\left(\mu^{p*}\sqrt{\mu^{p*2} - M^{p*2}} - M^{p*2}\ln\left|\frac{\mu^{p*} + \sqrt{\mu^{p*2} - M^{p*2}}}{M^{p*}}\right|\right) -$$

$$-\frac{N_c}{2\pi^2}\left[G_\sigma - \frac{G_\delta}{2}\right] \times M^{n*}\left(\mu^{n*}\sqrt{\mu^{n*2} - M^{*2}} - M^{n*2}\ln\left|\frac{\mu^{n*} + \sqrt{\mu^{n*2} - M^{n*2}}}{M^{n*}}\right|\right) \quad (3.4)$$

$$M^{n*} = M - \frac{1}{8\pi^2}\left[(4N_c + 1)G_\sigma + 4G_\omega - G_\rho - (2N_c + 1)G_\delta\right] \times$$

$$\times M^{n*}\left(\mu^{n*}\sqrt{\mu^{n*2} - M^{n*2}} - M^{n*2}\ln\left|\frac{\mu^{n*} + \sqrt{\mu^{n*2} - M^{n*2}}}{M^{n*}}\right|\right) - \frac{N_c}{2\pi^2}\left[G_\sigma - \frac{G_\delta}{2}\right] \times$$

$$\times M^{p*}\left(\mu^{p*}\sqrt{\mu^{p*2} - M^{p*2}} - M^{p*2}\ln\left|\frac{\mu^{p*} + \sqrt{\mu^{p*2} - M^{p*2}}}{M^{p*}}\right|\right) \quad (3.5)$$

For $k_{F_p}, k_{F_n}$, respectively, are the feces momentum for protons and neutrons and

$$\rho_B = \frac{1}{3\pi^2}\left(k_{F_p}^3 + k_{F_n}^3\right)$$

$$\rho_3 = \frac{1}{3\pi^2}\left(k_{F_p}^3 - k_{F_n}^3\right)$$

Based on experimental results, we choose the mass of nucleons and mesons, respectively, $M = 939\,MeV, m_\sigma = 550\,MeV, m_\omega = 783\,MeV, m_\rho = 770\,MeV, m_\delta = 983\,MeV$.

The calculation is done according to each of the following steps. Firstly, it is necessary to determine the value of the associated constants $G_\sigma$; $G_\omega$. To do so, first solve with the number of equations (3.4) or (3.5) for asymmetric nuclei (at this time ... Gρ = Gδ = 0) then replace the obtained root of function into the expressions $\epsilon_{bind}$ in equations (2.11) and (2.1). Two parameters $G_\sigma$; $G_\omega$ must have a value such that the binding energy $\epsilon_{bind}$= -15.8 MeV at the normal density of nuclear substance $\rho_B = \rho_0 = 16\,fm^{-3}$ as shown in Figure (3.2). Calculated results give $G_\sigma = 195.6/M^2$ and $G_\omega = 1.1215G_\sigma$.

The values of $G_\rho$ and $G_\sigma$ need to be used to determine the symmetry parameters of the Weiszaecker mass formula $a_4$ and the compression coefficient $K_0$. Here choose $a_4 = 30$ MeV and $K_0 = 240$ MeV, these values are close to the currently accepted values $a_4 = 31 \pm$ MeV and $K_0 \sim 200 \div 300$ MeV [6].

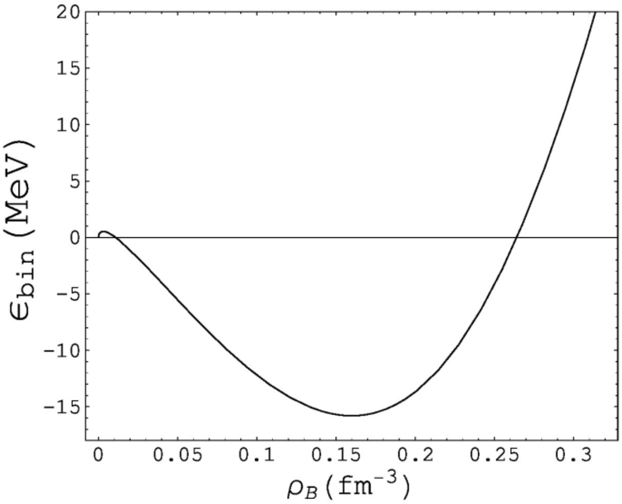

**Figure 3.1:** *Dependence of binding energy on symmetric nuclear substance on* $\rho_B$

The calculated result is $G_\rho = 0.5243 G_\sigma, G_\delta = 0.9318 G_\sigma$. Interestingly, in [3] $a_4 = 30$ MeV and $K_0 = 280$ MeV were obtained in the Walecka model near the mean field with the addition of the Goguta-Bodmer potential potential term.

Next we determine the energy dependence of the symmetric nuclear substance (NSE). Carry out numerical solutions for equations (2.1) and (2.11) and (3.1). We obtain the dependence of $E_{sym}$ on the density and can express that dependence by a function.

$$E_{sym}(\rho_B) \sim 30 \left(\frac{\rho_B}{\rho_0}\right)^{1.05} \tag{3.6}$$

It is clear that equation (3.6) is suitable for experiment as shown in [4] Thereby we determine the slope $L$ and $K_{sym}$ curves of NSE at the value $\rho_0$.

$$K_{sym} = 9\rho_0^2 \left(\frac{\partial^2 E_{sym}}{\partial \rho_B^2}\right)_{\rho_B=\rho_0}$$

The calculated result for $L = 99.54\,MeV,\ K_{sym} = -520.88\,MeV$ is within the acceptable value range when compared to

$$L = 88 \pm 25\,MeV, and\ K_{sym} = -500 \pm 50\,MeV$$

in [5].

## 4. CONCLUSION

A systematic study of the effective method of CJT at zero and finite temperatures, along with some specific examples.

Based on numerical calculations, it was found that the presence of delta mesons could reduce the value of the uncompressed coefficient as expected. We also obtained the values of most of the basic parameters of nuclear substances such as specific binding energy, symmetry energy and related quantities such as slope, uncompressed coefficients… In general, the results we obtained are in good agreement with other authors and experimentally. However, to further clarify the properties of nuclear substances, it is necessary to conduct a comprehensive investigation of the phase structure. That is the issue that will be implemented in the near future.

## REFERENCES

1. Baran. V, Colona. M, Greco. V, and Di Toro. M (2005), *Phys.Rep*. **410**, 335.
2. Chen. L. W, Ko. C. M, and Li. B. A (2005), *Phys.Rev*. **C72**, 064309.
3. Kubis. S and Kutschera. M (1997), *Phys. Lett*. **399**, 191.
4. Li. B. A and Chen. L. W, (2005), *Phys. Rev*. **C72**, 064611
5. Matsubara.T, Prog, (1955), *Theor. Phys*. 14 351.
6. Steiner. A. W, Prakash.M, Lattimer.J.M, and Ellis. P. J, (2005), *Phys.Rep***.** **411**, 325
7. Tran Huu Phat, Nguyen Tuan Anh, and Nguyen Van Long, (2008), *Phys.Rev*. **C77**, 054321.
8. Tran Huu Phat, Nguyen Tuan Anh, Le Viet Hoa and Nguyen Van Long, (2007), *Phys.Rev*. **C76**, 045202.

# KHẢO SÁT VAI TRÒ CỦA MESON DELTA TRONG CHẤT HẠT NHÂN BẤT ĐỐI XỨNG

***Tóm tắt:*** *Bằng cách mở mở rộng các tính toán chúng tôi đã khảo sát mô hình bốn nucleon của chất hạt nhân mà trong đó có tính tới meson delta. Các kết quả chính cho thấy không cần bổ xung thế Goguta-Bodmer vẫn thu được giá trị độ nén mong đợi* $K_0 = 240\ MeV$*, đồng thời độ dốc và độ cong của năng lượng đối xứng cũng phù hợp với thực nghiệm. Hơn nữa cần phải nhấn mạnh rằng, trong gần đúng trường trung bình Lgrangian 3.2 là tương đương với Lagrangian của mô hình Waleka là mô hình đã cho giá trị không phù hợp của độ nén* $K_0 = 540\ MeV$*. Điều này cho thấy rằng đóng góp của giản đồ loop đã làm tăng độ xốp của hạt nhân, như thế một lần nữa khẳng định vai trò quan trọng của các loop. Chính vì vậy, việc nghiên cứu mô hình bốn nucleon ở mức gần đúng cao hơn gần đúng trường trung bình sẽ là phù hợp nhất cho việc khảo sát nhiều hiện tượng cơ bản của cả vật lý hạt nhân và vũ trụ học.*

***Từ khóa:*** *Meson delta, sigma, omega*

# EVALUATION OF ALLELOPATHIC POTENTIAL OF SOME VIETNAMESE RICE (ORYZA SATIVA L.) LANDRACES AGAINST THE GROWTH OF BARNYARDGRASS (ECHINOCHLOA CRUS-GALLI P. BEAUV) IN THE LABORATORY CONDITION

**Nguyen Nhu Toan[1], Khuat Huu Trung[2], Dao Xuan Duc[2],**
**Tran Dang Khanh[2]*, Nguyen Truong Giang[3], Nguyen Lam Phuc[4]**
*[1] Hanoi Metropolitan University*
*[2] Agricultural Genetics Institute*
*[3] Department of Science Technology and Environment - Ministry of Agriculture and Rural Development*
*[4] University of Science - Hanoi National University*

***Abstract:*** *Allelopathy is a biological phenomenon by which an organism produces one or more biochemicals that influence the germination, growth, survival and reproduction of other organisms. In plants, Allelopathy can simply be comprehended as the ability of plants to inhibit or stimulate the growth of vicinity plants in nature. The objective of this study was to evaluate the allelopathic potential of 20 Vietnamese rice landraces against the growth of barnyard grass (Echinochloa crus-galli) in laboratory condition. The results showed that allelopathic activity of the rice showed landrace – dependence and origin dependence. All rice landraces showed significant average inhibition on the shoot and root length of barnyardgrass 17.71%, and 58.67%. Typically, the highest suppressing the shoot length was G170 OM504-JP (30.19%), followed by G423 N22 (29.49%) and G22 Tr. Trang (29.67%). For the root length inhibition, the maximum suppression was found HT9 (65.96%), while the lowest inhibition was Ble Blaudo (43.0%). Generally, the rice landraces used in this study revealed the remarkable inhibition over 50.0%. The results of this study might provide useful information for improving the weed-suppressing ability of rice in this country.*

***Keywords:*** *Allelopathy, barnyard grass, landrace, rice*

Email: nntoan@hnmu.edu.vn

Received 21 October 2019
Accepted for publication 25 November 2019

## 1. INTRODUCTION

Rice (*Oryza sativa* L.) is the main crop and is providing daily food for over half of world population. Vietnam has been ranked as one of the second-biggest rice exporters in the world. According to the report of MARD (2016) [1], 4.88 million tons of rice was and exported and earned 2.2 billion USD. However, rice export volume has decreased by 27.0% similar with reduction of rice export turnover by 22.0% to compare with the year of 2016.

Currently, rice crop in Vietnam has encountered biotic and biotic factors, leading to low rice yield compared to other rice-producing countries. Among the adverse factors, weed infestation is a major biotic constraint and one of the biggest challenges to rice yield in Vietnam. Causing severe economic losses. In the Mekong Delta, weeds cause over 46% rice yield losses on average in direct-sowing rice areas [2, 3]. Traditional weed managements in Vietnam are hand-weeding, water management, land preparation and sowing/seedling techniques. All these methods are dependent on weather conditions, are time-consuming and require intensive labor. Following urbanization and economic growth, a decrease in the labor force in the agricultural sector is occurring in Vietnam, causing a rapid increase in pesticide and herbicide uses [4]. Herbicide utilization can minimize the time spent on weed control and stabilize the rice yield. However, the overuse of synthetic chemicals for weed control is a serious problem in Vietnam, causing environmental pollution, unsafe agricultural products and human health concerns [2, 5].

Biological control of weeds in rice is somewhat less known and has carried out sporadically in this country [6]. Therefore, reducing the dependency on synthetic herbicides and agrochemicals in agricultural production in Vietnam is an important task to develop environment-friendly and maintain sustainable agricultural production.

Alleopathy or weed suppressing of host plant can be known as both beneficial and deleterious biochemical interactions between plants and microorganisms via the secondary metabolites that release into the environment and cause influence on the growth and development of vicinity plants [7].

Exploitation of allelopathy can improve crop production via avoidance of negative impacts, exploitation of stimulatory effects management and development of allelopathic crops and cultivars to suppress weeds as well as utilizing plant growth inhibitor as nature herbicides [6]. In another hand, biological weed management by using allelopathy may affect a yield improvement without environmental cost, which is one of the most important considerations for this country. Therefore, the objective of this study is to evaluate allelopathy potential of the 20 selected Vietnamese rice landraces in laboratory condition. The result may provide useful information to further develop rice allelopathy for sustainable agriculture production in this country.

## 2. MATERIALS AND METHODS

### 2.1. Preparation of rice landraces and barnyard grass seeds

Twenty rice landraces were kindly provided by Vietnam Plant Resource Center in 2017 as shown in Table 1. Barnyard grass seeds (*Echinochloa crus-galli* P. Beauv. Var *oryzicola* Ohwi) were grown and harvested at Agricultural Genetics Institute (AGI) - Lai Yen Experimental Station in 2018.

**Table 1:** *List of the 20 Vietnamese native rice landraces used in this study*

| No | Rice landraces | No | Rice landraces |
|---|---|---|---|
| 1 | Ble Blau do | 11 | G223 Pok |
| 2 | Bulu Pan dark | 12 | Lua den |
| 3 | G170 OM504 | 13 | Nep tu le |
| 4 | G423 N22 | 14 | G168 OM1490 |
| 5 | Huong Chiem | 15 | G45 Nep cuc |
| 6 | G22 Tr.Trang | 16 | HT9 |
| 7 | G133 A330 | 17 | G59 nep man |
| 8 | Nep TTHP | 18 | SH8 |
| 9 | GL 106 (GL) | 19 | BT09 |
| 10 | G176 K.B.Duong | 20 | J022 |

### 2.2. Bioassay

The empty and undeveloped seeds were discarded by floating in tap water. The remaining seeds were air-dried and then hermetically stored at -20◦C. Before conducting the experiment for breaking of dormancy, both rice and barnyardgrass seeds were incubated at 40◦C for five days. Before use in the bioassay, barnyardgrass seeds were sterilized with 1% sodium hypochlorite for 30 sec and rinsed several times with distilled water. In the germination test, the germination ratio of seeds was randomly checked and showed to be more than 90%.

A total of 20 Vietnamese rice landraces were screened in the laboratory for their allelopathic potential against barnyardgrass. Twenty healthy seeds of each rice landraces were evenly sown in a Petri dish (9 cm diameter) lined with filter paper and added to 10 ml of distilled water. Simultaneously, 20 seeds of barnyardgrass were evenly inter-planted between the rice seeds (Figure 1). The Petri dishes were transferred into a growth chamber (25◦C, 4000 lux, lighted time: 9:00-17:00h; humidity: 75%). After seven days. The numbers of germinating barnyardgrass seeds were counted and the length of shoots and roots was measured. Additionally, the inhibition percentage (%) between treatment and the control was calculated by the equation:

*Inhibition (%) = [(control-rice variety treatment)/control] x 100*

The inhibition magnitudes against barnyardgrass growth including the SL, DW of the sampled barnyard grass were recorded as an average inhibition (AI).

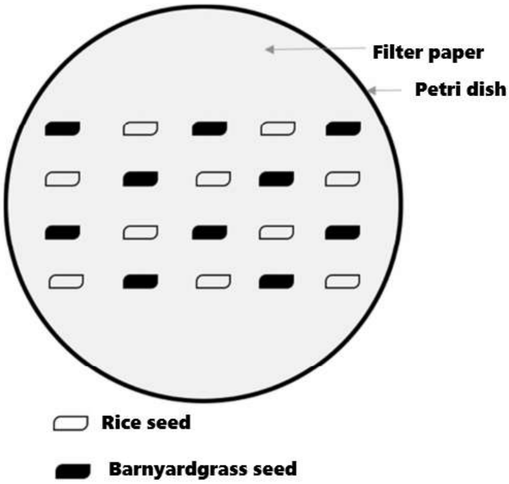

**Figure 1:** *Diagram of seed distribution in a Petri dish*

## 2.3. Statistical analysis

The experiments in laboratory screening were done in a completely randomized design with 3 replications. Statistical analysis was performed using analysis of variance to analyze treatment differences [9]. The means were separated on the basis of the least significant differences (LSD) at the 0.05 probability level.

## 3. RESULTS AND DISCUSSION

In the current study, barnyard grass was selected as the indicator plant because it is one of the most noxious paddy weeds available grown in upland and lowland paddy fields in Vietnam and caused rice yield significant reduction and troublesome to farmers.

In this study, the selected 20 Vietnamese rice landrace were used to assess their allelopathic properties on the growth of barnyardgrass. For the average of the shoot and root length inhibition, most of the rice landraces showed the inhibition on the growth of barnyardgrass was 17.71%, and 58.67%, respectively. The highest suppressing the shoot length was G170 OM504-JP (30.19%), followed by G423 N22 (29.49%) and G22 Tr.Trang (29.67%). It noted that 9 rice landraces reduced the shoot length of barnyardgrass by over 20% including: Lua den (28.73%), G133A330 (27.98%), G168 OM1490 (24.60%), HT9 (24.25%), Bulu Pan dark (22.28%), G223 Pokkali (21.40%), G176 K.B.Duong (20.88%), JO2 (20.48%), respectively. There were 8 rice landrace showing the shoot length inhibition less than 20% as following: Nep Tu le (16.75%), BT09 (16.87%), SH8 (13.67%), G45 nep cuc (13.14%), nep TTHP (12.21%), G59 nep man (12.15%), Huong chiem (10.93%). Only the Ble Blaudo landrace was found to be promoted the shoot length of barnyardgrass by 32.46% (Table 2).

**Table 2:** *Allelopathic potential of the 20 selected Vietnamese rice landraces on the growth of barnyardgrass in the laboratory condition*

| No | Rice landraces | Shoot length (cm) | Shoot length inhibition (%) | Root length (cm) | Root length inhibition (%) |
|---|---|---|---|---|---|
| 1 | Ble Blau Do | 7.95 | -32.46 | 3.26 | 43.00 |
| 2 | Bulu Pan dark | 4.45 | 22.28 | 2.28 | 60.08 |
| 3 | G170 OM504 | 4.00 | 30.19 | 1.99 | 65.15 |
| 4 | G423 N22 | 4.04 | 29.49 | 2.35 | 58.85 |
| 5 | Huong Chiem | 5.10 | 10.93 | 2.56 | 55.24 |
| 6 | G22 Tr.Trang | 4.03 | 29.67 | 1.96 | 65.79 |
| 7 | G133 A330 | 4.13 | 27.98 | 2.05 | 64.04 |
| 8 | Nep TTHP | 5.03 | 12.21 | 2.87 | 49.70 |
| 9 | GL 106 (GL) | 5.09 | 11.11 | 2.98 | 47.90 |
| 10 | G176 K.B.Duong | 4.53 | 20.88 | 2.13 | 62.64 |
| 11 | G223 Pok | 4.50 | 21.40 | 2.07 | 63.81 |
| 12 | Lua den | 4.08 | 28.73 | 2.06 | 63.98 |
| 13 | Nep tu le | 4.77 | 16.75 | 2.48 | 56.64 |
| 14 | G168 OM1490 | 4.32 | 24.60 | 2.83 | 60.01 |
| 15 | G45 Nep cuc | 4.98 | 13.14 | 2.59 | 54.72 |
| 16 | HT9 | 4.34 | 24.25 | 1.95 | 65.96 |
| 17 | G59 nep man | 5.03 | 12.15 | 2.06 | 63.86 |
| 18 | SH8 | 4.95 | 13.67 | 2.25 | 60.60 |
| 19 | BT09 | 4.76 | 16.87 | 2.33 | 59.20 |
| 20 | J022 | 4.56 | 20.48 | 2.74 | 52.09 |
|  | Control | 5.73 | 0.0 | 5.72 | 0.0 |
|  | Total inhibition | 4.71 | 17.71 | 2.36 | 58.67 |
|  | LSD $_{(0.05)}$ |  | 0.72 |  | 0.91 |

*Note: (-) implies the promotion of barnyargrass's growth*

For the root length inhibition, all rice landraces showed a significant inhibition over 40.0%, ranged from 43.0% to 65.79%, respectively. The maximum suppression was found HT9 (65.96%), while the lowest inhibition was Ble Blaudo (43.0%). Generally, the rice landraces used in this study revealed the remarkable inhibition over 50.0% as the order: HT9 (65.96%), G22Tr.trang (65.79%), G170 OM504 (65.15%), G133 A330 (64.04%), Lua den (63.98%), G59 nep man (63.86%), G223 pok (63.81%), G176 K.B.Duong (62.64%), SH8 (60.60%), G168 OM490 (60.01%), BT09(59.20%), G423 N22 (58.85%), Nep tu le (56.64%), Huong Chiem (55.24%), G45 nep cuc (54.72%) and J022 (52.09%), respectively (Table 2).

For average inhibition on the growth of barnyardgrass, there are 10 rice landraces showing suppressing ability over 40.0%, of which the highest suppression of barnyardgrass growth was found in G22 Tr.Trang (47.73%) and G170 OM504 (47.67%), respectively. Eight rice landraces showed average inhibition on the growth of barnyardgrass by over 30.0% were as the order: BT09 (38.04%), G59 nep man (38.01%), J022 (36.92%), Nep Tu le (36.70%), G45 Nep cuc (33.93%), Huong Chiem (33.09%) and Nep TTHP (30.96%), respectively. The weakest allelopathic average inhibition was found in Ble Blaudo (5.72%), followed by GL 106 (GL) (29.51%), respectively (Figure 2).

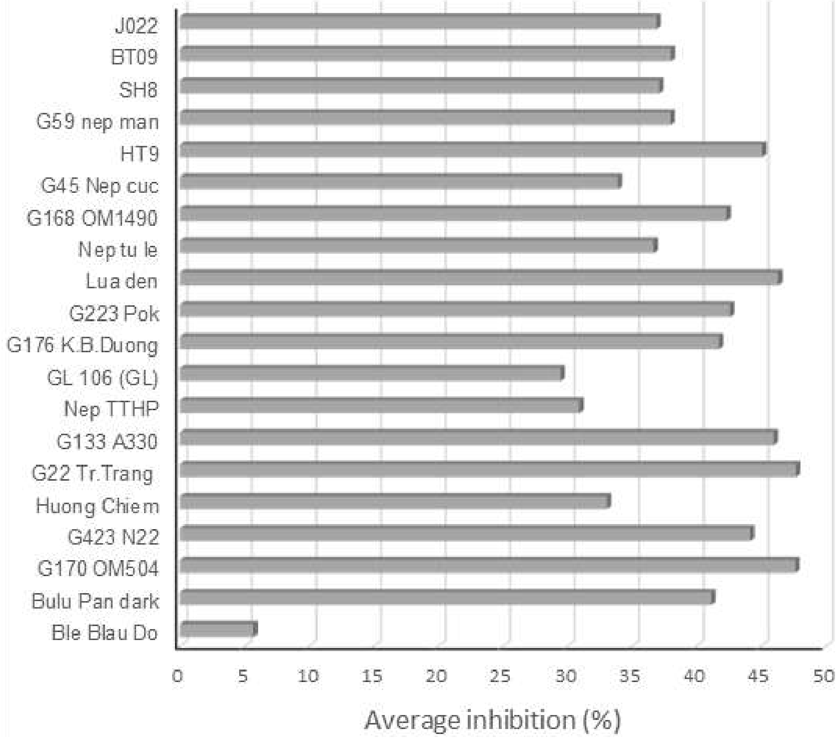

**Figure 2:** *The average inhibition of the 20 selected rice landraces against the growth of barnyardgrass*

In some last years, many works have been carried out to evaluate allelopathic potential of rice in field condition. Dil day et al (2000) [10] reported 412 among 12.000 rice landraces displayed alleopathic activity against duck salad in-field evaluation. So far, thousands of rice landraces have been assessed their alleopathic activity. The results showed that germplasm from china and Japonica rice landraces had more allelopathic potential than other rice varieties [11]. Recently, 73 landraces with different varietal groups against the growth of barnyard in laboratory, greenhouse and field conditions were evaluated. It showed that hybrid variety showed highest inhibition than non-sticky varieties, followed by foreign and traditional sticky rice varieties. The lowest inhibition was found in upland sticky rice varieties [6]. Allelopathic rice landraces have been induced by many allelopathic chemicals which were previously reported involving in numerous phytotoxins such as phenolic acids, diterpenoids, glucopyranosides, momilactones, oryzaexin, and stigmastanols etc. were isolated from the leaf, stem, root and root exudates [5].

It was similar with our current work because most rice landraces used in this study were traditional and upland rice landrace with the exception of G170 OM504, G168 OM1490, J022 and HT9 is the improved rice varieties which exhibited allelopathic property rather high than other landraces.

## 4. CONCLUSIONS

In summary, the 20 selected rice landraces were evaluated the allelopathic allelopathic potential in laboratory condition. Rice allelopathy activity showed landrace - dependence and origin – dependence. All rice landraces showed remarkable weed-suppressing on the growth of barnyardgrass. Further research on assess the allelopathic properties of those landraces should be conducted in the greenhouse and field conditions as well as isolating allelochemicals which may be responsible for weed inhibition ability. The current results might be useful for the improvement of the weed-suppressing ability of rice in this country.

***Acknowledgement:*** *Authors would like to thank Miss Dang Thi Mai Huong for her efforts to contribute to this experiment.*

## REFERENCES

1. MARD - Ministry of Agriculture and Rural Development (2016), *Annual report of rice production.* December. 2016.

2. Chin. D.V. (2001), “Biology and management of barnyard grass. Red sprangletop and weedy rice”- *Weed Biology and Management.* 1:37-41.

3. Khanh T.D., Xuan T.D., Chin D.V., Chung I.M., Abdelghany E.A., Tawata S. (2006), “Current status of biological control of paddy weeds in Vietnam”- *Weed Biology and Management.* 6:1-9.

4. Khanh T.D, Linh L.H, Linh T.H, Quan N.T, Trung K.H, Cuong D.M, Hien V.T.T; Ham L.H, Xuan T.D (2013), "Integration of allelopathy to control weeds in rice. In: Herbicides" – *Current Research and Case Studies in Use*. Andrew. J (eds). 75-99.
5. Khanh T.D. Xuan T.D, Chung I.M. (2007), "Rice allelopathy and possibility for weed management"- *Annals of Applied Biology*. 151:325-339.
6. Khanh T.D, Cong L.C, Chung I.M, Xuan T.D (2009), "Variation of weed-suppressing potential of Vietnamese rice cultivars against barnyard grass (*Echinochloa crus-galli*) in laboratory"- *Greenhouse and field screenings*. *Journal of Plant Interactions*. 4:209-218.
7. Rice E.L., (1984), Allelopathy.2nd ed. Academic Press Inc. Orlando. FL; p.422.
8. Ahn J.K, Hahn. S.J, Kim. J.T, Khanh. T.D, Chung. I.M. (2005), *Evaluation of allelopathic potential among rice (Oryza sativa L.) germplasm for control of Echinochloa crus galli P. Beauv in the field.* Crop Protection. 24:413-419.
9. *SAS Institute*. (1997), SAS/STAT User's Guide. 6.12 Ed. SAS Institute. Cary.NC.
10. Dilday. R.H, Mattice J.D, Moldenhauer K.A. (2000), "Anoverview of rice allelopathy in the USA" - *In Proceedings of International Workshop in Rice Allelopathy*. 17–19 August 2000. Kyungpook National University.pp.15–26. Taegu. Korea: Institute of Agricultural Science and Technology. Kyung-Pook National University.
11. Dilday R.H, Mattice J.D, Moldenhauer K.A, Yan A.W. (2001), "Allelopathic potential of rice germp lasm against duck salad. Red stem and barnyard grass" - *Journal of Crop Production*. 4.287–301.

# ĐÁNH GIÁ TIỀM NĂNG ALLELOPATHIC Ở MỘT SỐ LOÀI LÚA CỦA VIỆT NAM CHỐNG LẠI SỰ PHÁT TRIỂN CỦA LOÀI CỎ BARNYA TRONG ĐIỀU KIỆN PHÒNG THÍ NGHIỆM

***Tóm tắt:*** *Allelopathy là một hiện tượng sinh học, nó được sản sinh ra bởi sinh vật hoăc điều chế sinh hóa học, nó có ảnh hưởng đến sự nảy mầm. Ở thực vật, allelopathy có thể được hiểu một cách đơn giản nó như là khả năng của thực vật để ức chế hoặc kích thích sự sinh trưởng của các loại thực vật gần nó. Mục đích của nghiên cứu này đã đánh giá khả năng của allelopathic ở 20 giống lúa của Việt Nam chống lại sự phát triển của cỏ barnyard (echinochloa crus-galli) trong điều kiện phòng thí nghiệm. Kết quả nghiên cứu đã chỉ ra rằng allelopathic hoạt động ở lúa phụ thuộc vào điều kiện phát triển và phụ thuộc vào nguồn gốc của nó. Tất cả các loài lúa bản địa cho thấy sự ức chế sự phát triển chiều dài của chồi và rễ ở cây cỏ Barnya 17,71% và 58,67%. Điển hình, chiều dài của chồi bị hạn chế cao nhất là G170 OM504 JP (31,19%), tiếp theo là G423 N22 (29,49%) và G22 Tr.Trang (29,67%). Với sự ức chế chiều dài của rễ, sự ức chế tối đa đã được tìm thấy HT9 (65,96%), trong khi sự ức chế thấp nhất là Ble Blaudo (43,0%). Nói chung, các loại lúa địa phương được sử dụng trong nghiên cứu này đã cho thấy sự ức chế đáng chú ý trên 50,0%. Kết quả của nghiên cứu này có thể cung cấp thông tin hữu ích để cải thiện khả năng tiêu diệt cỏ của lúa ở Việt Nam.*

***Từ khóa:*** *Allelopathy, cỏ barnyard, địa phương, lúa*

# A SPECIFICATION OF HANOI METROPOLITAN UNIVERSITY MANAGEMENT SYSTEM

**Tran Thi Thu Phuong, Nguyen Quoc Tuan**
*Hanoi Metropolitan University*

***Abstract:*** *The paper proposes a specification for a management system of the Hanoi metropolitan university (HNMU) based on the ERP system. By describing the organizational structure and limitations of the current system, we propose a system which has functional modules for the university's tasks, but still ensure the interoperability and consistency due to use a common database. The advantages and limitations of implementing the system are also indicated to help HNMU and other universities can consider applying the system in managing the university's activities to achieve the goals.*

***Keywords:*** *specification, university, management system, ERP, module, common database*

Email: tttphuong2@hnmu.edu.vn

Received 15 October 2019
Accepted for publication 25 November 2019

## 1. INTRODUCTION

In the education environment, universities meet many challenges, from how to effectively manage a large number of students and staffs with a variety of training activities which require the innovative programs and methods of teaching and learning follow the trend of information exchange and integration with other universities. In addition, many universities have multiple campuses in different places, since a problem for most universities is to find an effective model to support the university in the organization of management and unified management.

Hanoi Metropolitan University (HNMU) - formerly Hanoi Pedagogical College established in 1959, located at 98 Duong Quang Ham, Cau Giay. This is the only university directly under the Hanoi People's Committee, a multi-disciplinary, career-oriented, high-quality university, pioneering in fundamental and comprehensive innovation of education and training. The university has three locations with over 6000 students and nearly 400 staffs. The university's activities are coordinated by 11 departments, 13 faculties and 13 affiliated units [1]. Moreover, the teaching and learning activities are organized according to credit with hundreds of training disciplines, then how to effectively manage university’s activities is very difficult.

To solve that situation, the university's management system [2] has been operating for many years. The current system has ensured resource availability for users through email systems, electronic portals providing students and staffs with timely information, forms and administrative documents. However, in some cases, the information is not consistent and not connected with each other. For example, when the training department changes the schedule exam, but this information is not communicated with the examination department, then the distribution of the schedule is not accurate, the current system has not yet provided effective tools for academic advisors to promptly update their students' learning outcomes… In short, the system does not guarantee data interconnection between functional components due to not using a single database source.

ERP (Enterprise Resource Planning) is standardized management process in the environment information technology. The system uses a common database that provides information across the enterprise using normalized data based on common definitions and user experiences [3]. In recent years, the trend of ERP application in the modern environment, learning is growing strongly and bringing a lot of advantages in operating universities’ activities. The world's leading ERP providers such as ORACLE, SAP, PEOPLESOFT have been successful with the ERP model for many major universities in the world like England, America, Germany.

This paper proposes a specification a management system based on the ERP system to help help HNMU and other universities can consider applying the system in managing school activities to achieve the educational requirements of a modern society.

## 2. WHAT IS ERP SYSTEM?

ERP, or enterprise resource planning, is a modular software system designed to integrates information from all areas of a business into one complete enterprise system. Therefore, the data can be shared across departments in real-time in order to streamline processes and automate common tasks [4]. For example, instead of using individual software such as financial software - accounting, HR management software, production management software, salary management, CRM software... and data not available cohesion and inheritance, the ERP system will integrate all on a single software and the data will be inherited, linked together.

As its definition, there are three main characteristics of ERP system. The first is “*central database*”, this mean that enter data once into your ERP solution and it can be accessed by any other user. The second is "*the operate in real time*", this mean once information is placed into the ERP software, it updates throughout the system, providing up-to-date information in real time for all of its users. And the last is "*Comprehensive*", this mean that most of your daily business functions and processes should be able to operate within the ERP software.

At its core, an ERP system is a database management system, creating and managing a database of business processes including [5]:

**Human Resource**: The module helps to HR team for efficient management of human resources. HR module helps to manage employee information, track employee records, manage salaries, payment reports etc.

**Inventory**: Inventory module can be used to track the stock of items. Items can be identified by unique serial numbers. Using that unique number inventory system can keep track of the item and trace its current location in the organization.

**Sales and Marketing**: The module helps to manage the typical sales process includes processes like Sales queries and inquiry, analysis and handling, quotation drafting, accepting sales orders, drafting sales invoices with proper taxation, dispatch/Shipment of material or service, tracking pending sales order.

**Purchase:** The modules take care of all the processes that are part of the procurement of items or raw materials that are required for the organization.

**Finance and Accounting:** Whole inflow and outflow of money/capital is managed by the finance module.

**Customer Relationship Management (CRM):** CRM department is helping to boost the sales performance through better customer service and establishing a healthy relationship with customers. All the stored details of the customer are available in the CRM module

**Engineering/ Production:** Production module is a great help for the manufacturing industry for delivering the product.

**Supply Chain Management (SCM)**: SCM module manages the flow of product items from manufacturer to consumer and consumer to manufacturer.

The primary differences between ERP system and stand-alone targeted software is a common central database from which the various ERP system modules access information, some of which is shared with the other modules involved in a given business process. This means that companies using ERP are largely saved from having to make double entries to update information because the system shares the data, in turn enabling greater accuracy and collaboration between the organization's departments.

## 3. PROPOSED ERP SYSTEM FOR HNMU

Formally, an ERP solution is a system that integrates all management modules stages in the production process of the business, including: planning, inspection, and supplies input, output products, distribution, accounting, human resources... This is a special product combination information technology (IT) with standardized management process. Therefore, the investment for one ERP solutions are not merely buying software, but standardizing business processes with IT. In the university environment, ERP must be adjusted, add and remove some modules accordingly, such as a human resource management module (officers, students), and subdivisions financial management system, library management module, diploma management module, learning management module, training, facilities…

In HNMU, the operational organization is outlined as follows:

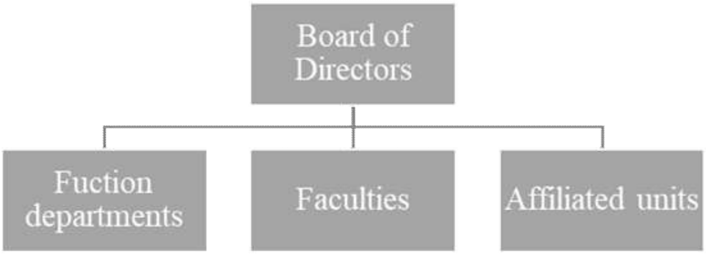

**Figure 1:** *The operational organization of HNMU*

**Board of Directors**: Has the highest authority in the university, runs all of its activities.

**Function departments**: There are 11 functional departments in HNMU. They manage issues related to training, personnel, facilities, examination, research…

**Faculties**: There are 13 faculties in HNMU. They manage training-related issues (teaching, learning, education program, research…).

**Affiliated units**: There are 11 affiliated units in HNMU. They manage issues related to relationships within and outside the university.

Therefore, we suggest modules that ERP needs to deploy in the university as follows:

**Profile management module**: The module helps to manage profiles of students, staffs, diplomas and credits.

**Academic management module**: The module help to manage activities of student and staffs, for example, the learning process of students and teachers' teaching such as: Managing training programs, teaching plan, studying, examination (timetable), and assessing learning outcomes, resource management (Accounts, information services (portal)).

**Financial management module:** Manage the student finance (the fee, scholarships...) and the finance staffs (salary, taxes…).

**Human resource management module**: Manage the recruitment, development and training of human resources, retirement…

**Facilities management module**: Manage classrooms, equipment for training.

**Customer support module**: Employment consulting, market research and marketing brand promotion.

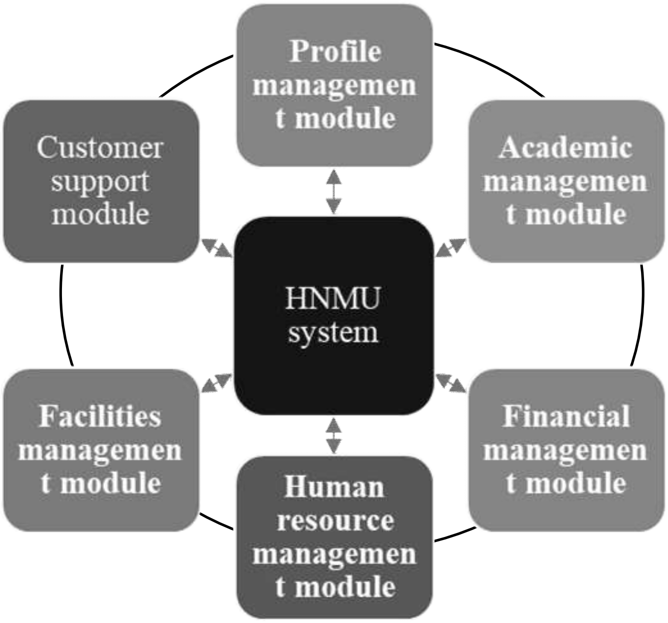

**Figure 2:** *The model of HNMU system*

These modules can be standardized according to individual processes and possible application runs on local databases (for example, financial management programs may have their own databases the process of paying students' fees and running on the office of the finance department). However, these applications must be integrated into an interchangeable system information with each other (for example, the database of student fees must be shared application of the training module to know the schedule of study or exam) to provide information for the management director.

We also suggest some interface images to illustrate a few modules as follows:

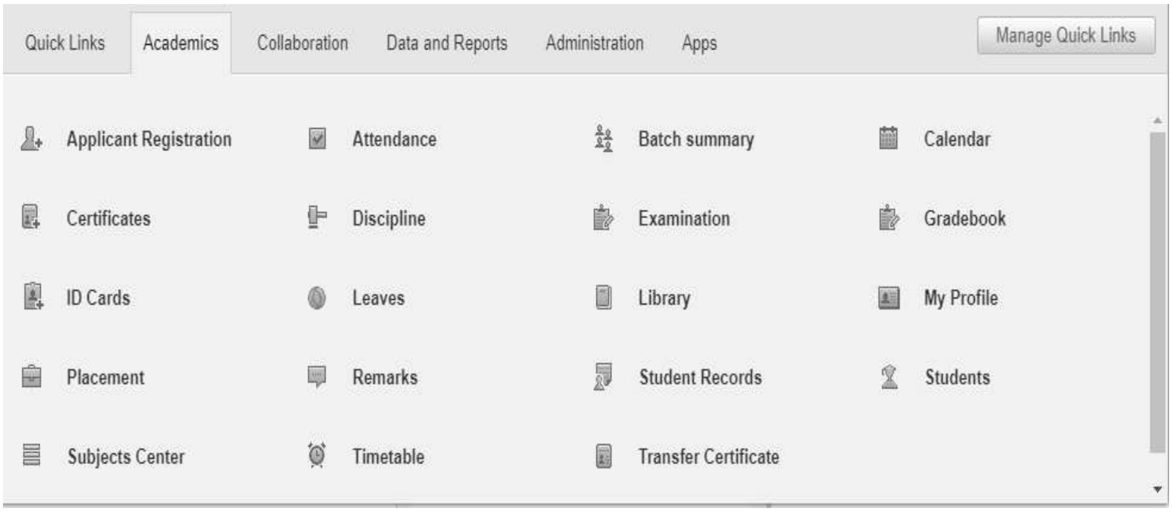

**Figure 3:** *The academic management module*

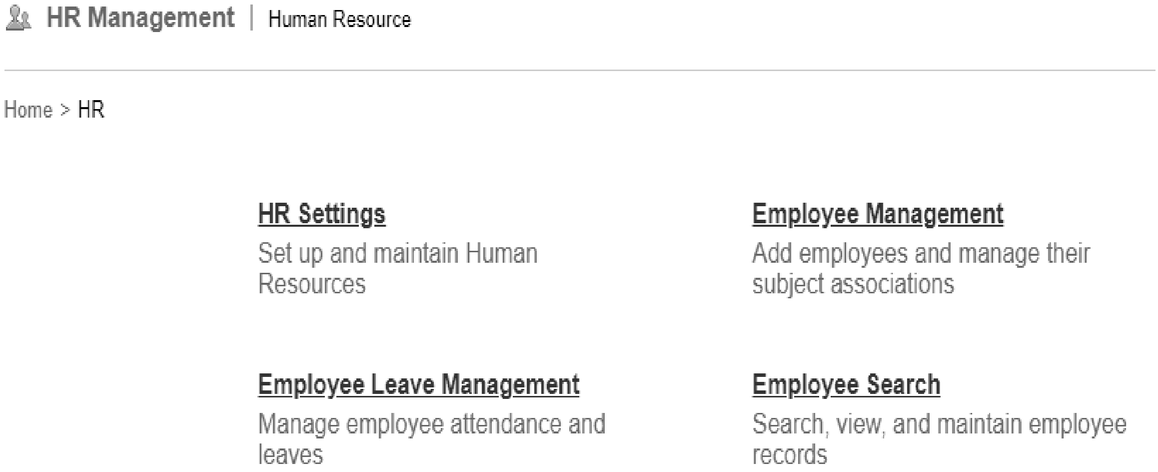
HR Management | Human Resource

Home > HR

HR Settings
Set up and maintain Human Resources

Employee Management
Add employees and manage their subject associations

Employee Leave Management
Manage employee attendance and leaves

Employee Search
Search, view, and maintain employee records

**Figure 4:** *The human resource management module*

From the above analysis, ERP solutions for HNMU according to the following process:

**Step 1 - Building local management modules** (Profile management module, Academic management module, financial management modules, Human resource management module, customer support module and facilities management modules): These local modules are possible using data in different formats.

**Step 2 - Strategic planning for information exploitation of the whole system**: Determining the usage requirements and data sharing between modules, analyzing data, administrative issues and data security.

**Step 3 - Building integrated modules of the system**: Transmission (network), collecting and transferring data, system redundancy.

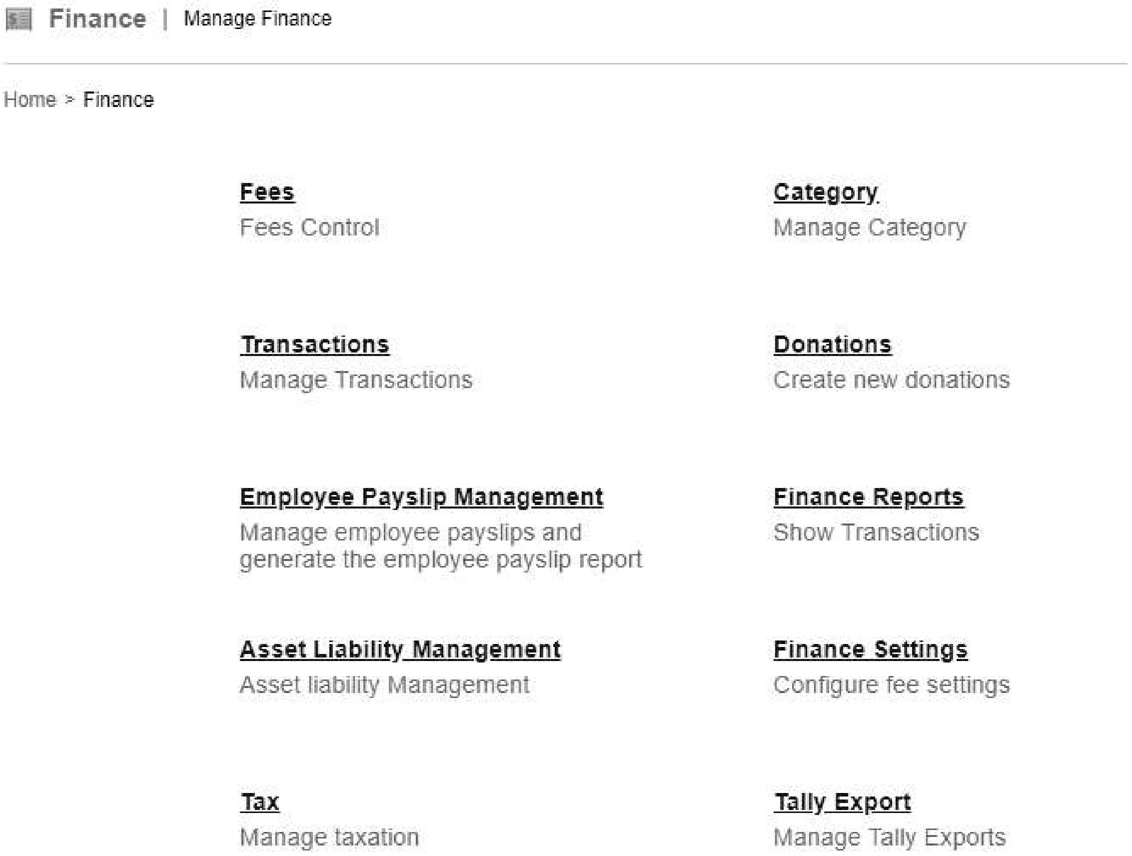

Finance | Manage Finance

Home > Finance

**Fees**
Fees Control

**Category**
Manage Category

**Transactions**
Manage Transactions

**Donations**
Create new donations

**Employee Payslip Management**
Manage employee payslips and generate the employee payslip report

**Finance Reports**
Show Transactions

**Asset Liability Management**
Asset liability Management

**Finance Settings**
Configure fee settings

**Tax**
Manage taxation

**Tally Export**
Manage Tally Exports

**Figure 5:** *Financial management module*

## 4. CONCLUSION

In this paper, we proposed a method for the specification of HNMU system based on the ERP system. The ERP implementation for universities is an inevitable trend of universities which want to build a modern educational environment in order to meet the requirements of education management innovation. ERP brings great benefits to the university enhances the management capacity of the leadership, the work efficiency of the departments and especially create a unified environment that allows the university to exploit information and exchange information conveniently.

The implementing ERP for HNMU as well as other universities has as some advantages as bellows:

- IT application is encouraged and creates opportunities for universities to improve their effectiveness in management and training.

- Universities have the same operating system as businesses, organized enterprises decentralize many departments such as: finance, personnel, planning, administration, supplies... therefore, universities also have issues to solve such as: financial management, human resource, facilities, in a consistent and effective way.

- Combined with IT achievements, especially computer networks and data mining such as data warehousing, distributed databases, ERP models has the advantage of organizing centralized management of geographic dispersed universities.

- ERP is particularly suitable in the trend of building a digital university as well as e-learning, remote online that requires the university to quickly invest in facilities and deployment strategies to meet the training requirements for society.

- Universities are promoting the application of IT to training activities such as the electronic textbooks, electronic library, electronic resources that are opportunities to deploy ERP for universities.

However, there are some difficulties in implementing ERP for universities:

- The biggest difficulty is standardizing the management process. When applying ERP universities must be standardized on the foundation application of information technology in a unified integrated system. The previous IT applications were very fragmented and could not exchange information with each other.

- Human issues should be attended: When implementing ERP for the university or for any business, it is necessary to have experts to advise, deploy and operate this system. Experts mainly support two jobs: standardizing the process of managing and building information technology solutions believe automation management process. Besides, a real problem in the university due to many reasons such as habits, lack of skills, many staffs afraid to access the management program by the regulation standardization process. This obstructs the ERP implementation process in the university.

## REFERENCES

1. The operational organization of HNMU. Available from: http://hnmu.edu.vn/so-do-to-chuc/so-do-to-chuc.html
2. The Hanoi Metropolitan University – the home page. Available from: http://hnmu.edu.vn/
3. Oracle team: *What is ERP?* Available from: https://www.oracle.com/applications/erp/what-is-erp.html
4. Jonas Hedman, Andreas Borell: *ERP Systems Impact on Organizations,* Idea Group Publishing, pp. 1-21, 2003.
5. Bret Wagner, Ellen Monk: *Enterprise Resource Planning,* Cengage Learning publishing, 3 edition (February 4, 2008).

# ĐẶC TẢ HỆ THỐNG QUẢN LÝ ĐỀ XUẤT CHO TRƯỜNG ĐẠI HỌC THỦ ĐÔ HÀ NỘI

***Tóm tắt:*** *Bài báo đề xuất một đặc tả cho một hệ thống quản lý của trường Đại học Thủ đô Hà Nội dựa trên hệ thống ERP. Bằng việc mô tả cơ cấu tổ chức, những hạn chế của hệ thống hiện tại, chúng tôi đề xuất một hệ thống gồm các module chức năng cho các tác vụ của trường nhưng vẫn đảm bảo tính liên thông và nhất quán dữ liệu do cơ sở dữ liệu dùng chung. Những ưu điểm và hạn chế khi triển khai hệ thống cũng được chỉ ra nhằm giúp HNMU và các trường đại học khác có thể xem xét áp dụng hệ thống trong quản lý hoạt động của trường để đạt các mục tiêu giáo dục.*

***Từ khóa:*** *Đặc tả, hệ thống quản lý, trường đại học, ERP, mô đun, cơ sở dữ liệu dùng chung.*

# STUDY ON ISOLATING AND DETERMINING THE STRUCTURE OF SOME ORGANIC COMPOUNDS IN TUBERS OF STEMONA TUBEROSA IN CENTRAL HIGHLANDS OF VIETNAM

**Pham Van Cong**
*Tay Bac University*

***Abstract:*** *5-hydroxymetylfurfural (1), bisdehydroneotuberostemonine (2) and a mixture containing neotuberostemonine (3) were isolated from Stemona tuberosa's climbing plant. The chemical structure of these compounds is determined by 1-dimensional and 2-dimensional magnetic resonance spectroscopy methods as well as comparison with references.*

***Keywords***: *Stemona tuberosa, fural, ankaloids, stemonine, Central Highlands of Vietnam*

Email: phamvancongdhtb@gmail.com

Received 19 October 2019
Accepted for publication 25 November 2019

## 1. PREAMBLE

Stemona is one of the precious medicinal plants used to cure many folk diseases such as cough, skin diseases... [1-3]. With such effects, cypress in Vietnam has been studied and researched for a long time by scientists and has found many valuable compounds, especially alkaloids [4].

Cypress tree is a shrub, grows wild in the plaints of Southern of Vietnam, Central Highlands of Vietnam, Northeast of Thailand. According to the folk experience in the South and Central Highlands of Vietnam, people have used the roots of the cypress tree to treat many effective diseases such as skin diseases, liver cancer... [1]. In addition, the bulbs have the ability to make insecticides, termites... The research on the trees in the Central Highlands of Vietnam is very limited, mostly only at the level of researching plant subspecies. There have not been any researches on the chemical composition and biological activity of this tree in the Central Highlands.

## 2. EXPERIMENTAL AND RESEARCH METHODS

### 2.1. Plant samples

Stemona tuberosa tubers of climbing trees are collected from Central Highlands in October, 2013. Sample issued by PhD. Do Huu Thu (Institute of Natural Resources and Environment Ecology, VAST) identifies the scientific name.

### 2.2. Chemicals and equipment

- Thin layer chromatography (TLC): Performed on a thin, pre-coated sheet of DC-Alufolien 60 F254 (Merck-Germany). Detect the substance with ultraviolet light in two wavelengths 254 and 368 nm, sulfuric acid reagent ($H_2SO_4$ + methanol + vanillin) dried at a temperature of > 100 $^oC$ until the color appears.

- Column chromatography (CC) is carried out with normal phase adsorbents (Silica gel 60-160 and 240-430 mesh, Merck).

- Nuclear magnetic resonance spectrum (NMR) was measured on the Bruker AM500 FT-NMR Spectrometer.

- MS, NMR spectra were measured at the Institute of Chemistry, Vietnam Academy of Science and Technology.

### 2.3. Extraction and isolation of substances

Cypress roots have a weight of 1.0 kilograms (dried, chopped), this amount of sample is soaked in solvent $H_2O$: MeOH = 80:20 (5 liters). The sample was soaked for 1 week, ultrasonic extraction several times. Carry out the separation of the yellow solution and the residue. The residue is further soaked in $H_2O$: MeOH solvent. Repeat several times until the filtered water remains only a pale yellow color. The portion of solution used for distillation of the evaporator is high yellow, liquid, gelatinous (PVC). After that, the total alkaloid extract was treated in the direction of the alkaloids extraction yielding 5.2 grams of the total alkaloid. The chromatographic column of silica gel column and crystallized were obtained with two pure substances, compound **1** [PVC2E2 (10 mgrs)], compound **2** [PVC2F2 (84 mgrs), and an alkaloid-rich fraction [PVC2E1 (48 mgrs)].

## 3. RESULTS

### 3.1. Compound 1 (PVC2E2)

$^1H$ NMR spectrum of compound **1** (figure 3.1) has 5 protons, including:

- A proton of the -CHO group has a chemical shift of 9.61 ppm.

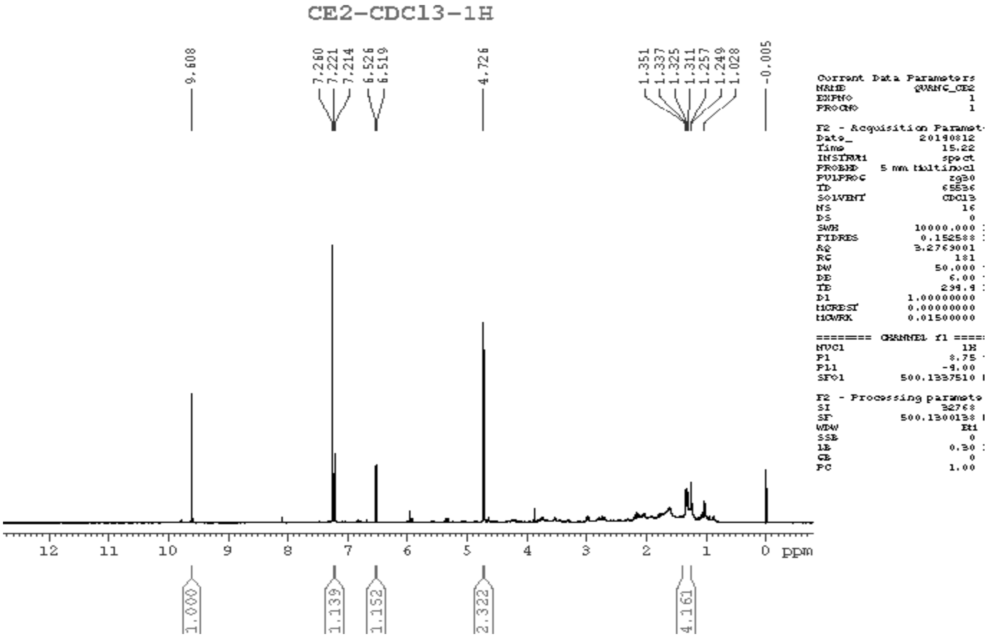

**Fig 3.1:** *$^1$H NMR spectrum of PVC2E2 compound*

- The two protons have a chemical shift at 7.22 and 6.52 ppm with a spin-spin separation constant J = 3.5 Hz, which is predicted to be two carbon-linked protons adjacent to each other. Compared to reference [6] we predict **1** contains furan rings.

- Two protons equivalent, with a chemical shift of 4.73 ppm are expected to be protons of the $–CH_2-O-$ group.

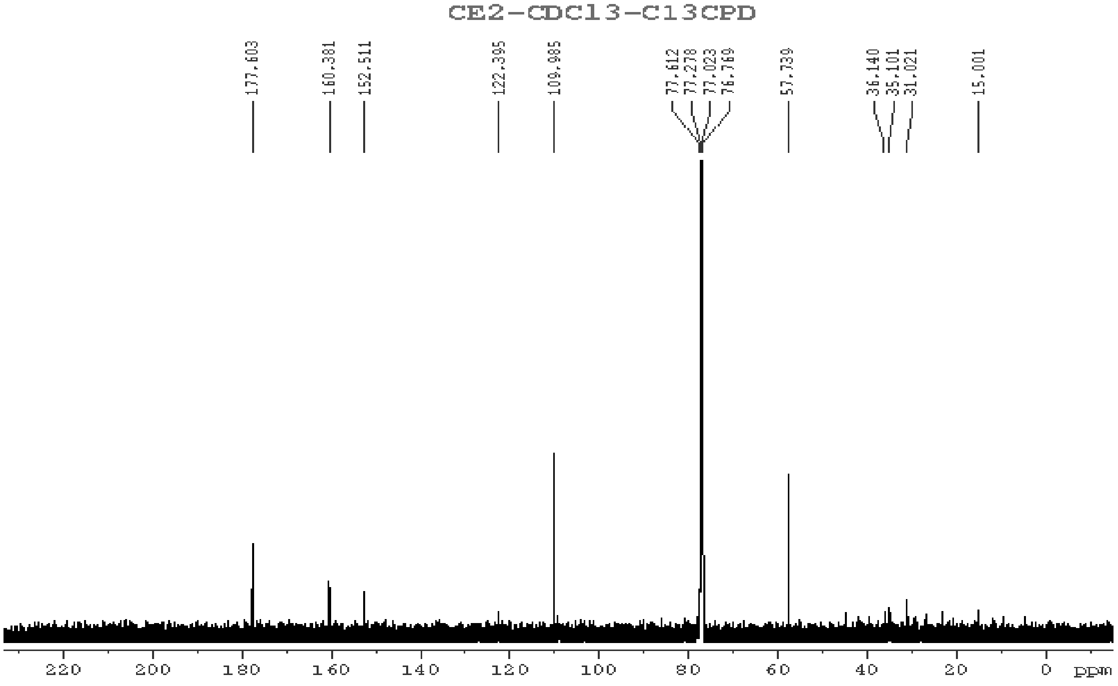

**Fig 3.2:** *$^{13}$C NMR spectrum of PVC2E2 compound*

- $^{13}$C NMR spectrum of compound **1** (Figure 3.2) has a signal at 177.6 ppm which is attributed to carbon of –CHO group.

- A signal at 57.7 ppm is attributed to the carbon of the $CH_2$-O group.

- Also there are 4 sp$^2$ hybrid carbon with a chemical shift of 160.4; 152.5; 122.4 and 110.0 ppm.

To determine the structure of this compound, we conducted 2D NMR spectroscopy which is HSQC and HMBC spectra.

- In the HSQC spectrum (Figure 3.3) there are the following correlations:

+ The 7.22 ppm signal is delivered with C at 122.4 ppm.

+ The proton signal at 6.52 ppm intersects with the C at 110.0 ppm.

+ The signal at 4.73 ppm intersects with the C at 57.7 ppm.

Finally, the structure of compound **1** is determined by the HMBC spectrum (Fig 3.4). Among them are the following interactions between proton and carbon:

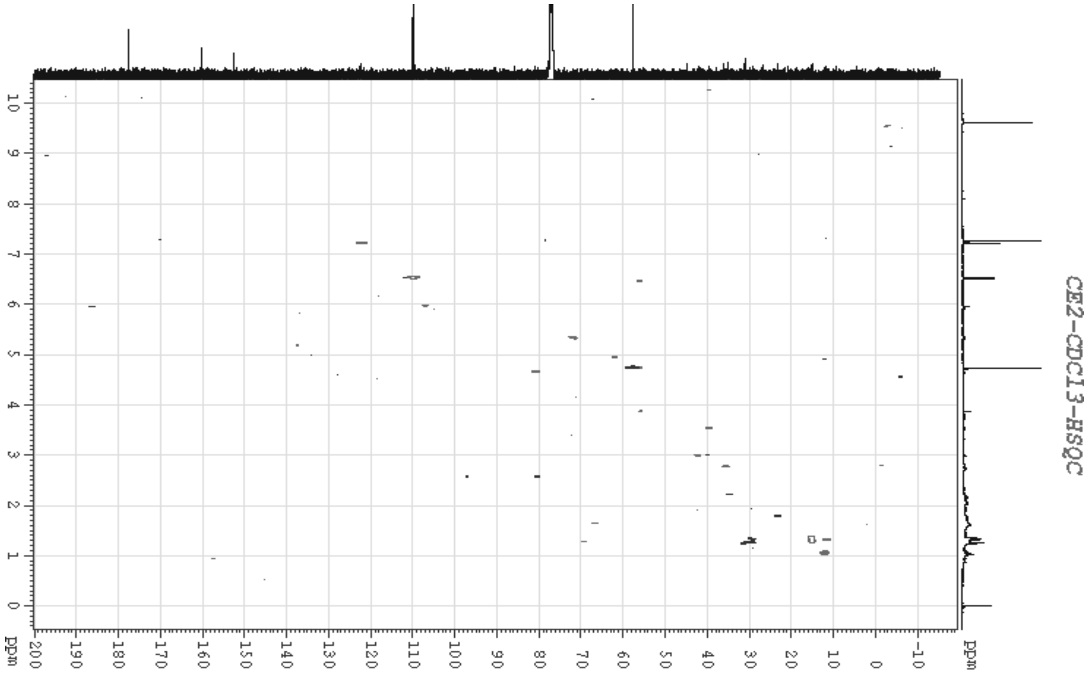

**Fig 3.3:** *HSQC spectrum of compound 1*

- Two protons at 4.73 ppm have a far interaction with C-4 (110.0 ppm) and C-5 (160.4 ppm), the –$CH_2OH$ group attaches to C-5 furan ring.

- Proton H-3 and H-4 have a long interaction with C-2 and C-5, thus deducing the group -CHO attached to C-2. Therefore, this compound contains furfural framework.

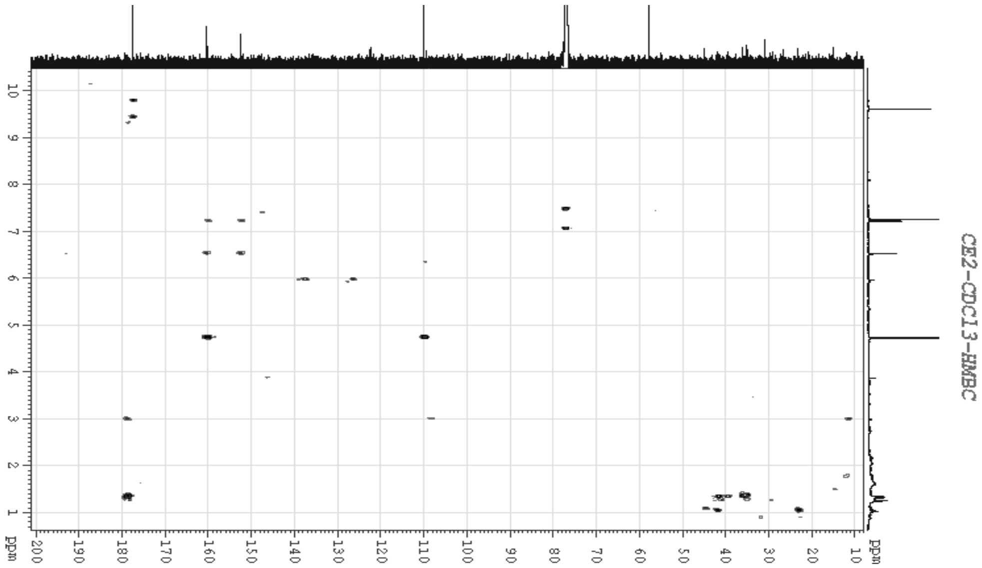

**Fig 3.4:** *HMBC spectrum of compound 1*

So, compound **1** is 5-hydroxymethylfurfural with the following structure:

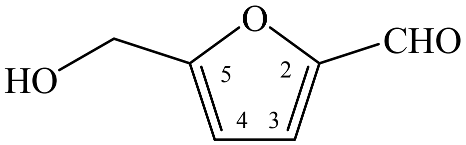

Compound structure **1**

**Table 3.1:** *The NMR spectrum data of 1 and compared with reference*

| Order number | Prussia $^{1}$H NMR | Prussia $^{13}$C NMR | Document [5] |
|---|---|---|---|
| 2 |  | 152,5 |  |
| 3 | 7,22, d, 3,5 Hz | 122,4 | 7,24, d, 3,4 Hz |
| 4 | 6,52, d, 3,5 Hz | 110,0 | 6,54, d, 3,4 Hz |
| 5 |  | 160,4 |  |
| 2-CHO | 9,61, s | 177,6 | 9,62, s |
| 5-CH$_2$OH | 4,73, s | 57,7 | 4,75, s |

## 3.2. Compound 2 (PVC2F2)

Compound No. 2 is purified by the method of recrystallization in ethanol solvent for white, needle-shaped crystals.

$^{1}$H NMR spectrum of compound 2 (Figure 3.5) has the following signals:

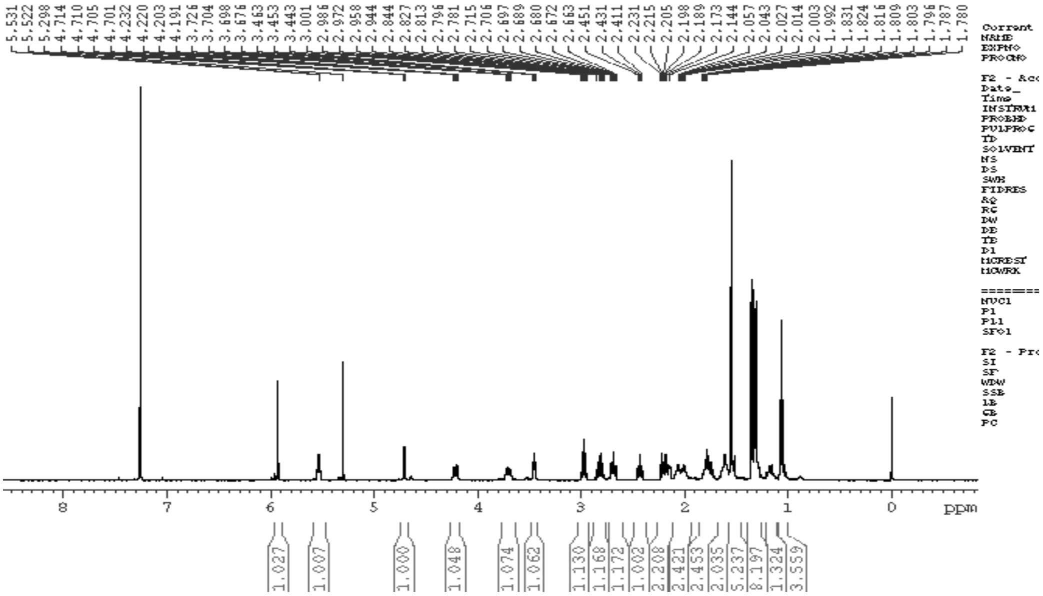

**Fig 3.1:** *$^1$H NMR spectrum of compound 2*

- There is a proton with a chemical shift of 5.93 ppm which is attributed as H attached to $sp^2$ hybridized carbon.

- The two methyl groups, which are double bonded with secondary carbon, have a chemical shift of 1.32 and 1.35 ppm.

- A methyl group has the shape of a triplet, deducing that with the $–CH_2\text{-}CH_3$ group.

Analysis of $^{13}C$ NMR spectrum of compound **2** shows:

- There are two groups of C = O with chemical shift at 178.7 and 178.8 ppm.

- There are 4 carbon hybrid $sp^2$.

- There are two carbon bonded to oxygen at 80.8 and 71.7 ppm. Comparing NMR spectrum data of compound **2** with bisdehydroneotuberostemonine, we found a good match. So compound **2** is bisdehydroneotuberostemonine [5].

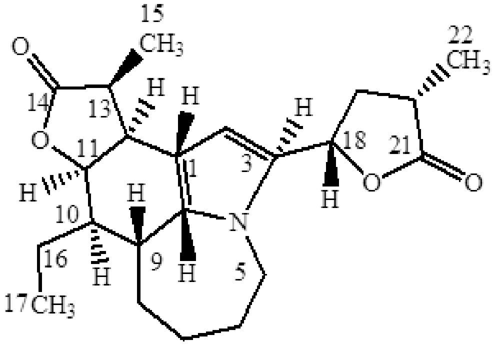

Compound structure **2**

**Table 3.2:** *The NMR spectrum data of 2 and compared with reference*

| Order number | $^1$H NMR | $^{13}$C NMR | $^1$H NMR [6] | $^{13}$C NMR [6] |
|---|---|---|---|---|
| 1 | | 107.1 | | 107.1 |
| 2 | 5,93, s | 108.6 | 5,95, s | 108.7 |
| 3 | | 137.5 | | 137.1 |
| 5 | 4,21, dd, 6.0, 14.5 | 44.8 | 4,20, ddd, 15.5, 5.0, 1.0 | 44.8 |
| | 3,70, dd, 14.0, 11.0 | | 3,73, dd, 15.0, 11.4 | |
| 6 | 2.00, m | 28.6 | 1.93, m | 28.6 |
| | 1,30, m | | 1.30, m | |
| 7 | 2,03, m | 29.1 | 2,03, m | 29.2 |
| | 1,52, m | | 1,45, m | |
| 8 | 1,18, m | 35.0 | 1.10, ddd, 11.7, 3.2, 8.2 | 35.1 |
| | 1,30, m | | 1.30, m | |
| 9 | 2,70, m | 36.0 | 2.73, m | 36.1 |
| 9a | | 127.5 | | 127.8 |
| 10 | 1,99, m | 34.8 | 1,90, m | 34.9 |
| 11 | 4,70, ddm 2.0, 4.5 | 80.8 | 4,62 brd, 5.0 | 80.8 |
| 12 | 3,45, brt, 5.0 | 39.5 | 3,51, dd, 7.1, 5.0 | 39.6 |
| 13 | 2,97, m | 41.9 | 2,95, dq, 7.1, 7.3 | 41.9 |
| 14 | | 178.7 | 1,30, d, 7.3 | 178.7 |
| 15 | 1,30, d, 7.0 | 15.0 | 1,75-1,85, m | 15.0 |
| 16 | 1,75-1,85, m | 23.2 | 1,03, t (7.5) | 23.2 |
| 17 | 1,06, t, 6.5 | 11.4 | 5,33, dd(5.2, 11.2) | 11.4 |
| 18 | 5,53, dd, 5.0, 8.0 | 71.7 | 2.77, ddd (5.2, 5.4, 11.7) | 71.7 |
| 19 | 2,70, m | 30.9 | 2.15, ddd (11.7, 11.9, 11.2) | 30.8 |
| | 2,15, m | | | |
| 20 | 2,81, m | 44.8 | 2.80, ddq (5.4, 11.9, 6.9) | 44.8 |
| 21 | | 178.8 | 1.35, d (6.9) | 178.7 |
| 22 | 1,35, d, 7.0 | 11.8 | | 11.8 |

## 3.3. Compound 3 (PVC2E1)

In addition, we isolated a segment of PVC2E1 that is rich in alkaloids. We conducted a TLC test and column chromatography, but couldn't be purer. Analysis of $^1$H NMR spectrum (Figure 3.6) of this mixture showed that many signals coincide with the spectrum of neotuberostemonine (3).

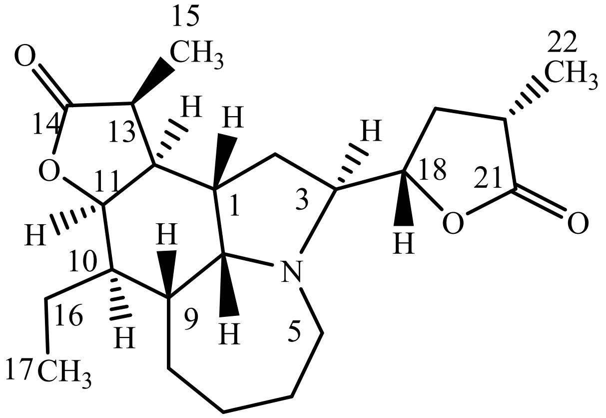

Compound structure **3**

Thus, from the extract of the vines, S. tuberosa collected from Central Highlands of Vietnam, we purified 5-hydroxymethylfurfural (1), bisdehydroneotuberostemonine (2) and a mixture containing neotuberostemonine (3).

## 4. CONCLUSION

By means of one-and-two-dimensional magnetic resonance spectroscopy, combined with reference, we have determined the structure of two compounds, 5-hydroxymethylfurfural (1) and bisdehydroneotuberostemonine (2), recommended structure of neotuberostemonine (3).

This result is completely consistent with the previous research results on alkaloids in tubers of climbing plants in Ha Nam of Vietnam [4] and Kunming of China [5].

## REFERENCES

1. Do Tat Loi (1977), *Vietnamese medicinal plants and herbs*, - Science and Technology Publishing House, Hanoi, p.180-181 (in Vietnamese).
2. Nguyen Tien Ban (2003), *List of Vietnamese plant species. 3*, - Publishing house. Agriculture (in Vietnamese).

3. Pham Hoang Ho (1999), *Vietnamese Plants*, Volume 3, - Young Publishing House (in Vietnamese)

4. Pham Huu Dien, Pham Van Kiem, Luu Van Chinh and Chau Van Minh (2000), "Alkaloids from Stemona tuberosa Lour root tubers, - *Journal of Chemistry*, volume 38, pp.64-67 (in Vietnamese).

5. Suqin Hu, Zhaofu Zhang, Jinliang Song, Yinxi Zhou and Buxing Han (2009), "Efficient conversion of glucose into 5-hydroxymethylfurfural catalyzed by a common Lewis acid SnCl4 in an ionic liquid", - *Green Chem.*, 2009, 11, pp.1746-1749.

6. Yang Ye, Guo-Wei Qin and Ren-Sheng Xu (1994), "Alkaloids from Stemona tuberosa", - *Phytochemistry*, 37, pp.1201-1203.

# NGHIÊN CỨU PHÂN LẬP VÀ XÁC ĐỊNH CẤU TRÚC MỘT SỐ HỢP CHẤT HỮU CƠ TRONG CỦ CÂY BÁCH BỘ THÂN LEO (STEMONA TUBEROSA) Ở TÂY NGUYÊN

***Tóm tắt***: *5-hydroxymetylfurfural (1), bisdehydroneotuberostemonine (2) và hỗn hợp chứa neotuberostemonine (3) đã được phân lập từ củ cây bách bộ thân leo Stemona tuberosa. Cấu trúc hóa học của các hợp chất này được xác định bằng các phương pháp phổ cộng hưởng từ hạt nhân 1 chiều và 2 chiều cũng như kết hợp so sánh với tài liệu tham khảo.*

***Từ khóa:*** *Stemona tuberosa, fural, ankaloids, stemonin, Tây Nguyên.*

# LAND USE AND MANAGEMENT: NATURAL CHARACTER ASSESSMENTS IN GIAO THUY, NAM DINH PROVINCE

**Ngo Thanh Son**[1] **, Nguyen Bich Ngoc**[2]
[1]*Hanoi Metropolitan University*
[2]*Hanoi University of Natural Resources & Environment*

***Abstract:*** *The results of general analysis of natural characteristics of climate, hydrology, soil and vegetation cover of a territory are defined as scientific bases to assess the function and role of the scene. Ecological mandates of the territory, for planning purposes, management of territorial resource development. Through the process of analysis and evaluation, the research has identified the characteristics of landscape structure in Giao Thuy district which are located in the tropical monsoon landscape system, the tropical monsoon landscape with cold winter, including: one plain landscape layer and one side landscape coastal plain with 20 different landscape types. On that basis, assessing the potential of the landscape, contributing to the district's orientation on land resource planning, agricultural and forestry development in association with environmental protection.*

***Keywords***: *landscape, landscape architecture, planning and agriculture – forestry*

Email: ntson@hnmu.edu.vn

Received 15 October 2019
Accepted for publication 20 November 2019

## 1. INTRODUCTION

Giao Thuy district (Nam Dinh province) is adjacent to the sea with a coastline of more than 32km. The potential advantages of the location allows the district to develop an integrated agricultural economy - forestry. However, the issue of natural resources exploitation and utilization for sustainable development is an urgent concern. The evaluation of natural conditions and assessing the landscape of Giao Thuy district would clarify the potential of the district as a scientific basis to propose a sustainable development orientation.

# 2. SUBJECT AND METHODS

## 2.1. Subject

Subject: natural characteristic and natual resources.

Evaluating sites: Giao Thuy distric, Nam Dinh province.

## 2.2. Method

***1. Reference collection:*** Documents, reports, research projects related to the topic were thoroughly collected and synthezised.

***2. Field survey:*** The survey on natural characteristics and territorial differentiation was carried out.

***3. Landscape classification:*** The PLCQ system in the study area was developed according to the PLCQ system designed by Pham Hoang Hai et.al. (1997).

***4. Landscape assessment*** [3]

*a) Criterion*

❖***Land classifying:*** characteristics of land, viewscape, water quality, soil quality etc...

❖***Slope:*** $15^0$

❖ ***Topographic:*** Characteristics of the plain and hills

❖***Rainfall and temperature:*** Optimal temperatures for agriculture range from $20^0$ – $25^0$C. Rainfall: heavy rain: ≥ 2.500mm, morderate rain: 1.500 - 2.500mm.

❖***Hydrology:*** evaluated based on water supply capacity

*b) Scale and weighting scale*

Table 1 showed the scale and weighting scale in this evaluation

**Table 1:** *Scale and weighting scale*

| TT | Scale | | Weighting scale | |
|---|---|---|---|---|
| | **Level** | **Score** | **Level** | **Score** |
| 1 | Well appropriate | 3 | Decisive influence | 3 |
| 2 | Appropriate | 2 | Strong influence | 2 |
| 3 | Less appropriate | 1 | Negligible influence | 1 |

*c) Scoring*

❖The CQ was calculated as the following equation:

$$\text{CQ}: X = X_1.n_1 + \ldots + X_i.n_i \tag{I}$$

where: X: general score of CQ; $X_i$ score for the criteria i; $n_i$ weighting scale; i criteria, i = 1,2,3…n

❖ Scale: $$\Delta D = \frac{D_{\max} - D_{\min}}{M} \quad \text{(II)},$$

where: $D_{rax}$ highest score; $D_{\min}$ lowest score; (M = 3)

## 3. RESUTLS AND DISCUSSIONS

### 3.1. Ecological landscape of Giao Thuy district, Nam Dinh province

*Topographical conditions:* Giao Thuy district is a relatively flat plain and tends to decrease from North to South. The territory is divided into 2 areas: inland areas and coastal alluvial areas with 32km of coastline. Large fishing grounds, diverse creatures and beautiful beaches create favorable conditions for fisheries and tourism.

*Land:* of the district is generally fertile with 6 different soil types: (Pb) Alluvial soil that is enriched annually; (P) Alluvial soil that is not accreted annually; (M) saline soil; (C) saline sandy soil; (Jmn) Salty muddy soil; (Sp) Potential alum soil.

*Climate:* Giao Thuy district is located in the humid monsoon tropics with four distinct seasons. The annual average temperature: $24^0$C. The average annual rainfall is approximately 1,775mm. The rainy season is from May to October. The dry season starts from November of the previous year to April of the following year [5].

*River system:* The district is surrounded by two main rivers: Red River and So River. The tide is diurnal tide with the average amplitude from 1.6 to 1.7 m (the largest is 3.3 m and the smallest is 0.1 m). The district has a coastline of 32km. The salinity varies with a very large variation from 11 ‰ - 30 ‰. In addition, the variation in salinity depends on the months of the year and the location of each site. In winter, the average salinity of seawater ranges from 28-30 ‰. In summer, the average salinity ranges from 20 to 27 ‰. The pH variation is from 8.0 - 8.4 depending on the amount of fresh water, seawater and physiological activities of aquatic animals. The pH between two periods of high tide and low tide in a cycle is 6.5.

### 3.2. Characteristics of landscape structure

Giao Thuy district in particular and the whole territory of Vietnam in general are located in the tropical monsoon region, which has the full characteristics of a tropical monsoon landscape system and the tropical monsoon landscape with cold winter influenced by the cold and dry Northeast monsoon, and the hot and humid Southeast monsoon.

Giao Thuy is in the plain, without hills and mountains, including the formations of Tertiary sediments, Neogen sediments, and Quaternary sediments, which are classified into the plain landscape.

Topography of Giao Thuy district has absolute height of 0.5-0.9m, It can be classified as a lowland terrain located at the door of Ba Lat beach.

Landscape type is divided based on the characteristics of the mutual relationship between plant communities and soil types, forming 20 types of landscapes corresponding to 3 landscape categories (Table 2).

**Table 2:** *Distribution of landscape types*

| **Class CQ** | **Type CQ** | **Soil type** | **Vegetation** | **Distribution** |
|---|---|---|---|---|
| Accruals clay silt sediments along river banks | 1 | $P_b$ | Paddy field | Hong Thuan, Giao Huong |
| | 2 | | Perennial tree | Hong Thuan, Giao Huong |
| | 3 | | Grasslands and shrubs | From Ngo Dong to Giao Huong |
| The delta clay silt deposits accumulating from river | 4 | P | Paddy field | Giao Tien, Ngo Dong, Hong Thuan, Giao Huong, Binh Hoa, Hoanh Son, Giao Nhan, Giao Hoa, Giao Thanh |
| | 5 | $M_i$, $M_{tb}$ | Paddy field | Giao Chau, Giao Yen, Giao Hai, Giao Xuan, Giao An, Giao Thanh, Giao Thien |
| | 6 | | Perennial tree | Quat Lam, Giao Phong |

| **Class CQ** | **Type CQ** | **Soil type** | **Vegetation** | **Distribution** |
|---|---|---|---|---|
|  | 7 |  | Freshwater aquatic plant | Giao Ha, Giao Yen |
|  | 8 | $S_p$ | Paddy field | Giao Tien, Giao Tan |
| Mud and organic humus sediments, | 9 | $M_n$ | Paddy field | Giao Thien, Giao An, Giao Lac, Giao Xuan, Giao Long |
|  | 10 |  | Perennial tree | Bach Long |
|  | 11 |  | Grasslands and shrubs | Bach Long |
|  | 12 |  | Brine-pan | Bach Long, Giao Phong, Quat Lam |
|  | 13 |  | Shellfish field | Con Lu |
|  | 14 |  | Shrimp pond | Giao Thien, Giao An, Giao Lac, Giao Xuan, Giao Long, Bach Long,, Giao Phong, Quat Lam, Con Ngan, Con Lu |
|  | 15 |  | Forest | Con Lu, Con Ngan, Giao Phong, Quat Lam |
|  | 16 | $C_m$ | Grasslands and shrubs | Coastal part in the SouthEast of the district |
|  | 17 |  | Shellfish field | Con Lu |
|  | 18 |  | Shellfish field | Con Xanh |
|  | 19 |  | Forest | Giao An, Giao Lac, Giao Xuan |
|  | 20 | $J_{mn}$ | Shellfish field | Con Lu |

Formula (I) and (II) were used to calculate the aggregate advantage level of each landscape type and to classify the degree of adaptation of landscape types. Table 3, 4, and 5 sumarized the obtained results.

**Table 3:** *Targets for crop development*

| Landscape type | Criteria | | | | | | | |
|---|---|---|---|---|---|---|---|---|
| | Soil | | Water | | Rainfall | Temperature | Current status | Final score |
| | Weighting scale | Score | Weighting scale | Score | | | | |
| 1 | 3 | 3 | 2 | 3 | 2 | 3 | 3 | 4.6 |
| 2 | 3 | 3 | 2 | 3 | 2 | 3 | 2 | 4.4 |
| 3 | 3 | 3 | 2 | 3 | 2 | 3 | 1 | 4.2 |
| 4 | 3 | 3 | 2 | 2 | 2 | 3 | 3 | 4.2 |
| 5 | 3 | 2 | 2 | 2 | 2 | 3 | 3 | 3.6 |
| 6 | 3 | 2 | 2 | 2 | 2 | 3 | 2 | 3.4 |
| 7 | 3 | 2 | 2 | 2 | 2 | 3 | 1 | 3.2 |
| 8 | 3 | 2 | 2 | 2 | 2 | 3 | 3 | 3.6 |
| 9 | 3 | 1 | 2 | 1 | 2 | 3 | 3 | 2.6 |
| 10 | 3 | 1 | 2 | 1 | 2 | 3 | 2 | 2.4 |
| 11 | 3 | 1 | 2 | 1 | 2 | 3 | 1 | 2.2 |

$L_1$ – Very appropriate : 4.6 – 3.8

$L_2$ – Appropriate : 3.7 – 3.1

$L_3$ – Less appropriate : 3.0 - 2.2

+ The landscape that is very suitable for farming (L1) : 1, 2, 3, 4.

+ The landscape that is suitable for farming (L2) : 5, 6, 7, 8.

+ The landscape that is less suitable for farming (L3) : 9, 10, 11

**Table 4:** *Targets for aquaculture development*

| Landscape | Criteria | | | | | | | |
|---|---|---|---|---|---|---|---|---|
| | Topography | | Hydrology | | Environment | Temperature | Current status | Final score |
| | Weighting scale | Score | Weighting scale | Score | | | | |
| 1 | 1 | 1 | 2 | 2 | 2 | 3 | 1 | 2.2 |
| 3 | 1 | 1 | 2 | 2 | 2 | 3 | 2 | 2.4 |
| 4 | 1 | 1 | 2 | 2 | 2 | 3 | 1 | 2.2 |
| 5 | 1 | 1 | 2 | 2 | 2 | 3 | 1 | 2.2 |
| 7 | 1 | 2 | 2 | 3 | 2 | 3 | 3 | 3.2 |
| 8 | 1 | 1 | 2 | 2 | 2 | 3 | 1 | 2.2 |
| 9 | 1 | 1 | 2 | 3 | 2 | 3 | 1 | 2.6 |
| 11 | 1 | 1 | 2 | 3 | 2 | 3 | 2 | 2.8 |
| 13 | 1 | 3 | 2 | 3 | 2 | 3 | 3 | 3.4 |
| 14 | 1 | 3 | 2 | 3 | 2 | 3 | 3 | 3.4 |
| 16 | 1 | 1 | 2 | 3 | 2 | 3 | 2 | 2.8 |
| 17 | 1 | 3 | 2 | 3 | 2 | 3 | 3 | 3.4 |
| 18 | 1 | 3 | 2 | 3 | 2 | 3 | 3 | 3.4 |
| 20 | 1 | 3 | 2 | 3 | 2 | 3 | 3 | 3.4 |

$T_1$ – Very appropriate : 3.4 – 3.0

$T_2$ – Appropriate : 2.9 – 2.5

$T_3$ – Less appropriate : 2.4 – 2.0

+ The landscape is very suitable for aquaculture (T1) : 7, 13, 14, 17, 18, 20.

+ The landscape is suitable for aquaculture (T2) : 11, 16.

+ The landscape is less suitable for aquaculture (T3) : 1, 3, 4, 5, 8, 9.

**Table 5:** *Indicators for forestry development*

| Landscape | Criteria | | | | | | Final score |
|---|---|---|---|---|---|---|---|
| | Soil | | Hydrology | | Rainfall | Current status | |
| | Weighting scale | Score | Weighting scale | Score | | | |
| 6 | 3 | 1 | 2 | | 2 | | 0.8 |
| 7 | 3 | 1 | 2 | | 2 | | 0.8 |
| 9 | 3 | 3 | 2 | | 2 | | 2.3 |
| 10 | 3 | 3 | 2 | | 2 | | 2.3 |
| 11 | 3 | 3 | 2 | | 2 | | 2.3 |
| 12 | 3 | 3 | 2 | | 2 | | 2.3 |
| 13 | 3 | 3 | 2 | 3 | 2 | 1 | 4.3 |
| 14 | 3 | 3 | 2 | 3 | 2 | 1 | 4.3 |
| 16 | 3 | 2 | 2 | 3 | 2 | 2 | 4.0 |
| 15 | 3 | 3 | 2 | 3 | 2 | 3 | 5.3 |
| 17 | 3 | 2 | 2 | 3 | 2 | 1 | 3.4 |
| 18 | 3 | 2 | 2 | 3 | 2 | 1 | 3.4 |
| 19 | 3 | 2 | 2 | 3 | 2 | 3 | 5.3 |
| 20 | 3 | 2 | 2 | 3 | 2 | 1 | 3.4 |

$R_1$ – Very appropriate : 5.3 – 3.8

$R_2$ – Appropriate : 3.7 – 2.2

$R_3$ – Less appropriate : 2.1 – 0.6

+ The landscape is very suitable for saline forests (R1) : 13, 14, 15, 16, 19.

+ The landscape is suitable for saline forests (R2) : 9, 10, 11, 12, 17, 18, 20.

+ The landscape is less suitable for saline forests (R3) : 6, 7

According the summary tables assessing the appropriateness of landscapes for each production purpose, and the reviewing of current situation and development orientation of the locality, the most appropriate landscapes for production purposes was selected to make suggestions on the orientation of agriculture - forestry development in Gao Thuy district and develop a map of the direction of using the territory for the item destination for economic development and environmental protection in Giao Thuy district (Table 6).

***Table 6.*** *The orientation of using landscape of Giao Thuy district*

| **Type of CQ** | **Function of CQ** | **Current status of CQ** | **Final results** | **Proposed orientation** |
|---|---|---|---|---|
| 1 | Producing | Paddy field | *L1,T3* | Rice cultivation |
| 2 | Producing | Perennial tree | *L1* | Rice cultivation |
| 3 | Producing | Grasslands and shrubs | *L1,T3* | Rice cultivation |
| 4 | Producing | Paddy field | *L1,T3* | Rice cultivation |
| 5 | Producing | Paddy field | *L2,T3* | Rice combined with short-day crops and cereals cultivation |
| 6 | Producing | Perennial tree | *L2,R3* | Rice combined with short-day crops and cereals cultivation |
| 7 | Producing | Freshwater aquatic plant | *L2,T1,R3* | Aquaculture |
| 8 | Producing | Paddy field | *L2,T3* | Rice combined with short-day crops and cereals cultivation |
| 9 | Producing | Paddy field | *R2,T3,L3* | Afforestation |
| 10 | Producing | Perennial tree | *R2,L3* | Afforestation, Perennial tree planting |
| 11 | Producing | Grasslands and shrubs | *T2,R2,L3* | Afforestation, Aquaculture |
| 12 | Producing | Brine-pan | *R2* | Saline forest |
| 13 | Producing | Shellfish field | *T1,R1* | Afforestation, Aquaculture |
| 14 | Producing | Shrimp pond | *T1,R1* | Afforestation, Aquaculture |
| 15 | Protecting, Producing | Forest | *R1* | Saline forest |
| 16 | Producing | Grasslands and shrubs | *T2,R1* | Afforestation |
| 17 | Producing | Shellfish field | *T1,R2* | Afforestation, Aquaculture |
| 18 | Producing | Shellfish field | *T1,R2* | Afforestation, Aquaculture |
| 19 | Producing | Forest | *R1* | Saline forest |
| 20 | Producing | Shellfish field | *T1,R2* | Afforestation, Aquaculture |

Accordingly, the CQ No 1, 2, 3 và 4 are best for Rice cultivation, while the CQ No 5, 6 and 8 are best for the combination of rice, short-day tree and cereals cultivation. Aquaculture should be developed in the CQ No 7, 17, 18, and 20. Both saline forest and aquaculture should be developed in the CQ No 11, 13 , and 14. The CQ No 9, 10, 12, 15, 16, 19 are appropriate for saline forest.

## 4. CONCLUSIONS

Thorough valuation of the different characteristics of the terrain, soil, climate, hydrology and vegetation conditions of Giao Thuy district, Nam Dinh province revealed the the full characteristics of the landscape. There is 1 landscape class and 1 landscape subclass, 3 landscape classes with 20 different landscape types belonging to the tropical forest type. The rainy season has a cold winter and lies in the tropical landscape system humid monsoon and sub-tropical monsoon tropical system of natural Vietnam. On that basis, orientations for rational planning of agricultural and forestry production activities, forming specialized cultivation areas and cultivation areas in combination with other crops were proposed.

## REFERENCES

1. Lai Huy Anh (1994), *Topographic features*, - Geomorphology of the North Central region, rational use recommendations, Geographical Institute Materials.
2. Pham Quang Anh (1996), *Analyzing landscape ecology and applying the orientation of Vietnam Green Tourism Organization*, - Dissertation of Geographic PTS, University of Natural Sciences, Hanoi.
3. Pham Hoang Hai, Nguyen Thuong Hung, Nguyen Ngoc Khanh (1997), *Landscape landscape of rational use of natural resources*, *protection of Vietnam's environmental territory*, - Education Publishing House, Hanoi.
4. Pham Hoang Hai (2006), “Researching Vietnam's landscape diversity, methodology and some practical research results”, - *Collection of 2nd National Science Conference reports*, Hanoi.
5. People's Committee of Giao Thuy district, Nam Dinh province (2018), “*Report on land use planning for the five years 2018 - 2025 and orientation for land use to 2030*”.

# NGHIÊN CỨU, ĐÁNH GIÁ CÁC ĐẶC ĐIỂM TỰ NHIÊN PHỤC VỤ QUẢN LÝ TÀI NGUYÊN ĐẤT TẠI HUYỆN GIAO THỦY, TỈNH NAM ĐỊNH

***Tóm tắt:*** *Kết quả phân tích tổng hợp các đặc điểm tự nhiên về điều kiện khí hậu, thủy văn, đất đai và lớp phủ thực vật của một khu vực được xác định là cơ sở khoa học để đánh giá được chức năng, vai trò của cảnh quan sinh thái của khu vực, phục vụ mục đích quy hoạch, quản lý phát triển tài nguyên khu vực. Qua quá trình phân tích, đánh giá nghiên cứu đã xác định được đặc điểm cấu trúc cảnh quan huyện Giao Thủy đều nằm trong hệ cảnh quan nhiệt đới gió mùa, phụ hệ cảnh quan nhiệt đới gió mùa có mùa đông lạnh, bao gồm 1 lớp cảnh quan đồng bằng và 1 phụ lớp cảnh quan đồng bằng ven biển với 20 loại cảnh quan khác nhau. Trên cơ sở đó, đánh giá tiềm năng cảnh quan, góp phần cho huyện định hướng quy hoạch tài nguyên đất, phát triển nông – lâm nghiệp gắn với bảo vệ môi trường.*

***Từ khóa****: Cảnh quan, cấu trúc cảnh quan, sử dụng hợp lý tài nguyên đất quy hoạch nông - lâm nghiệp*

# THE STATUS OF PRODUCTION AND DEMAND FOR ORGANIC VEGETABLES IN HANOI

**Nguyen Thi Hoai Thuong**[1], **Bui Thi Nuong**[2], **Mai Huong Lam**[3], **Bui Minh Tuyen**[4]
[1,2,3] *Ha Noi University of Natural resources and Environment.*
[4] *Ha Noi Metropolitan University*

***Abstract:*** *This study aims to assess the current status of organic vegetable production and consumption in order to propose solutions to develop organic vegetable production in Hanoi City. The data in this study was collected through reports, related research, focus group discussions and surveying random samples of 390 consumers in Hanoi. The research results show that organic vegetable production was facing some difficulties such as small, scattered farming area (only accounting for 0.41% of the total vegetable cultivated land area), low productivity (meeting for 0.1% of the local demand), organic vegetable's price was significantly higher than conventional vegetables (3-4 times). Hanoi consumers have been aware of food safety and already have demand for OV (25.6%), however, there were still several barriers in accessing and using OV. To sustainably develop the organic vegetable production in Hanoi, the study has proposed some specific solutions related to the overall planning policy, management mechanisms, and communication.*

***Keywords:*** *organic vegetables; consumption, production, demand, Hanoi city.*

Email: bmtuyen@hnmu.edu.vn

Received 10 October 2019
Accepted for publication 20 November 2019

## 1. INTRODUCTION

The overuse of plant protection drugs to improve crop yields has left serious consequences not only for the general living environment, but also for agricultural production itself. Uncontrolled use of pesticides has been shown to increase soil erosion, soil degradation [1], reduce biodiversity [2] and ecological imbalance [3]. At the same time, many studies have shown a close relationship among some chemicals commonly used in plant protection drugs (such as 2,4 D; Paraquat...) and cancer development. on people [4], [5]. According to the Ministry of Health's 2018 statistics, the incidence of cancer in Vietnam tends to increase at an alarming rate with more than 126,000 new cases and about 94,000 deaths each year [6].

In this context, a model of vegetable cultivation without using chemical fertilizers, pesticides and transgenic seedlings, called organic vegetables (OV), is of great interest. OV products are reported to have high nutrient content, be safe for users and minimize environmental pollution [7], [8]. With these advantages, the OV farming model is expected to help Vietnam's agriculture develop sustainably.

Hanoi capital is an area with a high population size, with an average income level which is being improved, accompanied by a sense of health and environment protection being changed positively gradually. According to a survey in 2018, nearly 90% of people in Hanoi rated safe vegetables, including OV, which is essential in their daily meals [9]. At the same time, Hanoi city after being expanded is considered very suitable for developing OV production models, especially in suburban districts such as Ba Vi, Thach That, Chuong My or Soc Son. Therefore, Hanoi is considered to be a potential consumption market of OV, and it also has many advantages to develop this production model. However, the current production of OV in the city still faces many difficulties. Therefore, we conduct research “The status of production and demand for organic vegatables in Hanoi”, in order to investigate the status of production and consumption of OV products, provide accurate information about the output market's potential, thereby proposing solutions to develop OV production model in Hanoi, meeting environmental and community health benefits.

## 2. MATERIALS AND METHODS

### 2.1. The method of data collection:

***Secondary data*:** Data related to production situation such as area, OV production... are inherited from the reports in 2018 published in the main magazines and websites of ministries and related organizations.

***Primary data*:** Information on distribution channels, quality inspection and monitoring activities as well as factors affecting OV production were collected from group discussions of OV producing households. Perceptions about OV, needs and access issues OV markets were collected by interviewing 390 users from 18 to 60 who were randomly selected by semi-structured questionnaires. The in-depth interview method is applied to retail store owners and organic production team leaders in order to collect information on origin, price, production management and consumption of OV.

### 2.2. Data processing methods

Descriptive statistical analysis, calculation of evaluation criteria and content analysis to provide the current status of OV production & consumption and needs as well as identify outstanding issues and propose solutions in order to develop production and consumption markets of OV in Hanoi.

## 3. RESULTS AND DISCUSSION

### 3.1. Assess the current status of OV production in Hanoi

Currently, organic farming systems have caused increasing attention and has become a development trend in many countries in recent years, especially in developing countries, while pressure on food hygiene and safety, the quality of agricultural products and the environment are increasing, the demand for organic products is increasing. With the active advocacy of the Vietnam Organic Agriculture Association and the government as well as state agencies began to pay attention to promoting the development of organic agriculture.

**Table 3.1:** *OV cultivation area in Hanoi*

| Number | Evaluation criteria | Area unit | Area | Proportion (%) |
|---|---|---|---|---|
| 1 | Total vegatables area | ha | 12000 | 100 |
| 2 | Safe vegatables | ha | 5000 | 42,6 |
| 3 | VietGap vegetables | ha | 224 | 1,9 |
| 4 | OV (certificated) | ha | 50 | 0,4 |

*(Source: Hanoi Department of Agriculture and Rural Development, 2018)*

According to 2018 data of the Department of Agriculture and Rural Development, Hanoi has a total area of 12,000 hectares of vegetables, of which 5,000 hectares are eligible for safe vegetable production, 224 hectares of VietGAP vegetables and 50 hectares of OV certified. From the above results, it shows that the planned area for growing vegetables in Hanoi is relatively large but the area for safe vegetable production and especially OV is not much, small and scattered area occupies only about 0.41% of total vegetable planning area. This is due to many reasons in which the environmental conditions (soil, water) and inputs (plant varieties, etc.) must meet strict OV standards, making the area of OV model not yet met expectation.

According to statistics, the total production of vegetables in Hanoi is approximately 569.802 tons/ year; be able to meet 60% of the demand for green vegetables (in which the output of vegetables produced by the OV production process reaches 972 tons/ year, meeting 0.1% of the city's vegetable demand). About 40% of the vegetables supply from other localities such as Bac Ninh, Hung Yen, Hai Duong, Hai Phong, Vinh Phuc, especially the amount of OV provided by Luong Son, Hoa Binh cooperative.

**Table 3.2:** *Area and types of OV in Hanoi city*

| **Number** | **Evaluation criteria** | **Area (ha)** | **Quantity (tons / month)** | **Types of vegetables** |
|---|---|---|---|---|
| 1 | Thanh Xuan Cooperative | 36 | 40-50 | Mustard greens, mustard greens, Chinese cabbage, bok choy, spinach, sweet potato, Chinese amaranth, red amaranth, rice amaranth, pickled mustard greens, Japanese jute, jute, bitter melon, cucumber, okra , pumpkin, zucchini, kohlrabi, gourd, doc mung, ripe bananas, lemongrass, guise leaves, basil, scallions, mugwort, black beans… |
| 2 | Tue Vien organic farm (Lien Viet Company) | 3 | 10-12 | Cabbage, mustard greens, mushrooms, squash, spinach, purple cress, pickled vegetables, papaya, zucchini, luffa, shallots, mugwort… |
| 3 | Hoa Vien Organic Farm (Hoa Lac Ecological Company) | 10 | 25-30 | Cruciferous vegetables, natural flowers, spinach, sweet potato, amaranth, zucchini, gourd, squash, chayote, kohlrabi, Red and sour amaranth, cucumber, squeegee, dandelion... |

*(Source: Hanoi Department of Agriculture and Rural Development, 2018)*

Each month the amount of OV from OV production models to the Hanoi market ranges from 40 to 60 tons, with about 40 types of vegetables, fruits and spices, the number and types of substitutes supplied to the market vary depending on the time of year. Some types of vegetables are often supplied to the market such as Brassicajuncea, Cucumber (Chrysanthemum coronarium L), Lettuce (Lactuca sativa Var.CapittaL.), herbs (Coriandrum sativum), Coriander (Coriandrum sativum), High-yielding green chili (Capsicum annum L.), Amaranth (Amaranthus mangostanus), Bitter melon (Momordica charantia)... These vegetables are mostly imported from Hanoi Agricultural University, so they are relatively high-quanlity. In addition, a number of organic indigenous vegetables are also being studied and tested such as spinach..., contributing to diversifying the supply to the OV market of Hanoi. The survey results also indicate that OV products are being favored and appreciated by consumers with positive consumption signals.

**Table 3.3:** *Comparison of organic and conventional vegetables productivity*

| **Chỉ tiêu** | **OV** | **Safe vegetables** | **Regular vegetables** |
|---|---|---|---|
| Productivity (quintal / ha / crop) | 260 | 300 | 320 |
| The difference in yield among organic and conventional vegetables | -60 | | |

*(Source: Results of group discussion, 2018)*

According to the Hanoi Plant Protection Department, there are currently two models involved in organic vegetable production: a model of production of a group of households with similar interests, such as a cooperative with a 36ha certified area, besides some businesses. also began to respond to participate in OV production such as: Viet Lien Company has an area of OV production of 3 hectares in Long Bien district; Hoa Lac Exploiting Potential Co., Ltd. OV production area reaches 10 hectares in Thach That district; OV production groups in Hanoi organize production in two forms. The first is concentrated production in groups, group members contribute land, work together, timekeeping, and share economic profits. The second is production in a separate form, the production plan follows the group's common plan, but the area of each household in the group takes care of itself, harvests and consumes it in groups. Enterprises mainly operate in the form of centralized production management, such as hiring fields and hiring employees to organize production. Comparison of vegetable production efficiency based on organic vegetable model are presented in the table. It can be observed that despite the high input cost, the yield of organic vegetables is significantly lower than that of conventional and safe vegetables. The low productivity is partly due to the limited management of weeds and pests, especially the herb drugs being used are not really effective in preventing pests.

Discuss some factors affecting OV production activities in Hanoi, the results show that certain initial achievements have been made, demonstrating the possibility of developing organic agriculture in the area. However, at present, these models are still facing many difficulties and challenges, making farmers not really want to convert to organic agricultural production due to the attraction of low income and unsatisfactory commitment consumption market, OV products have not been introduced to the majority of consumers. Moreover, the production process is rigorous, it takes a long time to improve the soil and create irrigation water to meet the quality requirements, so production and labor costs...

| Priority | Positive effect | Negative effect |
|---|---|---|
| 1 | There is support from the project on breeding | Awareness and confidence of consumers on OV is very limited |
| 2 | Change farming practices and use of pesticides of farmers, improve the responsibility of the people | Market and channel of consumption are not diverse and not guaranteed |
| 3 | Ensure health for producers and consumers | High labor costs, low productivity and many risks of pests and diseases |
| 4 | Create job opportunities, improve income | Current policies are indicative and not specific |

*(Source: Results of group discussion, 2018)*

### 3.2. Current status of consumption of OV products in Hanoi

Demand for Hanoi City for vegetables is quite large, estimated at 2,500-3,000 tons/ month. The survey results from OV producing households are mapped in Figure 3.1 showing the distribution channels and consumption of OV products to consumers in Hanoi market. Currently OV is consumed through two main channels: direct consumption channel and indirect consumption channel as follows.

Direct OV consumption channel: About 30% of the production OV is consumed in this form but this consumption channel is often unstable. This type of product consumption is mainly through contracts with safe agricultural stores, direct orders of households, local product introduction stores or direct contracts of supermarkets, hotels and restaurants and some retail stores of safe vegetables.

Indirect consumption channel: This is the main form of consumption (accounting for about 70%), OV products will be supplied to consumers through consumption contracts with organic product distribution businesses. In order to consume products through this channel, households must commit to product quality and be subject to internal supervision of enterprises during the production process. Businesses use their brand name and reputation to sell products to supermarkets / restaurants / hotels or follow retail chain of distribution of clean food. The volume and price discussed before changing, normally the purchasing price of fruits and vegetables of all kinds is stable on average 15,000 VND/ kg, participating in this consumption channel, on average, each household produces OV. have an income of about 5-7 million / month after deducting expenses.

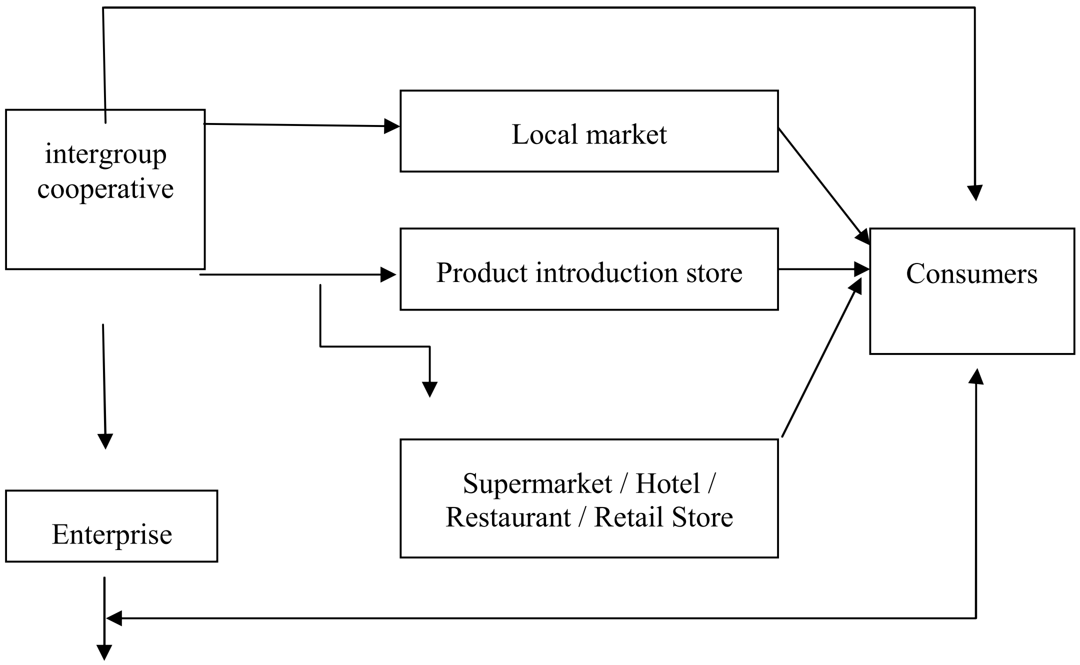

**Figure 3.1:** *OV distribution and consumption channel in Hanoi city*
*(Source: Results of group discussion, 2018)*

For the retail distribution system in Hanoi, OV has been being displayed at 41 supermarkets, shops, agents selling OV such as: Soi Bien clean food chain, Bac Tom clean food chain, Haprofood, Vian food 9 Food, Ecofood, Donavi, Top Green, Duyen Hai, Clever Food chain... Not only limited to specialized high-end shops, organic products are present in all supermarkets and hypermarkets such as Co.opmart, Co.opXtra, Big C, Lotte Mart, Aeon, Emart, Unimart, Michimart which are close to residential areas and offices, mostly concentrated in Thanh Xuan districts, Ha Dong, Hoan Kiem... According to OV products trading establishments, OV's products initially meet the needs of consumers but are limited in types and models of products. Moisture specifications products do not really meet the requirements of consumers. Survey results from OV products shops, the average number of customers of the store is 100-120 passengers/ day. The object of regular customers shopping is from 35 to 50 years old. OV sales are usually highest in the summer, as the number and model of supplies are more diverse. The survey results show that the majority of OV products (about 80%) are sold at the chains of clean food stores, supermarkets or stores when they reach the consumers with the cost is 3-4 times as the cost of regular vegetables. Survey results show that the average price of 1 kg of OV sold in the market is from VND 32,000/kg, some organic herbs cost 65,000 VND/kg. Whereas ordinary selling price is only about VND 8,000 - 10,000/kg. On the other hand, there still exists the fact that about 20% of OV vegetables consumed in local markets are not sold at OV prices that may even be lower than regular vegetables. This can be explained by the bad design due to the invasion of pests, diverse species and consumers who do not really know the value of OV and often equate OV and other common vegetables. This is one of the barriers to OV model development. OV prices in the market are summarized in Table 3.3.

**Table 3.4:** *OV prices in the market of some OV stores*

| Store | Cost (VNĐ) | | |
|---|---|---|---|
| | **Leafy vegetables (kg)** | **Fruit vegetable (kg)** | **Root vegetables (kg)** |
| System of Soi Bien stores | 32.000 | 30.000 -60.000 | 35.000 - 80.000 |
| Duyen Hai store | 32.000 | 30.000 -60.000 | 35.000 -80.000 |
| The system of Bac Tom stores (VinaGap Company) | 32.000 -50.000 | 35.000 -70.000 | 35.000 -100.000 |

*(Source: Summary of survey data, 2018)*

## 3.3. Demand for using OV products in Hanoi city

*About consumer awareness of vegetable quality in the market:* Plays an important role in the consumption of organic vegetables. When people understand the situation as well as the nature and role of vegetables quality, they actively seek for quality and safe vegetables and are willing to buy at a higher price than those who have less knowledge. Survey results on consumers' perceptions of vegetable quality in the study area show that over 71% of the respondents confirmed that regular vegetables are unsafe because they do not know the origin as well as the production process and are known at the same time. Additional information regarding plant protection drug abuse. However, up to 10% do not know if vegetables are safe or not pay much attention to vegetable quality, about 15% of consumers think that vegetable quality is quite safe. This indicates that people have begun to recognize health risks from using unsafe vegetables on the market.

**Table 3.5:** *Assessment of consumers on vegetable quality in Hanoi (N = 390)*

| Number | Evaluation criteria | Respondent | Proportion (%) |
|---|---|---|---|
| 1 | Absolute safe | 4 | 1 |
| 2 | Safe | 69 | 18 |
| 3 | Not safe | 277 | 71 |
| 4 | Do not know, do not care | 39 | 10 |
| Total | | 390 | 100 |

*(Source: Summary of survey data, 2018)*

*About the choice of vegetable supply channel:* partly reflects the consumers' need for safe vegetable quality. In the study area, consumers access different supply channels such as markets, supermarkets, clean / organic food stores, in the garden. In which people mainly come to the market to buy food including vegetables for their families because it is easy to choose thanks to a variety of vegetables that are plentiful, convenient and especially cheap in line with the financial spending of the majority of consumers in Hanoi. However, there are many consumers who choose safe supermarkets or vegetable shops to buy high-quality and safe products for their families, although the price is high and it is not convenient to buy. A small number of consumers living in suburban areas choose to buy vegetables at the acquaintances' garden because of the trust in quality and affordable prices.

**Table 3.6:** *Factors affecting the selection of vegetable supply channels of consumers (N = 390)*

| Number | Supply channel | The number of people | Reason for choosing |
|---|---|---|---|
| 1 | Markets | 200 | Diversity, convenience and cheap cost |
| 2 | Supermarkets | 150 | Convenience, quality assurance and safety |
| 3 | Clean vegetable/ OV stores | 40 | Safety |
| 4 | At the garden of acquaintances | 20 | Quality belief and cheap cost |

*(Source: Summary of survey data, 2018)*

*Current situation of demand for vegetables / OV:* In order to assess the status of full or partial use of OV in daily meals, the results are shown in Table 3.7.

**Table 3.7:** *Vegetable consumption characteristics of surveyed consumers (N = 390)*

| Number | Features of vegetable consumption | Frequency | Proportion (%) |
|---|---|---|---|
| 1 | Consumption of regular vegetables only | 290 | 74,4 |
| 2 | Consumption of OV only | 8 | 2,1 |
| 3 | Most OVs, sometimes with regular and safe vegetables | 20 | 5,1 |
| 4 | Most common vegetables and safe vegetables, sometimes with OV | 58 | 14,9 |
| 5 | Regular vegetables, safe vegetables and OV are equal | 14 | 3.5 |
| **Total** | | **390** | **100** |

*(Source: Summary of survey data, 2018)*

The summary results in Table 3.4 show that most consumers in Hanoi area still use regular vegetables (accounting for 74.4%), the number of consumers who choose to use OV products at different levels in family meals is significant (accounting for 25.6%). This also shows that the benefits of OV have been a significant part of consumers. However, the percentage of consumers using OV only accounts for a modest percentage (2%), possibly not only related to cognitive problems, but also due to income and status issues, the availability, accessibility and reliability of OV domestically products.

*About information channels of OV products:* This is a very important issue, even directly affecting the choice of consumers, because of the accuracy, completeness and reliability of OV products. In the context that the information channels that consumers access are quite diverse, the structure of the main types of information channels is shown in Figure 3.2:

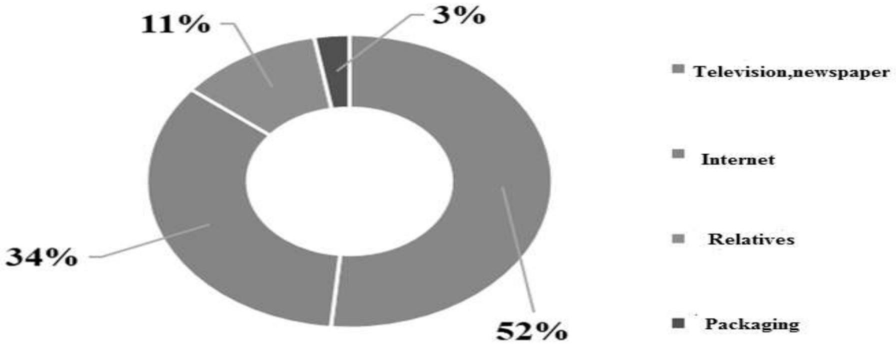

**Figure 3.2:** *Channels that receive OV product information of customers in Hanoi*
*(Source: Summary of survey data, 2018)*

The survey results show that the most popular OV information channel for consumers is via TV (newspaper, radio) and internet. Television (newspapers, radio - accounting for 52%) is a traditional information channel with high origin and high quality because it is censored by the authorities. Recently, food safety issues including OV are increasingly concerned and mentioned in many categories, integrated into many news programs. It can be seen that this information channel contributes a big part in introducing OV to consumers. The second most popular channel is the Internet (accounting for 34%), which is a potential information channel which is a trend in the 4.0 era. The internet channel is accessible to young workers, although the information is multidimensional but the quality is difficult to censor, sometimes inconsistent. This is an information channel which is evaluated as an active way of consumers, having the opportunity to introduce OV to consumers simply and quickly.

In addition, the information channel from product packaging is very important, due to the factors of origin, nutritional composition, branding... and especially the licensing of the authorities. However, at present the information on the packaging of OV products in the country is often incomplete and transparent, only recorded in a very general manner, following the OV standards. This situation creates a matrix of OV items, inconsistencies, causing bad consequences, making consumers not trust and decide not to use.

*About the type of OV that consumers prefer:* Survey results on 390 people with 04 OV groups showed that the OV group eating leaves (cabbage, lettuce...) was used the most (202/390 people, accounting for 51.8%), on the contrary, group of vegetables with tubers (sweet potatoes, potatoes, carrots...) is less popular (23/390 people, accounting for 5%).

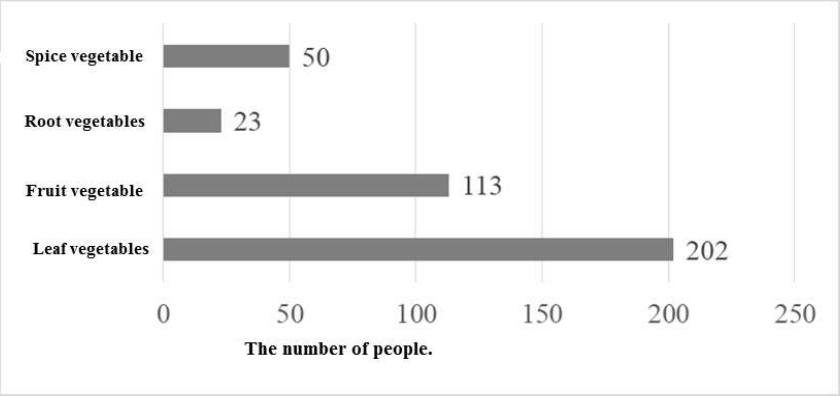

**Figure 3.3:** *The OV category is popular with consumers*
*(Source: Summary of survey data, 2018)*

The imbalance in the structure of the preferred OV species can be explained by the fact that consumers believe leafy vegetables are the most heavily affected group of abuse of plant protection drugs because of direct contact with chemicals used for spraying and watering. Meanwhile, root vegetables do not come in direct contact, or have a thick skin and are removed during cooking, so it is believed to be less affected by chemicals. In addition, this issue is related to the eating habits or culture of the main consumer department.

## 3.4. Factors affecting access and demand for OV products

**Table 3.8:** *Some barriers to OV access and use in Hanoi City*

| Number | Evaluation criteria | Respondent (390) | Proportion (%) |
|---|---|---|---|
| 1 | Do not know where OV is sold | 58 | 9.7 |
| 2 | Do not trust OV | 180 | 30.0 |
| 3 | The price of OV products are too high | 290 | 48.3 |
| 4 | Not available and less diverse in categories | 30 | 5.0 |
| 5 | Not accessible, not convenient | 42 | 7.0 |

*(Source: Summary of survey data, 2018)*

The results in the table show that high price is the main factor, nearly 70% of respondents think that high price compared to income is a big barrier to the intention to access OV products. In addition, consumers' confidence in OV products is not high due to lack of clear information and control, monitoring and evaluation to ensure the quality of the authorities is still loose. Many consumers assert that if quality assurance, the price of OV is 30-40% higher than normal vegetables still acceptable. In addition, the not diversified variety and unfavorable locations for selling vegetables are also preventing consumers from accessing OV market.

## 3.5. Proposing some solutions to develop OV model in Hanoi

The results of the above assessment of OV production and consumption have shown that the problem exists at all stages of the OV supply chain, it is necessary to have a series of synchronous solutions, with participation and cooperation with the authorities, production facilities and consumers, to promote the development of this model in Hanoi. The research team would like to offer some specific solutions as follows:

- General solution of land fund: fragmented land planning and small-scale production scale are major factors affecting the development of OV production model. The government needs to have a comprehensive planning policy to minimize the impact of normal vegetable production activities in the area, make the most of the area reserved for OV development, create favorable conditions for the construction and Infrastructure management which inherently requires very strict criteria.

- Solutions to reduce OV product cost: OV product price is a major obstacle to OV consumption of people. In order to reduce the cost of OV products, the government needs practical support policies and programs (such as loan support, technology transfer in farming, etc.) to reduce costs and increase production efficiency, improve quality, help increase competitiveness with other vegetables on the market.

- Solutions to strengthen consumers ' confidence in OV products: by strengthening control and management of OV production and distribution; Training qualified human resources for OV quality monitoring and supervision, strengthening OV safety and quality control in the process of production and consumption in the market; Strengthening OV sales network through supermarkets, OV specialty shops, distribution systems which have partly trusted consumers' quality of products; Focus on branding by providing complete information on labels and product packaging, with customer service promotion.

- Communication solutions: It is very important to raise consumers' awareness about OV, so that consumers can understand correctly and fully, proceed to accept and be willing to pay for OV products. Propaganda programs need to be conducted regularly, in a variety of forms, practical and specific. It is necessary to concentrate investment and build propaganda programs through regular information channels.

- Solutions to build and expand OV distribution system: integrate clean food chains into regular distribution forms to create favorable conditions for consumers to easily access OV supply.

## 4. CONCLUSION

Through the study, we can draw some conclusions as follows:

- The model of organic vegetable production is proving to be a potential model with the participation of many different subjects such as farmer groups and enterprises, which have initially achieved certain successes, but the model are still facing many difficulties and challenges such as small planning area, low productivity, high production costs, and guiding policies that are not specific.

- The situation of OV consumption is quite positive with many distribution channels, but the high price of products compared to the average income of consumers is an issue of concern.

- People have had awareness of food safety issues and have demand for OV, but meeting the demand depends on many factors. The study has shown many practical solutions related to communication, planning and management to develop OV model in Hanoi.

## REFERENCES

1. Rahman, K. and D. Zhang, Effects of fertilizer broadcasting on the excessive use of inorganic fertilizers and environmental sustainability. Sustainability, 2018. **10**(3): p.759.
2. Kanekar, P.P., et al., Biodegradation of organophosphorus pesticides. Proceedings-Indian National Science Academy Part B, 2004. **70**(1): p.57-70.
3. Sánchez-Bayo, F., S. Baskaran, and I.R. Kennedy, Ecological relative risk (EcoRR): another approach for risk assessment of pesticides in agriculture. Agriculture, Ecosystems & Environment, 2002. **91**(1-3): p.37-57.
4. Park, S.K., et al., Cancer incidence among paraquat exposed applicators in the Agricultural Health Study: a prospective cohort study. International journal of occupational and environmental health, 2009. **15**(3): p.274-281.
5. Bassil, K.L., et al., Cancer health effects of pesticides: systematic review. Canadian Family Physician, 2007. **53**(10): p.1704-1711.

6. Ministry of Health, Statistical Report. 2018.

7. Conacher, J. and A. Conacher, Organic farming and the environment, with particular reference to Australia: a review. Biological Agriculture & Horticulture, 1998. **16**(2): p.145-171

8. Crinnion, W.J., Organic foods contain higher levels of certain nutrients, lower levels of pesticides, and may provide health benefits for the consumer. Alternative Medicine Review, 2010. 15(1)

# ĐÁNH GIÁ HIỆN TRẠNG SẢN XUẤT VÀ NHU CẦU SỬ DỤNG RAU HỮU CƠ TRÊN ĐỊA BÀN THÀNH PHỐ HÀ NỘI

***Tóm tắt:*** *Nghiên cứu này nhằm đánh giá thực trạng sản xuất và tiêu dùng rau hữu cơ, đề xuất giải pháp phát triển mô hình rau hữu cơ tại thành phố Hà Nội. Các dữ liệu trong nghiên cứu này được thu thập thông qua các báo cáo, nghiên cứu, thảoluận nhóm người sản xuất rau hữu cơ và kết quả phỏng vấn 390 người tiêu dùngđược lựa chọn ngẫu nhiên trên địa bàn thành phố Hà Nội. Kết quả nghiên cứu cho thấy, mô hình này đang vấp phải một số khó khăn như diện tích quy hoạch nhỏ lẻ (chiếm 0,41% tổng diện tích đất canh tác), năng suất thấp (đáp ứng 0,1% nhu cầu của khu vực), giá thành sản phẩm còn cao hơn đáng kể so với rau thông thường (gấp 3-4 lần). Người tiêu dùng Hà Nội đã bước đầu nhận thức về an toàn thực phẩm và đã có nhu cầu sử dụng RHC (25,6%), tuy nhiên, còn nhiều rào cản trong việc tiếp cận và sử dụng RHC. Để phát triển bền vững mô hình rau hữu cơ tại Hà Nội, nghiên cứu đã đề xuất một số giải pháp cụ thể liên quan đến chính sách quy hoạch tổng thể, cơ chế quản lý và truyền thông.*

***Từ khóa:*** *Rau hữu cơ; tiêu thụ, sản xuất, nhu cầu, thành phố Hà Nội.*

# CALL FOR PAPERS

1. Scientific Journal is the official journal of Hanoi Metropolitan University. The issues are published monthly including specific fields: Social Science and Education; Natural Science and Technology.
2. The submission of an article implies that the work described has not been published previously and should be sent to the bellow email. The manuscripts will be revised for publication by the Editorial Board Members.
3. Manuscript format: *Abstract* (the abstract should state briefly the purpose of the research, the principal results and major conclusions); *Introduction*; *Content*; *Conclusion* và *REFERENCES.*

   The full-text is not exceeding 10 pages on A4 paper, font Times New Roman (Unicode), size 12 with a margin of 3 cm on left, 2 cm on right, 2.5 cm on top and at bottom.

   The *Abstract* is not exceeding 10 lines including Vietnamese and English. Attaching the author's full name, title, phone number and email address at the end of the manuscript.
4. The *REFERENCES* should be arranged orderly such as:
   1. John Steinbeck (1994), *Chùm nho phẫn nộ* (Phạm Thủy Ba dịch, tập 2), Nxb Hội nhà văn, H., tr.181.
   2. Bloom, Harold (2005), *Bloom's guides: John Steinbeck's The Grapes of Wrath*, New York: Chelsea House, pp.80-81.
   3. W.A Farag, V.H Quintana,. G Lambert-Torres (1998), "A Genetic-Based Neuro-Fuzzy Approach to odelling and Control of Dynamical Systems", *IEEE Transactions on neural Networks Volume*: 9 Issue: 5, pp.756-767.

---

***Scientific Journal - Hanoi Metropolitan University***
*No.98, Duong Quang Ham, Quan Hoa, Cau Giay, Ha Noi*
*Tel: 024.3.767.1409; Fax: 024.3. 833.5426*
*Email: tapchikhoahoc@hnmu.edu.vn*